



Justus-Liebig-Universität Gießen

Klinik Für Neurologie



---

# **Efficacy of Fibroblast Growth Factor Receptor (FGFR) inhibitor Infigratinib on Experimental Autoimmune Encephalomyelitis (EAE), a mouse model of Multiple sclerosis (MS)**

---

**Inaugural Dissertation**

Submitted to the

**Faculty of Biology and Chemistry**

In partial fulfillment of the requirements for the

Dr. rer. nat. Degree

To the Faculty of Biology and Chemistry  
of the Justus Liebig University Giessen, Germany

By

**Vinothkumar Rajendran**

Giessen, 2021

Germany

## **Multiple Sclerosis Research Group**

Department of Neurology, Justus-Liebig-University Giessen, Germany

First Supervisor:

**Prof. Dr. Reinhard Lakes-Harlan**  
Faculty 08 Biology and Chemistry  
Institute of Animal Physiology  
Department of Integrative Sensory Physiology  
Justus-Liebig-University Giessen, Germany

Second Supervisor:

**Prof. Dr. med. Martin Berghoff**  
Faculty 11 Medicine  
Multiple Sclerosis Research Group  
Neurology Clinic  
Justus-Liebig-University Giessen, Germany

Committee members:

**Prof. Dr. Christoph Rummel**  
Faculty 10 Veterinary Medicine  
Institute for Veterinary Physiology and Biochemistry  
Department of Veterinary Medicine  
Justus-Liebig-University Giessen, Germany

**Prof. Dr. Reinhard Dammann**  
Faculty 08 Biology and Chemistry  
Institute of Genetics  
Justus-Liebig-University Giessen, Germany

Doctoral Defense: 03.12.2021

*I dedicate this thesis to my family members  
(Especially to the memory of my beloved Grandmother and Father)*

*&*

*Relatives and Friends*

*I love you all dearly*



**திருக்குறள்**

வான்நின்று உலகம் வழங்கி வருதலால்  
தான்அமிழ்தம் என்றுணரற் பாற்று

**திருவள்ளுவர்**

**Tirukkural**

By the continuance of rain the world is preserved in  
existence; it is therefore worthy to be called ambrosia

**Thiruvalluvar**



## **DECLARATION**

I hereby declare that the present thesis is my original work and that it has not been previously presented in this or any other university for any degree. I have also abided by the principles of good scientific conduct laid down in the charter of the Justus Liebig University of Giessen in carrying out the investigations described in the dissertation.

**Vinothkumar Rajendran**

Giessen, Germany

**INDEX**

<b>INDEX.....</b>	<b>1</b>
<b>ABBREVIATIONS.....</b>	<b>4</b>
<b>LIST OF FIGURES.....</b>	<b>5</b>
<b>LIST OF TABLES.....</b>	<b>7</b>
<b>ABSTRACT.....</b>	<b>8</b>
<b>1 INTRODUCTION.....</b>	<b>9</b>
1.1 Multiple sclerosis .....	9
1.1.1 Etiology of MS .....	10
1.1.2 Symptoms of MS .....	10
1.1.3 Immunopathology of MS.....	11
1.1.4 Subtypes of MS .....	12
1.1.5 MS diagnosis .....	13
1.1.6 MS treatment .....	14
1.2 Experimental autoimmune encephalomyelitis (EAE).....	15
1.2.1 Subtypes of EAE models used in MS research .....	16
1.3 Oligodendrocytes, myelin in MS and EAE.....	17
1.4 Fibroblast growth factors (FGFs).....	18
1.5 Fibroblast growth factor receptors (FGFR).....	20
1.6 Fibroblast growth factor/FGF receptor interaction .....	20
1.7 FGFR in oligodendrocyte lineage .....	21
1.8 FGF/FGFR in demyelinating disease MS and its animal model EAE.....	22
1.9 Functional role of FGFR1 and FGFR2 in MOG <sub>35-55</sub> -induced EAE.....	22
1.10 FGFR inhibitors in clinical trails.....	24
1.11 Selective FGFR inhibitor infigratinib .....	26
<b>2 AIMS.....</b>	<b>28</b>
<b>3 MATERIALS AND METHODS.....</b>	<b>29</b>
3.1 MATERIALS .....	29
3.1.1 Animals.....	29
3.1.2 Cell lines .....	29
3.1.3 Kits.....	29
3.1.4 Primary Antibodies.....	30
3.1.5 Secondary Anibodies .....	31

---

3.1.6 Ladders .....	31
3.1.7 Primers.....	31
3.1.8 Chemicals and Solutions .....	32
3.1.9 Laboratory consumables.....	33
3.1.10 Laboratory instruments.....	35
3.1.11 Buffers .....	36
3.1.12 Software.....	37
<b>3.2 METHODS.....</b>	<b>38</b>
3.2.1 Animal experiment procedures.....	38
3.2.2 Molecular biology methods .....	41
3.2.3 Protein biochemistry .....	42
3.2.4 Histopathology and immunohistochemistry (IHC) .....	43
3.2.5 Cell culture experiments .....	45
3.2.6 Statistical analysis.....	47
<b>4 RESULTS .....</b>	<b>48</b>
<b>4.1 Efficacy of infigratinib in MOG<sub>35-55</sub>-induced EAE .....</b>	<b>48</b>
4.1.1 EAE clinical scoring.....	48
<b>4.2 Infigratinib applied from the time of EAE induction (Preventive protocol) .....</b>	<b>49</b>
4.2.1 Infigratinib given from day 0-9 p.i. reduces the severity and relapses in EAE.....	49
4.2.2 Immune cells infiltration was reduced by infigratinib.....	52
4.2.3 Regulation of inflammatory mediators in the whole spinal cord during EAE .....	55
4.2.4 Infigratinib decreases demyelination and increases axonal density .....	57
4.2.5 Myelin inhibitor expression is modulated by infigratinib .....	57
4.2.6 Infigratinib enhances the number of OPCs, mature oligodendrocytes, and motor neurons, and myelin protein expression .....	60
4.2.7 Infigratinib modifies FGFR signalling and BDNF/ TrkB receptors expression .....	68
<b>4.3 Infigratinib applied from the time of onset of disease (Suppressive protocol) .....</b>	<b>71</b>
4.3.1 Infigratinib given from day 10-19 p.i. suppresses severity and relapses of EAE....	71
4.3.2 Migration of immune cells into the CNS was reduced by infigratinib.....	74
4.3.3 Pro-inflammatory cytokine changes induced by infigratinib .....	77
4.3.4 Infigratinib decreases demyelination and increases axonal density .....	79
4.3.5 Expression of inhibitor of remyelination.....	79
4.3.6 Infigratinib enhances the number of mature oligodendrocytes, motor neurons and myelin protein expression.....	83
4.3.7 Infigratinib on FGFR signalling and BDNF/TrkB receptors expression .....	90

---

<b>4.4 <i>In vitro</i> experiments.....</b>	<b>94</b>
4.4.1 The effects of FGFR inhibition with infigratinib in OLN93 oligodendrocytes .....	94
<b>5 DISCUSSION.....</b>	<b>96</b>
5.1 Inhibition of FGFR by infigratinib reduces severity of EAE.....	96
5.2 Infigratinib reduces immune cell infiltration into the CNS .....	97
5.3 Modulatory effects of infigratinib on pro-inflammatory cytokines .....	97
5.4 Effect of infigratinib on myelin inhibitors .....	99
5.5 Effects of infigratinib on oligodendrocytes, demyelination and axons.....	100
5.6 Effects of infigratinib on FGFR and dependent signalling pathways .....	100
<b>6 SUMMARY .....</b>	<b>104</b>
<b>ZUSAMMENFASSUNG .....</b>	<b>105</b>
<b>REFERENCES.....</b>	<b>106</b>
<b>ACKNOWLEDGEMENTS .....</b>	<b>118</b>
<b>PUBLICATIONS.....</b>	<b>120</b>

---

**ABBREVIATIONS**

BBB	Blood Brain Barrier
BDNF	Brain-derived neurotrophic factor
BSA	Bovine serum albumin
CNS	Central nervous system
CSF	Cerebrospinal fluid
CX3CL	Chemokine (C-X3-C motif) Ligand 1 (Fractalkine)
CX3CR	Chemokine (C-X3-C motif) receptor 1
DIS	Dissemination in space
DNA	Deoxyribonucleic acid
EAE	Experimental autoimmune encephalomyelitis
ECL	Enhanced chemiluminescence
ERK	Extracellular signal-regulated kinases
FGF	Fibroblast growth factor
FGFR	Fibroblast growth factor receptor
GAPDH	Glyceraldehyde 3-phosphate dehydrogenase
H and E	Hematoxylin and Eosin
IL	Interleukins
i.p.	Intraperitoneal
iNOS	Inducible Nitric oxide synthase
LFB/PAS	Luxol fast blue/periodic acid Schiff
MBP	Myelin Basic protein
MOG	Myelin oligodendrocyte glycoprotein
mRNA	Messenger Ribonucleic acid
MS	Multiple sclerosis
NAWM	Normal-appearing white matter
OPC	Oligodendrocyte progenitor cells
p.i.	Post immunization
PBS	Phosphate buffered saline
PFA	Paraformaldehyde
PLP	Proteolipid protein
RT	Room temperature
RT-PCR	Real time-Polymerase chain reaction
SDS	Sodium dodecyl sulfate
TBS	Tris buffered saline
TBST	Tris buffered saline with Tween 20
TFG- $\beta$	Transforming growth factor beta
TNF	Tumor necrosis factor
TrkB	Neurotrophic tyrosine kinase receptor, type 2
WML	White matter lesions

---

**LIST OF FIGURES**

Figure 1. Prevalence of multiple sclerosis 2020 .....	9
Figure 2. Risk factors for multiple sclerosis .....	10
Figure 3. Immunopathology of multiple sclerosis .....	11
Figure 4. The clinical course of multiple sclerosis .....	12
Figure 5. Timeline of therapeutic drug developments in multiple sclerosis.....	14
Figure 6. Mouse model of chronic EAE .....	16
Figure 7. Mouse model of adoptive transfer EAE .....	17
Figure 8. Structure and FGF receptor specificity of the fibroblast growth factor family .....	19
Figure 9. Structure of FGFR, FGF ligand binding, and FGF/FGFR signalling pathways .....	21
Figure 10. Oligodendroglial specific deletion of <i>FGFR1</i> and <i>FGFR2</i> in EAE.....	23
Figure 11. Chemical structure of the FGFR inhibitor fingertinib.....	27
Figure 12. Experimental design illustrating the timeline of EAE induction, fingertinib treatment, clinical scoring and tissue analysis till acute and chronic phase of EAE .....	40
Figure 13. Clinical symptoms of MOG <sub>35-55</sub> -induced EAE (placebo arm).....	48
Figure 14. Fingertinib reduces the severity of relapses in MOG <sub>35-55</sub> -induced EAE .....	50
Figure 15. Effect of fingertinib on EAE onset and body weight .....	51
Figure 16. Inflammation and immune cell infiltration in spinal cord WML at day 17 p.i. ....	53
Figure 17. Inflammation and immune cell infiltration spinal cord WML at day 41 p.i. ....	54
Figure 18. Fingertinib on cytokines and chemokines in spinal cord at day 17/41 p.i. ....	56
Figure 19. Fingertinib on demyelination and axonal density in the spinal cord at day 17 p.i.	58
Figure 20. Fingertinib on demyelination and axonal density in the spinal cord at day 41 p.i.	59
Figure 21. Expression of remyelination inhibitors in the whole spinal cord at day 17/41 p.i.	60
Figure 22. OPCs populations in spinal cord WML at day 17/41 p.i.....	62
Figure 23. OPCs populations in spinal cord NAWM at day 17/41 p.i. ....	63
Figure 24. Mature oligodendrocyte populations in spinal cord WML at at day 17/41 p.i.....	64
Figure 25. Mature oligodendrocyte populations in spinal cord NAWM at day 17/41 p.i. ....	65
Figure 26. Motor neuron populations in spinal cord grey matter at day 17/41 p.i. ....	66
Figure 27. Myelin protein expression in the spinal cord at day 17/41 p.i.....	67
Figure 28. FGF/FGFR and BDNF/TrkB expression in the spinal cord at day 17 p.i. ....	69
Figure 29. FGF/FGFR and BDNF/TrkB expression in the spinal cord at day 41 p.i. ....	70
Figure 30. Fingertinib suppresses the severity of relapses in MOG <sub>35-55</sub> -induced EAE.....	72

---

Figure 31. Effect of fingertinib on EAE onset and body weight .....	73
Figure 32. Inflammation and immune cell infiltration in spinal cord WML at day 20 p.i. ....	75
Figure 33. Inflammation and immune cell infiltration in spinal cord WML at day 42 p.i. ....	76
Figure 34. Expression of cytokines/chemokines in spinal cord at day 20/42 p.i.....	78
Figure 35. Fingertinib on demyelination and axonal density in the spinal cord at day 20 p.i.	80
Figure 36. Fingertinib on demyelination and axonal density in the spinal cord at day 42 p.i.	81
Figure 37. mRNA expression of remyelination inhibitors in spinal cord at day 20/42 p.i.....	82
Figure 38. OPCs cell populations in spinal cord WML at day 20/42 p.i.....	84
Figure 39. OPCs cell populations in spinal cord NAWM at day 20/42 p.i.....	85
Figure 40. Mature oligodendrocyte populations in spinal cord WML at day 20/42 p.i. ....	86
Figure 41. Mature oligodendrocyte populations in spinal cord NAWM at day 20/42 p.i. ....	87
Figure 42. Motor neuron populations in spinal cord grey matter at day 20/42 p.i. ....	88
Figure 43. Myelin protein expression in the spinal cord at day 20/42 p.i.....	89
Figure 44. FGF/FGFR and BDNF/TrkB expression in the spinal cord at day 20 p.i. ....	91
Figure 45. FGF/FGFR and BDNF/TrkB expression in the spinal cord at day 42 p.i. ....	92
Figure 46. Proliferation effects of fingertinib on OLN93 cells. ....	94
Figure 47. Expression of FGF/FGFR dependent signalling molecules and myelin proteins. .	95

---

**LIST OF TABLES**

Table 1. The 2017 McDonald criteria for the diagnosis of multiple sclerosis.....	13
Table 2. Myelin peptides are used to induce EAE.....	17
Table 3. Selective FGFR inhibitors in clinical development.....	25
Table 4. Disease severity (Prevention protocol).....	49
Table 5. Immune cell infiltrations (Prevention protocol).....	52
Table 6. Demyelination and axonal density (Prevention protocol).....	57
Table 7. Oligodendrocyte population (Prevention protocol).....	61
Table 8. Disease severity (Suppression protocol).....	71
Table 9. Immune cell infiltrations (Suppression protocol).....	74
Table 10. Demyelination and axonal density (Suppression protocol).....	79
Table 11. Oligodendrocyte population (Suppression protocol).....	83
Table 12. Summary of findings from EAE study.....	93



**ABSTRACT**

Multiple sclerosis (MS) is associated with oligodendrocytes damage resulting in demyelination, failure of remyelination and functional loss of neurons. Present therapeutic disease modifying drugs for MS are acting predominantly anti-inflammatory and there is a lack of substances with improving mechanisms of myelin repair. Recent findings in MS patients and its animal models suggested that fibroblast growth factors (FGF) and its receptor (FGFR) signalling plays a role in the pathology of MS and its models. Recent studies on the function of FGFR in MOG<sub>35-55</sub>-induced experimental autoimmune encephalitis (EAE) showed that deletion of *FGFR1* and *FGFR2* in oligodendrocytes leads to a less severe disease course, decreased lymphocyte and macrophage infiltration and increased remyelination. Here, we hypothesized that the oral application of a selective FGFR inhibitor infigratinib decreases disease severity and enhance neuronal protection in experimental autoimmune encephalomyelitis. Oral application of infigratinib resulted in a constant decline of disease severity in MOG<sub>35-55</sub>-induced EAE. The ameliorated disease course was associated with a reduction of cellular inflammation in the CNS, as well as neuroprotective and neuroregenerative effects. The number of mature oligodendrocytes within demyelinating lesions was increased, degeneration of myelin and axons was reduced following application of infigratinib. The limited expression of FGFRs in the spinal cord suggests that infigratinib crosses over the blood-brain barrier and acts in the CNS. Further, infigratinib induces the increased expression of BDNF/TrkB and myelin proteins MBP, PLP, CNPase in spinal cord. The results of this study suggest that short-term administration of infigratinib has the efficiency of ameliorating the severity of EAE by reducing immune cell infiltration and enhancing myelin protein expression.

## 1 INTRODUCTION

### 1.1 Multiple sclerosis

Multiple sclerosis (MS) is a chronic demyelinating inflammatory disorder of the central nervous system (CNS) that damages the myelin sheath, the insulating layer that covers and protects the nerves (Goldenberg 2012). Jean-Martin Charcot first described the pathology and symptoms of multiple sclerosis in 1868 (Kumar et al., 2011). The nature and severity of the MS are heterogeneous and characterized by relapse and remission timing. Multiple sclerosis typically attacks adults between the ages of 20 to 40 years and is higher among women than men (Goldenberg 2012). Approximately 2.8 million individuals globally affected by multiple sclerosis (Tafti et al., 2020). The prevalence of MS differs with geography, race, sex, and it is higher in temperate regions of the world (Nicholas et al., 2013) (Figure 1). Multiple sclerosis is associated with reduced health-related quality of life, mental distress, loss of career opportunities, and higher health care costs (Kidd et al., 2017). The life expectancy is shortened for people affected with MS, most of the causes of the death being the severity of MS or associated complications such as respiratory dysfunction and infections (Marrie et al., 2015).

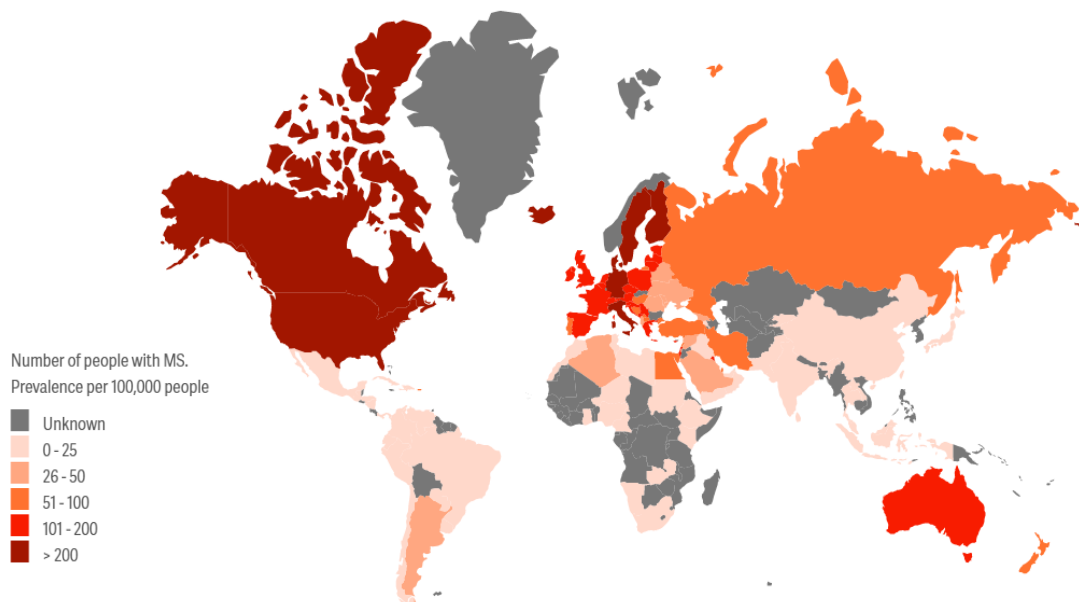


**Figure 1. Prevalence of multiple sclerosis 2020** (Source: The MS International Federation's Atlas of MS).

### 1.1.1 Etiology of MS

The etiology of MS is still unknown, but substantial evidence suggests that the interplay of genetic susceptibility and environmental stimulus contributes to MS development (Doshi et al., 2016). A higher percentage of genetic sharing within families such as monozygotic twins has a risk of developing MS. On genome-wide association studies, more than 200 genetic risk variants were identified for MS, and every genetic risk variant has a minor effect on the development of MS (Filippi et al., 2018). Several scientific studies showed risk associations with cigarette smoking, less sunlight exposure, vitamin D deficiency, and obesity during adolescence. People with previous Epstein–Barr virus infection have a higher risk of MS than those without (Dobson et al., 2019) (Figure 2). Human migration studies support, migrants from low-risk countries and children born to migrants in Europe are at high risk of MS (Dobson et al., 2018). The risk of MS is high in biological relatives of patients with MS (Tafti et al., 2020).

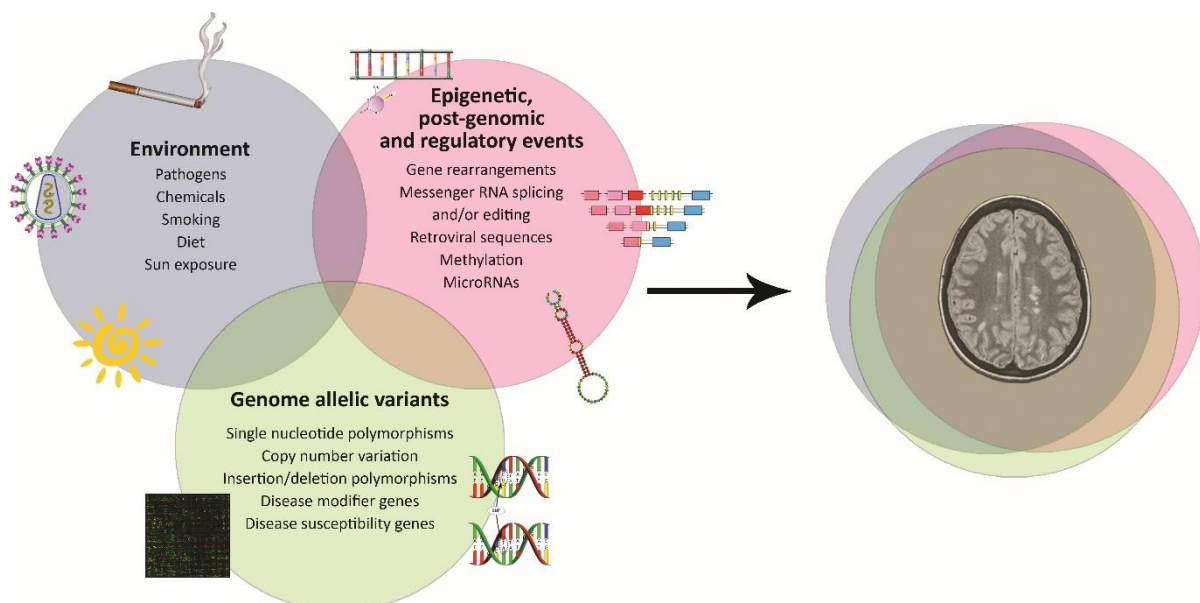


**Figure 2. Risk factors for multiple sclerosis** (Jorge R. Oksenberg/Cambridge University Press).

### 1.1.2 Symptoms of MS

The neurological signs and symptoms of MS vary widely and reflect the extent of lesions and their location (Hunter et al., 2016). The condition mostly affects optic nerves, brain and spinal

cord resulting in cognitive decline, difficulties in speech and swallowing, muscle weakness, ataxia, tremor, spasticity, paralysis, balance disorder, changes in vision, vertigo, sensory deficits, impairment of bladder and bowel function, pain, fatigue, and mental depression (Halabchi et al., 2017).

### 1.1.3 Immunopathology of MS

Multiple sclerosis is a chronic autoimmune inflammatory, demyelinating and neurodegenerative CNS disease (Filippi et al., 2018). The white matter in the brain and spinal cord is the focal area of inflammation and demyelination. The immune reactions are led by the activation of peripheral autoreactive T-lymphocytes following the loss of self-tolerance toward autoantigens such as myelin and other CNS antigens (Yamout et al., 2018). Leukocytes (including T cells) cross the blood-brain barrier (BBB) to perform the regular human CNS's immune surveillance. The mechanism of BBB disruption is mediated by activated leukocytes which initiate the production of numerous molecules such as cytokines, chemokines, adhesion molecules, integrins, and reactive oxygen species. The loss of barrier function of the BBB enhanced the massive transmigration of activated leukocytes (including T cells, B cells, and macrophages) into the CNS, which leads to further inflammation and demyelination (Legroux and Arbour 2015) (Figure 3).

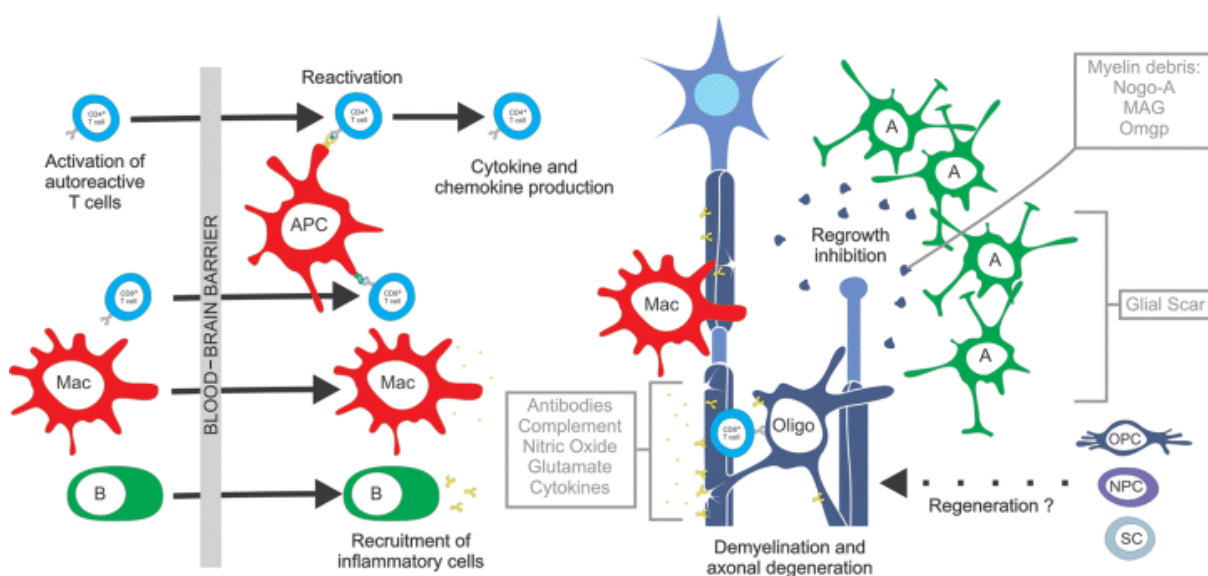


**Figure 3. Immunopathology of multiple sclerosis** (Source: McQualter et al., 2007).

In the CNS, autoreactive T cells are reactivated by local antigen-presenting cells and initiate the release of pro-inflammatory cytokines, chemokines and recruit other T cells, B cells, and macrophages resulting in oligodendrocyte destruction, myelin loss, and axonal damage. In parallel, immune-modulatory networks are triggered to limit excessive inflammation and initiate myelin repair, which results in at least partial remyelination and is associated with clinical remission (Baecher-Allan et al., 2018 and Yamout et al., 2018).

### 1.1.4 Subtypes of MS

U.S. National Multiple Sclerosis Society introduced new descriptors of activity and progression of MS in 2014. The clinically isolated syndrome (CIS) refers to a first episode of inflammatory demyelination in the central nervous system that could become MS if the additional activity occurs. Relapsing remitting MS (RRMS) episodes of acute worsening of neurologic functioning (new symptoms or the worsening of existing symptoms) with total or partial recovery and no apparent progression of the disease ( $\approx 85\%$  of patients have RRMS). Primary progressive MS (PPMS) shows steadily worsening neurologic function from the onset of symptoms without initial relapses or remissions ( $\approx 15\%$  of people with PPMS). Secondary progressive MS (SPMS) follows an initial relapsing remitting course, and the disease becomes more steadily progressive, with or without relapses (Klineova and Lublin 2018) (Figure 4).

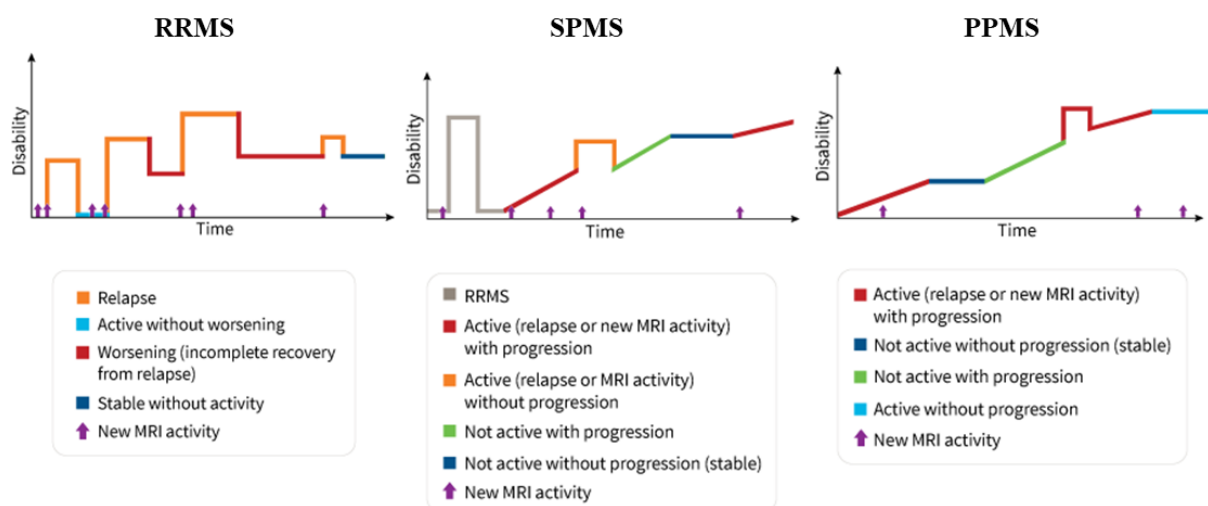


**Figure 4.** The clinical course of multiple sclerosis (Source: Lublin et al., 2014).

### 1.1.5 MS diagnosis

There is no single diagnostic test for MS. The diagnosis relies on clinical symptoms attributable to white matter lesions, supported by magnetic resonance imaging (MRI) and CSF analysis. Criteria for MRI techniques have evolved continuously, and MRI remains the sensitive method to detect MS lesions, disease activity, measure brain atrophy and disease progression (Hunter et al., 2016). Diagnostic criteria for MS, the most commonly used one is the McDonald criteria initially proposed in 2001 and revised in 2005, 2011, and recently in 2017. New parameters of the McDonald criteria 2017 were designed to facilitate earlier MS diagnosis (Zipp et al., 2019) (Table 1).

**Table 1. The 2017 McDonald criteria for the diagnosis of multiple sclerosis in patients with an attack at the onset.** (Revisions to MS diagnosis, Thompson et al., 2018 and The National Multiple Sclerosis Society, USA)

Clinical presentation	Additional data needed for a MS diagnosis
2 or more attacks and clinical evidence of 2 or more lesions; OR 2 or more attacks and clinical evidence of 1 lesion with clear historical evidence of prior attack involving lesion in different location	None
2 or more attacks and clinical evidence of 1 lesion	DIS shown by one of these criteria: - additional clinical attack implicating different CNS site - 1 or more MS-typical T2 lesions in 2 or more areas of CNS: periventricular, cortical, juxtacortical, infratentorial or spinal cord
1 attack and clinical evidence of 2 or more lesions	DIT shown by one of these criteria: - Additional clinical attack - Simultaneous presence of both enhancing and non-enhancing MS-typical MRI lesions, or new T2 or enhancing MRI lesion compared to baseline scan (without regard to timing of baseline scan) - CSF oligoclonal bands
1 attack and clinical evidence of 1 lesion	DIS shown by one of these criteria: - Additional attack implicating different CNS site - 1 or more MS-typical T2 lesions in 2 or more areas of CNS: periventricular, cortical, juxtacortical, infratentorial or spinal cord <b>AND</b> DIT shown by one of these criteria: - additional clinical attack - Simultaneous presence of both enhancing and non-enhancing MS-typical MRI lesions, or new T2 or enhancing MRI lesion compared to baseline scan (without regard to timing of baseline scan) - CSF oligoclonal bands

...in a person who has steady progression of disease since onset	
1 year of disease progression (retrospective or prospective)	DIS shown by at least two of these criteria: - 1 or more MS-typical T2 lesions (periventricular, cortical, juxtacortical or infratentorial) - 2 or more T2 spinal cord lesions - CSF oligoclonal bands

DIT = Dissemination in time, CNS = central nervous system, CSF = cerebrospinal fluid

DIS = Dissemination in space, T2 lesion = hyperintense lesion on T2-weighted MRI

### 1.1.6 MS treatment

Currently, there are no curative drug therapies for MS. Current MS treatment can be divided into three categories: acute relapse management, slowing disease progression with disease-modifying therapies (DMTs), and symptomatic treatments (Hart et al., 2016). High-dose corticosteroids are used to treat the acute management of MS relapses. These drugs (methylprednisolone and dexamethasone) facilitate faster functional recovery and protect from more severe deficits in the first weeks but unclear about long-term benefits (Filippi et al., 2018).

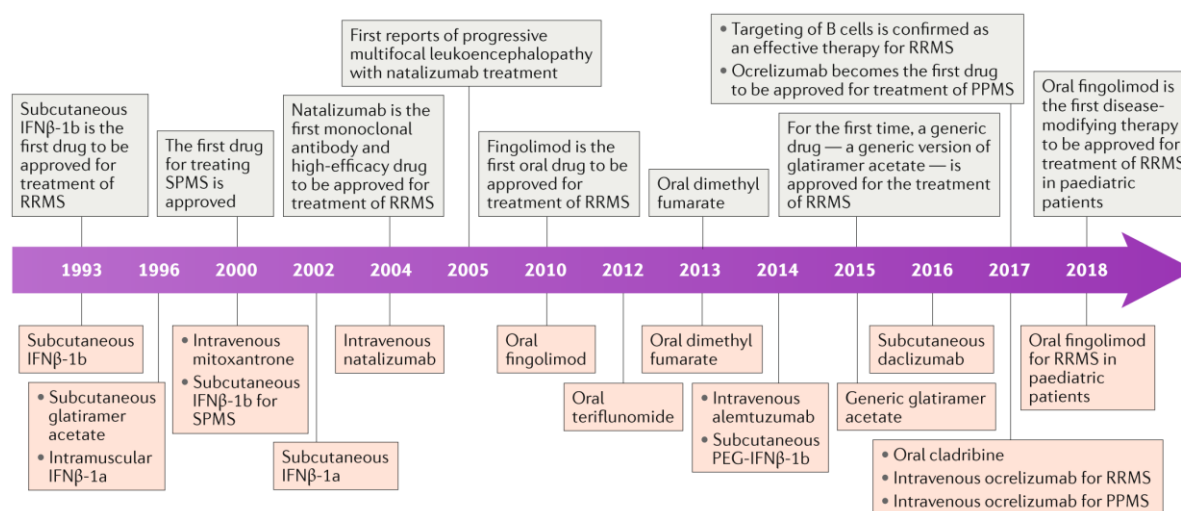


**Figure 5. Timeline of therapeutic drug developments in multiple sclerosis.** Significant milestones in the development are shown in green boxes, and drugs approved by the FDA or European Medicines Agency are shown in orange boxes. (Source: Tintore et al., 2019).

There are more than 15 FDA (U.S. Food and Drug Administration) approved DMTs available for treating RRMS (De Angelis et al., 2018) (Figure 5). The mechanism of action of DMTs is linked to the pathology of MS (Hart et al., 2016). Each DMT's varying in its mechanisms of action and is not fully understood, but many of these DMTs actions decrease circulating T cells, B cells, macrophages, and cytokine production. However, circulating lymphocytes represent approximately 2% of the total population; they may not be an accurate indicator of the body's total lymphocyte population and function (Fox et al., 2019). Several DMTs decrease the occurrence of relapses, slow or reduce disability worsening, and modify the overall MS disease course (Vermersch et al., 2020 and De Angelis et al., 2018). Most of the current MS DMTs are focused on selective or general suppression of the immune response. These medications would either attempt to deplete complete B-cell or both B and T-cells (e.g., ocrelizumab and alemtuzumab), sequestering away inflammatory immune cells from the CNS (natalizumab and sphingosine-phosphate receptor modulators), or inhibit the increase of activated lymphocytes (teriflunomide and cladribine) (Jakimovski et al., 2020). DMTs have immunosuppressive activity and the potential to increase infection risk. Dalfampridine is the FDA-approved drug for symptomatic therapy to improve walking speed in patients with MS (Goldenberg 2012).

## **1.2 Experimental autoimmune encephalomyelitis (EAE)**

Three animal models that have been used to study MS are (i) experimental autoimmune encephalomyelitis (EAE), (ii) virally-induced chronic demyelinating disease, known as Theiler's murine encephalomyelitis virus (TMEV) infection, and (iii) toxin (cuprizone) induced demyelination (Procaccini et al., 2015). EAE is a widely used animal model, effective for studying the immunopathogenic process of MS and preclinical testing for developing drugs (Farooqi et al., 2010). Many drug therapies were successfully translated from EAE to MS (e.g., Glatiramer acetate). The significant difference between MS and EAE is that external immunization is required to induce EAE, whereas an MS causative agent is unknown. (Hart et al., 2011). EAE can reproduce many of the clinical and immunoneuropathological aspects of MS (Gold et al., 2006). EAE can be induced in the rat, mouse, rabbit, guinea pig, and monkey. However, mice have become the most widely used species.



### 1.2.1 Subtypes of EAE models used in MS research

EAE can be induced in mice by two different active or passive immunizations. Active EAE mice are immunized with myelin peptides emulsified in complete Freund's adjuvant (CFA) accompanied by an intraperitoneal application of pertussis toxin on the day of immunization and 48 hrs later. Pertussis toxin mediates blood brain barrier breakdown to enhance migration of peripherally myelin activated T cells into the CNS. Migrated T cells in CNS are reactivated by local and inflammatory immune cell infiltration that occurs in CNS (Figure 6). Depending on the mouse strain and the antigen (e.g., myelin oligodendrocyte glycoprotein (MOG), myelin basic protein (MBP), myelin proteolipid protein (PLP)) required for autoimmunity induction varies (Bittner et al., 2014) (Table 2). MOG has emerged as an important target in MS. MOG-reactive T cells and autoantibodies are more readily detected in demyelinating lesions and cerebrospinal fluid of MS patients than PLP and MBP reactive T cells (Glatigny and Bettelli 2018). Immunization with MOG<sub>35-55</sub> peptide in the C57BL/6 mouse is the most frequently used mouse model for relapsing-remitting or chronic disease courses of MS. The first signs of EAE disease start 9-14 days post immunization, and then severity worsens and is followed by incomplete recovery (Bittner et al., 2014).

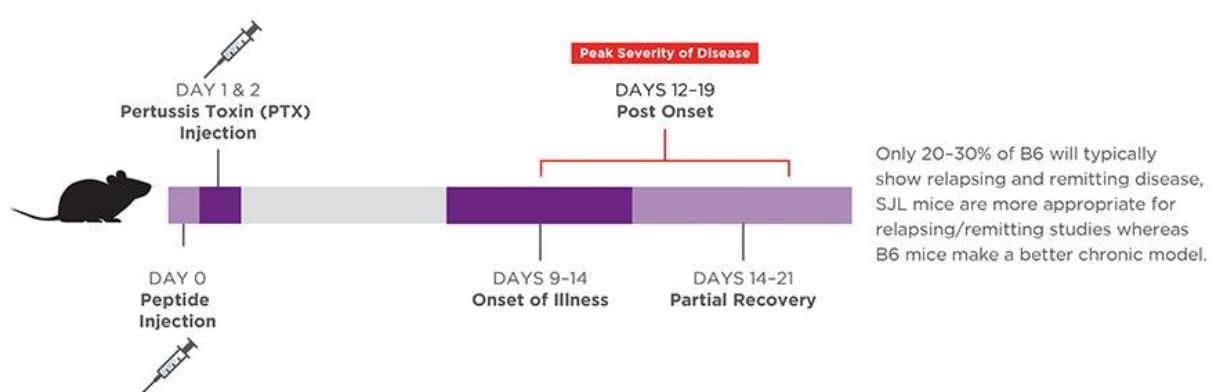


**Figure 6. Mouse model of chronic EAE** (Source: Taconic Biosciences, Inc).

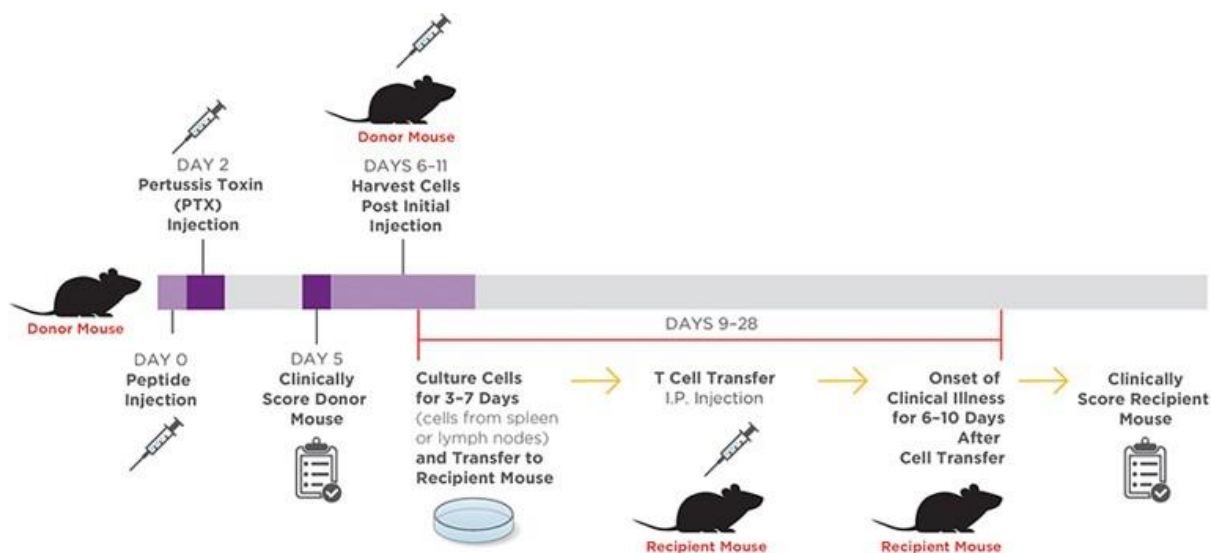


**Figure 7. Mouse model of adoptive transfer EAE** (Source: Taconic Biosciences, Inc).

In passive EAE (adoptively transferred), the disease is induced by injecting activated myelin antigen-specific CD4<sup>+</sup> T cells to develop EAE. The activated T cells are generated in donor animals from the same strain by active immunization with myelin protein or peptide emulsified in CFA. Then, generated activated T cells are transferred to recipient animals to develop a relapsing and remitting form of EAE (Racke 2001) (Figure 7).

**Table 2. Myelin peptides are used to induce EAE** (Racke 2001).

Peptide	Predominant mouse strains	Encephalitogenic sequence
MBP <sub>Ac1-11</sub>	PL/J, B10.PL	ASQKRPSQRSK
MBP <sub>89-101</sub>	SJL	FKNIVTPRTPPP
PLP <sub>139-151</sub>	SJL	HSLGKWLGHDPKF
MOG <sub>35-55</sub>	B6	MEVGWYRSPFSRVVHLYRNGK

### 1.3 Oligodendrocytes, myelin in MS and EAE

Oligodendrocytes are one of the glial cell types in the CNS and derive from oligodendrocyte precursor cells (OPCs). OPCs arise from ventricular zones of the brain and spinal cord and can proliferate, migrate, and differentiate into myelinating oligodendrocytes (Bergles and Richardson 2016). Oligodendrocytes produce myelin, a lipoprotein membrane that wraps around multiple segments of various nerve axons (up to 50), which enables proper nerve conduction and axonal integrity (Patel and Balabanov 2012). Myelin in the CNS plays a major

role in normal sensation, cognition, and motor function. The mammalian CNS contains 70% of its dry weight as myelin. The molecular composition of myelin is 70-75% of lipids and 25-30% of proteins. MBP, PLP, and their isoforms are the most abundant proteins in the compacted myelin (Jahn et al., 2009).

In MS, myelin-specific T cells initiate the series of an autoimmune response that leads to simultaneous destruction of myelin-producing oligodendrocytes and myelin followed by axonal damage. The infiltrating monocytes and microglia mediate myelin's destruction from the axonal segments. After myelin destruction during the early stages of MS, OPCs differentiate into remyelinating oligodendrocytes and restores myelin sheaths and axonal conduction. However, in chronic stages of the MS, remyelination process are ineffective because OPCs lose the differentiation capability into oligodendrocytes. The density of myelinating oligodendrocytes accounts for only 30% of MS lesions. The remaining 70% of the lesion areas contain a higher number of OPCs that were incapable of differentiating and producing myelin. (Domingues et al., 2016).


EAE closely mimics the disease process of human demyelinating disease (MS). The primary region of demyelination is the spinal cord; however, some degree of demyelination occurs in the optic nerve, cerebral cortex, and cerebellum (Palumbo and Pellegrini 2017). EAE induced with cuprizone and lyssolecithin lacks the immune response, infiltration of immune cells to the demyelinated areas, and the importance of immune cells in the demyelination. These models do not recapitulate any of the typical MS symptoms but are particularly useful for examining the remyelination mechanisms without continued demyelination (Kuhn et al., 2019). In contrast, MOG induced EAE is different from cuprizone-induced demyelination. Surprisingly, myelin damage and excessive formation of myelin, but not complete loss of myelin in the axons, are typical myelin abnormalities at inflammatory areas in MOG induced EAE (Bando 2015).

#### **1.4 Fibroblast growth factors (FGFs)**

Fibroblast growth factors (FGFs) are protein mitogens and regulate a wide variety of cellular process including proliferation, migration, differentiation, and survival. FGF signalling plays a vital role in tissue development, metabolism, and homeostasis (Xie et al. 2020). Mammals contain 22 FGF types, grouped into five paracrine subfamilies, one endocrine subfamily, and

one intracellular subfamily based on biochemical function, sequence homology, and phylogeny (Ornitz and Itoh 2015). Five paracrine subfamilies contain the FGF1 subfamily (FGF1, FGF2), FGF4 subfamily (FGF4, FGF5, FGF6), FGF7 subfamily (FGF3, FGF7, FGF10, FGF22), FGF8 subfamily (FGF8, FGF17, FGF18), and FGF9 subfamily (FGF9, FGF16, and FGF20). The endocrine subfamily of FGF is FGF19, FGF21, and FGF23 (Xie et al. 2020). The intracellular subfamily of FGF11 is FGF11, FGF12, FGF13, and FGF14. These intracellular FGFs are not secreted and no interaction with FGFRs.

Heparin/heparan sulfate (HS) proteoglycans (HSPGs) is a required cofactor for paracrine FGF signalling. HSPGs act as an extracellular buffer that preserves the FGF from degradation, and it plays a vital role in forming a complex between the FGF ligand and the FGFR. HSPGs restrict the movements of paracrine FGFs in the extracellular matrix from their secretion site. Each FGF ligand in the paracrine subfamily has a discrete affinity (moderate to high) to HSPGs. The endocrine FGF subfamily has a lower affinity to heparin/HS, and  $\alpha$ Klotho,  $\beta$ Klotho are the required cofactor for receptor binding (Ornitz and Itoh 2015; Laestander and Engstrom 2014) (Figure 8).

LIGANDS			RECEPTORS		
Scheme	Family	Members	FGFR	Isoforms	Scheme
	cFGFs	FGF4	FGF3	1, 2	IIIb
			FGF4	1, 2, 3, 4	IIIc
			FGF6	1, 2, 4	
		FGF5	FGF1	1, 2, 3, 4	IIIb, IIIc
			FGF2	1, 2, 3, 4	IIIc
			FGF5	1, 2	
		FGF8	FGF8	1, 2, 3, 4	IIIc
			FGF17	1, 2, 3, 4	
			FGF18	2, 3, 4	
		FGF9	FGF9	2, 3	IIIb, IIIc
	FGF16		2, 3	IIIc	
	FGF20		1, 2, 3, 4	IIIb, IIIc	
	FGF10	FGF7	2, 4	IIIb	
		FGF10	1, 2		
		FGF22	1, 2		
hFGFs	FGF15/19	FGF15/19	1, 2, 3, 4	IIIb, IIIc	
		FGF21	1, 2, 3, 4		
		FGF23	1, 2, 3, 4		
iFGFs	FGF11	FGF11			
		FGF12			
		FGF13			
		FGF14			

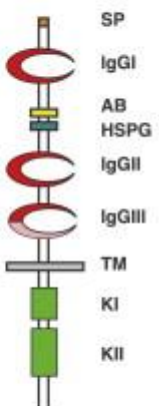


**Figure 8. Structure and FGF receptor specificity of the fibroblast growth factor family** (Guillemot and Zimmer 2011).

## 1.5 Fibroblast growth factor receptors (FGFR)

The fibroblast growth factor receptor (FGFR) family contains four members FGFR1-4 encoded by separate genes. These receptors share common structural features, a high percentage of sequence homology (56% to 71%), and consist of an extracellular ligand-binding domain, a transmembrane domain, and an intracellular tyrosine kinase catalytic domain (Dai et al., 2019). The extracellular portion consists of three immunoglobulin-like (IgI-IgIII) domains, a heparin-binding motif for FGFs, heparan cofactors, and partner proteins. The linker region between the IgI and IgII loop is called the acidic region due to its rich in aspartate acids. The second and third Ig-domains (IgII-IgIII) facilitate FGF ligand binding to the receptor (Astolfi et al., 2020), the IgIII domain of FGFR producing three isoforms (IgIIIa, IgIIIb, and IgIIIc). The IgIIIa isoform encoded by exon 7, IgIIIb and IgIIIc encoded by alternative splicing of exon 7/8 and exon 7/9. Commonly observed splice variants in FGFR1-3 are IgIIIb and IgIIIc (Tiong et al., 2013). The signal transduction from the extracellular domain into the cytoplasmic domain is mediated by the cell membrane bound transmembrane domain. The intracellular domain facilitates the FGFR tyrosine kinase activity. FGF ligand binding specificity of FGFRs is determined by IgIII domain isoforms (Figure 9).

## 1.6 Fibroblast growth factor/FGF receptor interaction

The FGF/FGFR signalling system is associated with the activation of multiple cellular functions such as proliferation, differentiation, survival, and motility (Tiong et al., 2013). The FGFs binding to inactive FGFRs will trigger the receptor dimerization, resulting in a conformational shift in receptor structure, which enables intracellular tyrosine kinase domain trans-autophosphorylation and initiating the onset of four key downstream signal transduction pathways such as RAS-RAF-MAPK, PI3K-AKT, signal transducer, and activator of transcription (STAT) and phospholipase C $\gamma$  (PLC $\gamma$ ). The adaptor proteins (FGFR substrate 2, SOS, and GRB2) docking to the activated FGFR, which resulted in the activation of the RAS/RAF/MAPK pathway mediate the regulation of cell proliferation. PI3K/AKT pathway is activated by docking of adaptor proteins GRB1 and GAB2 to activated FGFR, which is responsible for cell survival. FGFR activation stimulates other pathways such as the STAT pathway or PLC $\gamma$  (Astolfi et al., 2020) (Figure 9).

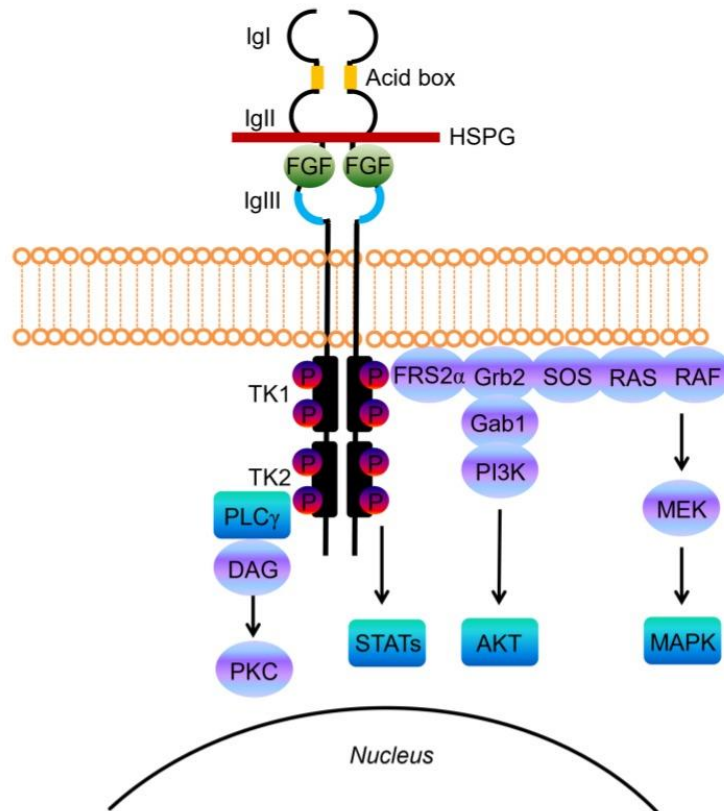


**Figure 9. Structure of fibroblast growth factor receptor (FGFR), FGF ligand binding, and FGF/FGFR signalling pathways (Astolfi et al., 2020).**

### 1.7 FGFR in oligodendrocyte lineage

The FGF receptor is differentially expressed in different stages of oligodendrocyte lineage progression. FGFR1 is expressed throughout oligodendrocyte development from OPCs to mature oligodendrocytes. FGFR2 is expressed in mature oligodendrocytes, and FGFR3 is expressed in the early and late progenitor stage. FGFR4 is not expressed at any stage of oligodendrocyte development. FGF2 upregulates OPCs proliferation via an increase of FGFR1 mRNA expression, and FGF2 mediates the downregulation of FGFR2 mRNA expression in mature oligodendrocytes (Bansal et al., 1996). FGF8 interaction with FGFR3 inhibits oligodendrocyte progenitor differentiation (Oh et al., 2003). FGF9 leads to growth of mature oligodendrocytes by activating FGFR2 (Nakamura et al., 1999).

## 1.8 FGF/FGFR in demyelinating disease MS and its animal model EAE

In MS, increased expression of the *FGF1* gene and the FGF1 protein in remyelinated lesions and that promotes both myelinations during development and remyelination. FGF1 is found in astrocytes, neurons, oligodendrocytes, microglia, and infiltrating lymphocytes. FGF1 inhibits the differentiation of OPCs into mature oligodendrocytes *in vitro* (Mohan et al., 2014). FGF2 levels are significantly increased in serum and cerebrospinal fluid of MS patients (Harirchian et al., 2011; Sarchielli et al., 2008). In cuprizone experimental demyelination *FGF2*<sup>-/-</sup> mice showed increased repopulation of oligodendrocyte in demyelinated lesions (Armstrong et al., 2002). In contrast, MOG<sub>35-55</sub>-induced EAE, *FGF2*<sup>-/-</sup> mice showed increased infiltration of CD8<sup>+</sup> cytotoxic T cells, macrophages/microglial cells, increased nerve fiber degeneration, and axonal loss (Rottlaender et al., 2011). Increased glial (astrocytes and oligodendrocytes) expression of FGF9 was observed in demyelinated lesions of MS patients and it inhibits remyelination.

In dissociated myelinating/cerebellar slice cultures revealed that FGF9 inhibits myelination/remyelination and induces the expression of pro-inflammatory chemokine genes such as *Ccl2* and *Ccl7* that are involved in recruitment of macrophages and microglia to the demyelinated lesions (Lindner et al., 2015). Increased expression of FGFR1 was found in OPCs within active lesions and surrounding chronic-active and chronic-inactive lesions of MS patients (Clemente et al., 2011). In a mouse model of cuprizone induced demyelination, oligodendrocytes specific deletion of *FGFR1* leads to increases of oligodendrocyte cell population in the lesion area and promotes remyelination following chronic demyelination (Zhou et al., 2011). *In vitro* activation of FGFR1 by FGF2 results in downregulation of myelin proteins in mature oligodendrocytes (Fortin et al., 2005). Expression of BDNF/TrkB and myelin proteins PLP and CNPase in OLN93 oligodendrocytes is increased by FGFR inhibition (Rajendran et al., 2021)

## 1.9 Functional role of FGFR1 and FGFR2 in MOG<sub>35-55</sub> induced EAE

Previously, our group described the role of oligodendroglial specific deletion of *FGFR1* (*Fgfr1*<sup>ind/-</sup> mice) in a mouse model of MOG<sub>35-55</sub>-induced EAE. Oligodendroglial specific deletion of *FGFR1* in B6.Cg-Tg(PLP1-cre/ERT)3-Pop *Fgfr1*<sup>tm5.1Sor</sup> mice is achieved by intraperitoneal injection of tamoxifen. The ablation of oligodendroglial *Fgfr1* in a mouse model

of MOG<sub>35-55</sub>-induced EAE showed a milder EAE disease course, reduced myelin loss, and increased axonal density in the lesion area (Figure 10 A). The inflammatory infiltrates in the white matter lesions such as CD3(+) T cells, B220(+) B cells, and Mac3(+) macrophages/microglia were decreased in *Fgfr1*<sup>ind/-</sup> mice. The underlying mechanisms for milder EAE disease course in *Fgfr1*<sup>ind/-</sup> mice includes reduced mRNA levels of pro-inflammatory cytokines (TNF $\alpha$ , IL1 $\beta$  and IL6), chemokine (CX3CL1 and CX3CR1), and remyelination inhibitor Lingo-1 in spinal cord tissues. Furthermore, higher phosphorylation of FGFR downstream signalling molecules ERK and Akt and increased expression of brain-derived neurotrophic factor (BDNF) and TrkB are found in *Fgfr1*<sup>ind/-</sup> mice spinal cord homogenates. Deletion of *FGFR1* does not change the oligodendrocyte lineage cell number in spinal cord white matter lesions (Rajendran et al., 2018).

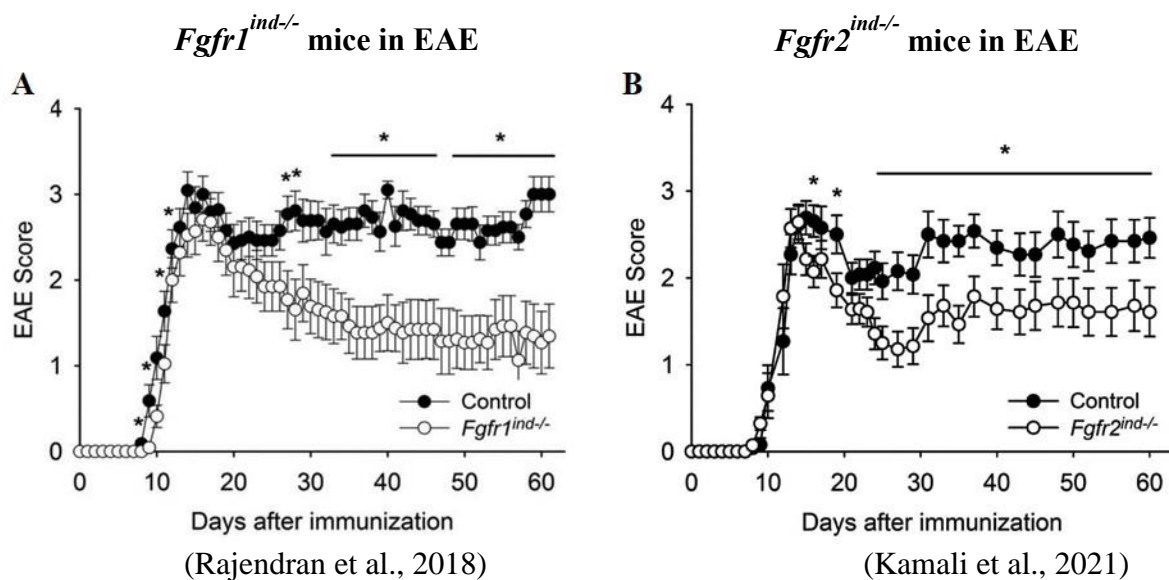


**Figure 10. Oligodendroglial specific deletion of *FGFR1* and *FGFR2* in a mouse model of MOG<sub>35-55</sub>-induced EAE.** (A) *Fgfr1*<sup>ind/-</sup> mice showed milder disease course from day 33 p.i. to till the end of the experiment (with exception of days 47 and 48) (Rajendran et al., 2018). (B) Less severity of the disease was observed in *Fgfr2*<sup>ind/-</sup> mice compared with controls from day 24 p.i. until the end of the experiment (Kamali et al., 2021).

Similarly, oligodendroglial specific deletion of *FGFR2* (*Fgfr2*<sup>ind/-</sup> mice) in MOG<sub>35-55</sub>-induced EAE showed less motor deficits, myelin and axonal degeneration (Figure 10 B). Moreover, less CD3(+) T cells, B220(+) B cells, and Mac3(+) macrophages/microglia infiltration were observed in white matter lesions of *Fgfr2*<sup>ind/-</sup> mice. *FGFR2* deletion in oligodendrocytes leads



to reduced protein expression levels of FGF2, FGF9, proinflammatory cytokines (TNF $\alpha$  and IL1 $\beta$ ), remyelination inhibitors (TGF $\beta$  and SEMA3A), and increased myelin protein PLP in spinal cord homogenates. Deletion of *FGFR2* regulates downstream signalling proteins, phosphorylation of ERK was decreased, and Akt was increased in *Fgfr2<sup>ind/-</sup>* mice (Kamali et al., 2021). Both studies, *Fgfr1<sup>ind/-</sup>* and *Fgfr2<sup>ind/-</sup>* mice in MOG<sub>35-55</sub>-induced EAE suggest that FGF/FGFR signalling plays an important role in inflammation and myelination in MS. FGFRs in oligodendrocyte is a potential therapeutic target in multiple sclerosis.

### 1.10 FGFR inhibitors in clinical trails

FGFR is a receptor tyrosine kinase (RTK) that plays significant roles in various physiological cellular processes, such as proliferation, differentiation, apoptosis, and migration. Recent preclinical studies indicate that aberrantly expressed FGFRs are connected with multiple cancer types and also noncancerous diseases. (Chae et al., 2017 and Lahiry et al., 2010). In animal model of MS, EAE induced with MOG<sub>35-55</sub> peptide in *Fgfr1<sup>ind/-</sup>* and *Fgfr2<sup>ind/-</sup>* mice showed less disease severity, myelin, and axonal degeneration (Rajendran et al., 2018 and Kamali et al., 2021). FGFR inhibitors are divided into three groups according to their binding behaviors, (i) receptor tyrosine kinase inhibitors (TKIs) are largely ATP-competitive, bind to the FGFR cytoplasmic kinase domain and inhibit the catalytic activity, (ii) antagonistic antibody or peptide inhibitors are competitive with FGFs, bind to the FGFR extracellular domain and blocking the FGF/FGFR complex and FGFR dimerization; (iii) FGF ligand traps are able to bind multiple FGF ligands and receptors preventing FGF/FGFR interaction (Chae et al., 2017). The early development of FGFR tyrosine kinase inhibitors (anlotinib, ponatinib, dovitinib, lucitanib, lenvatinib and nintedanib) inhibit multiple targets, including FGFRs and vascular endothelial growth factor receptors, KIT, RET, among others. It led to the lack of a profound FGFR inhibition and occurrence of harmful side effects. The current development of FGFR inhibitors is selectively inhibiting FGFR phosphorylation with nanomolar concentrations (Facchinetti et al., 2020). Selective FGFR inhibitors are less toxic than multikinase inhibitors (Ahnert et al., 2019). FGFR inhibitors are emerging targeted therapies that have demonstrated promising results in harboring *FGFR* aberrations (Kommalapati et al., 2021). At least 89 studies are actively recruiting patients to investigate the efficacy of FGFR inhibitors in several cancer types (clinicaltrials.gov).

The United States Food and Drug Administration granted accelerated approval to few selective FGFR inhibitors such as erdafitinib (Janssen Pharmaceuticals) to treat metastatic urothelial carcinoma harboring *FGFR2/3* alterations; infigratinib (QED Therapeutics), futibatinib (Taiho Oncology, Inc.) and pemigatinib (Incyte Corporation) to treat unresectable locally advanced or metastatic cholangiocarcinoma harboring *FGFR2* gene rearrangements, including gene fusions (<https://www.fda.gov>). The selective FGFR inhibitors that are in clinical trials are summarized in Table 3.

**Table 3. Selective FGFR inhibitors in clinical development** (Facchinetti et al., 2020).

Drug	Company	Targets	Inhibition type	Dose adopted in ongoing trials	Phase of ongoing trials
Erdafitinib (JNJ-42756493)	Janssen-Johnson & Johnson	FGFR1-4	Reversible	8 mg daily	III
Infigratinib (BGJ398)	BridgeBio/QED Therapeutics	FGFR1-3	Reversible	125 mg daily 3w on / 1w off	III
Pemigatinib (INCB054828)	Incyte Corp	FGFR1-3	Reversible	13.5 mg daily	III
Rogaratinib (BAY1163877)	Bayer	FGFR1-3	Reversible	800 mg twice daily	III
TAS-120	Taiho Oncology	FGFR1-4	Covalent	20 mg daily	II
Derazantinib (ARQ 087)	Basilea Pharmaceutica	FGFR1-4	Reversible	300 mg daily	II
LY2874455	Eli Lilly	FGFR1-4	Reversible	16 mg twice daily	I
AZD4547	AstraZeneca	FGFR1-3	Reversible	80 mg twice daily	II
Debio 1347 (CH5183284)	Debiopharm Group	FGFR1-3	Reversible	80 mg daily	II
BLU-554	Blueprint Medicines	FGFR4	Irreversible	600 mg daily	I extension

### 1.11 Selective FGFR inhibitor infigratinib

Infigratinib is an orally bioavailable, ATP-competitive, reversible inhibitor of the FGFR family of tyrosine kinase receptors. It selectively binds to FGF receptors and inhibits the FGFR1-3 activities with high potency but 38-fold lower potency for FGFR4 and 100-fold lower potency for other tyrosine kinases (Botrus et al., 2021). Infigratinib competitively and non-covalently interacts with the ATP binding pocket of the cytoplasmic tyrosine kinase domain and inhibits the activation of FGFR. The concentration of infigratinib required for half maximal inhibition range from 0.9 to 1.4 nM for FGFR1-3 to 60 nM for FGFR4 (Dai et al., 2019). Infigratinib is an investigational drug, currently undergoing several preclinical studies and phase I to phase III clinical trials of various human cancers, mostly solid tumours (clinicaltrials.gov and Wohrle et al., 2012). Daily treatment in an orthotopic xenograft bladder cancer mouse model with 10 and 30 mg/kg infigratinib for 12 days led to a reduction in tumour growth without losing bodyweight. Mice treated with 30 mg/kg infigratinib showed 10% body weight gain (Guagnano et al., 2011). Many phase I clinical trials have been conducted to evaluate the tolerance and safety of infigratinib in patients with multiple types of advanced solid tumors. In a large study, 132 patients were enrolled who had solid tumors with FGFR alterations. Infigratinib has a tolerable safety profile, with most patients (95.5%) experiencing at least one adverse event. The most common adverse events across all doses were hyperphosphatemia (74.2%), constipation (40.2%), and anorexia (40.2%) and less commonly fatigue, alopecia, and nausea (Botrus et al., 2021). These adverse effects of infigratinib were reversible (Chae et al., 2017).

Infigratinib exhibited a high plasma clearance and a large volume of distribution at a steady state. *In vitro* hepatic systems metabolize infigratinib predominantly to 2 pharmacologically active metabolites BHS697 (desethyl metabolite) and BQR917 (N-oxide). Biotransformation of infigratinib to both metabolites was seen in human hepatocyte cultures. *In vivo* safety pharmacology studies in rats and dogs did not show any effects on the central nervous system or respiratory system and on hemodynamic or electrocardiographic parameters, respectively (Seiwert 2018 and clinicaltrials.gov).

Infigratinib is also used in the animal model of noncancerous disease. In a mouse model of X-linked hypophosphatemia, long-term treatment with oral infigratinib (50 mg/kg) led to complete recovery from hypophosphatemia and hypocalcemia caused by malfunction of the FGF23/FGFR complex (Wohrle et al., 2012). The subcutaneous dosage of infigratinib (2 mg/kg) ameliorated achondroplasia (ACH) caused by a gain-of-function mutation in the *FGFR3* gene in a mouse model of achondroplasia (Komla-Ebri et al., 2016). Currently, infigratinib is in phase I and II clinical studies of children with achondroplasia (QED Therapeutics). U.S. FDA granted accelerated approval to infigratinib to treat metastatic cholangiocarcinoma harboring FGFR2 fusion.

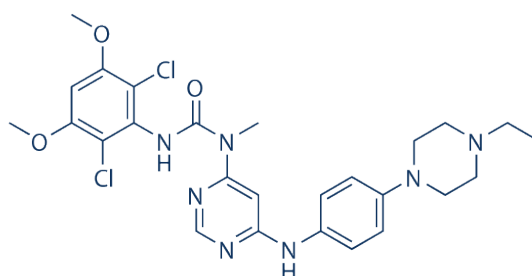


**Figure 11. Chemical structure of the FGFR inhibitor infigratinib. IUPAC Name:** 3-(2,6-dichloro-3,5-dimethoxyphenyl)-1-[6-[4-(4-ethylpiperazin-1-yl)anilino]pyrimidin-4-yl]-1-methylurea, **Molecular Formula:** C<sub>26</sub>H<sub>31</sub>Cl<sub>2</sub>N<sub>7</sub>O<sub>3</sub>, **Molecular weight:** 560.48 g/mol, **Other names:** BGJ398 and NVP-BGJ398. (Source: Selleck Chemicals)

## 2 AIMS

Our recent studies revealed that cell-specific deletion of oligodendroglial *FGFR1* and *FGFR2* exhibited a less severe disease course and reduced inflammation, myelin and axonal degeneration in MOG<sub>35-55</sub>-induced EAE. Further, expression of the myelination inhibitor Lingo-1 was decreased and expression of the neurotrophin BDNF and its receptor TrkB, myelin protein PLP was increased in *Fgfr1<sup>ind/-</sup>* and *Fgfr2<sup>ind/-</sup>* mice with EAE (Rajendran, R. et al., 2018 and Kamali, S. et al., 2021). We hypothesize here that prevention and suppression of EAE can be achieved with selective tyrosine kinase tyrosine inhibitors. Therefore, the aim of the present study is to decipher the impact of FGFR inhibitors on the prevention of relapses and suppression of symptoms using the EAE mouse model.

**Objective 1:** To characterize the efficacy of the FGFR inhibitor infigratinib on prevention and suppression of MOG<sub>35-55</sub>-induced EAE. Therefore, C57BL/6J mice will be treated with FGFR inhibitor either on days 0 - 9 or 10 - 19 p.i. and the disease course will be assessed till day 41-42 p.i.

**Objective 2:** To study the effect of the FGFR inhibitor infigratinib on myelin, axonal degeneration, and inflammation in MOG<sub>35-55</sub>-induced EAE. Hence, spinal cord tissue from C57BL/6J mice will be analyzed in the acute (day 18-20 p.i.) and chronic phases (day 41-42 p.i.) of EAE for morphological and structural alterations associated with disability.

**Objective 3:** To investigate the effect of the FGFR inhibitor infigratinib on the FGF/FGFR signalling pathways *in vivo* (EAE model) and *in vitro* (oligodendrocyte cell line).

### 3 MATERIALS AND METHODS

#### 3.1 MATERIALS

##### 3.1.1 Animals

###### 3.1.1.1 Mice provider and mice diet

**Mice line:** C57BL/6J

**Supplier:** Charles River (Charles River Laboratories, Sulzfeld, Germany)

**Animal facility:** JLU, Biomedical Research Center Seltersberg, Schubertstrasse 81, Giessen, Germany.

**Mice Diet:** Standard diet pellet (Art. Nr. 1324, Altromin Spezialfutter GmbH & Co. KG, Lage, Germany) DietGel Boost<sup>®</sup> (ClearH2O<sup>®</sup> Westbrook, Portland, USA), HydroGel<sup>®</sup> (ClearH2O<sup>®</sup> Westbrook, Portland, USA).

##### 3.1.2 Cell lines

Oligodendroglial cell line OLN93 derived from spontaneously transformed cells in primary rat brain glial cultures, kindly provided by Prof. Markus Kipp (University of Rostock, Germany).

##### 3.1.3 Kits

Kits	Manufacturer	Article. No	Method
BCA Protein Assay Kit	Pierce <sup>®</sup> Thermo Scientific, IL, USA	23225	Protein quantification
iTaq <sup>™</sup> Universal SYBR <sup>®</sup> Green Suppermix	Bio-Rad, CA, USA	1725124	Polymerase Chain Reaction (PCR)
peqGOLD Total RNA Kit	Peqlab Biotechnologie GmbH, Erlangen, Germany	12-6834-02	RNA isolation
QuantiTect <sup>®</sup> Reverse Transcription Kit	Qiagen GmbH, Hilden, Germany	205313	Reverse Transcription
Restore <sup>™</sup> Plus Western blot stripping buffer	Thermo Scientific, IL, USA	46430	Western Blot
SuperSignal <sup>®</sup> West Pico Chemiluminescent substrate	Thermo Scientific, IL, USA	34077	Western Blot

## 3.1.4 Primary Antibodies

Name	Host	Reactivity	Mol. Weight	Method	Art. No	Manufacturer
Anti-FGF2 (G2)	Mouse	H, M, R	18, 21, 24 kDa	WB	sc-365106	Santa Cruz Biotech, CA, USA
Anti-FGF9 (D8)	Mouse	H, M, R	30 kDa	WB	sc-8413	Santa Cruz Biotech, CA, USA
Anti-CNPase (B1)	Mouse	H, M, R	46 kDa	WB	sc-166019	Santa Cruz Biotech, CA, USA
Anti-MBP	Mouse	H, M, R, G	12,18 kDa	WB	78896S	Cell Signaling Tech, MA, USA
Anti-PLP	Rabbit	H, M, R	30 kDa	WB	85971	Cell Signaling Tech, MA, USA
Anti-pERK p-44/42	Rabbit	H, M, R, Hm, Mk	44, 42 kDa	WB	4370s	Cell Signaling Tech, MA, USA
Anti-pAkt (Ser473)	Rabbit	H, M, R, MK	60 kDa	WB	4060s	Cell Signaling Tech, MA, USA
Anti-Flg (M2F12) (FGFR1)	Rabbit	H, M, R	110 kDa	WB	sc-57132	Santa Cruz Biotech, CA, USA
Anti-Bek (C-8) (FGFR2)	Rabbit	H, M, R	120 kDa	WB	sc-6930	Santa Cruz Biotech, CA, USA
Anti-GAPDH	Mouse	H, M, R	37 kDa	WB	sc-365062	Santa Cruz Biotech, CA, USA
Anti-TrkB (794):sc12	Rabbit	H, M, R	145 kDa	WB	sc-377218	Santa Cruz Biotech, CA, USA
Anti-pro BDNF	Rabbit	H, M, R	14 kD	WB	sc-65514	Santa Cruz Biotech, CA, USA
MBP	Rabbit	M, R	staining	IHC	62301	Dako, Germany
Olig2	Mouse	H, M, R	staining	IHC	MABN50	MerckMillipore, Germany
P25	Rabbit	H, M, R	staining	IHC	ab 92305	Abcam, Cambridge, UK
NeuN	Rabbit	H, M, R	staining	IHC	ab177487	Abcam, Cambridge, UK

### 3.1.5 Secondary Antibodies

Antibody	Host	Art. No	Manufacturer
Anti-Rabbit-HRP	Goat	7074S	Cell Signaling Tech, MA, USA
Anti-Mouse-HRP	Horse	7076S	Cell Signaling Tech, MA, USA

### 3.1.6 Ladders

Marker	Manufacturer
PageRuler™ Prestained Protein Ladder	Thermo Scientific, IL, USA

### 3.1.7 Primers

Primer	5' → 3' Sequence
TNF $\alpha$	Forward CGGTCCCCAAAGGGATGAGAAGT
	Reverse ACGACGTGGGCTACAGGCTT
IL1 $\beta$	Forward TACCTGTGGCCTTGGGCCTCAA
	Reverse GCTTGGGATCCACACTCTCCAGCT
IL6	Forward CTCTGCAAGAGACTTCCA
	Reverse AGTCTCCTCTCCGGACTT
IL12	Forward AGACCACAGATGACATGGTGA
	Reverse ACGACGTGGGCTACAGGCTT
iNOS	Forward TTGGAGGCCTTGTGTCAGCCCT
	Reverse AAGGCAGCGGGCACATGCAA
GAPDH	Forward GGATGGGTCCTCATGCTCAC
	Reverse TGGTGCTGCAAGTCAGAGCAG
TGF $\beta$	Forward CTCCTGCTGCTTTCTCCCTC
	Reverse GTGGGGTCTCCCAAGGAAAG
SEMA3A	Forward GGATGGGTCCTCATGCTCAC
	Reverse TGGTGCTGCAAGTCAGAGCAG
Lingo-1	Forward TCATCAGGTGAGCGAGAGGA
	Reverse CAGTACCAGCAGGAGGATGG
CX3CR1	Forward CTGCTCAGGACCTCACCATGT
	Reverse ATGTCGCCCAAATAACAGGC
CX3CL1	Forward GCGACAAGATGACCTCACGA
	Reverse TGTCGTCTCCAGGACAATGG



## 3.1.8 Chemicals and Solutions

Compound	Company
10x PBS (DPBS)	Lonza, Köln, Germany
2-Mercaptoethanol	Sigma-Aldrich, Steinheim, Germany
3% Hydrogen peroxide	Carl Roth, Karlsruhe, Germany
Ammonium Persulphate (APS)	Carl Roth, Karlsruhe, Germany
bFGF	R&D Systems, MN, USA
Bromophenol Blue	Neolab, Heidelberg, Germany
Bovine Serum Albumin (BSA)	Capricorn Scientific GmbH, Ebsdorfergrund, Germany
complete Freund´s adjuvant	Sigma-Aldrich, Steinheim, Germany
Dimethylsulfoxide (DMSO)	Carl Roth, Karlsruhe, Germany
DMEM medium	Life Technologies Limited, Renfrew, UK
DNase	Qiagen, Hilden, Germany
EDTA	Carl Roth, Karlsruhe, Germany
Eosin	Merck, Darmstadt, Germany
Ethanol 100%	Sigma-Aldrich, Steinheim, Germany
FBS	PAA Laboratories, Pasching, Austria
Glucose	Carl Roth, Karlsruhe, Germany
Glutaraldehyde	Carl Roth, Karlsruhe, Germany
Glycerol	Carl Roth, Karlsruhe, Germany
Hematoxylin	Carl Roth, Karlsruhe, Germany
Hydrochloric acid 37%	Sigma-Aldrich, Steinheim, Germany
Infigratinib (BGJ398)	Selleckchem, Houston, TX, USA
Isoflurane 100%	Ecuphar, Greifswald, Germany
Ketamin 10%	bela-pharm GmbH, Vechta, Germany
Luxol-Fast-Blue	Sigma-Aldrich, Steinheim, Germany
Methanol	Sigma-Aldrich, Steinheim, Germany
MOG <sub>35-55</sub> peptide	Charité Berlin, Berlin, Germany
<i>Mycobacterium tuberculosis</i>	Difco Laboratories, Michigan, USA
Non-fat dry milk powder	Cell Signaling Technology, Inc. MA, USA

NP40	US Biologicals, MA, USA
Paraformaldehyde (PFA)	Sigma-Aldrich, Steinheim, Germany
Penicillin/streptomycin	Life Technologies Limited, Renfrew, UK
Pertussis Toxin	Merck KGaA, Darmstadt, Germany
Potassium chloride (KCL)	Carl Roth, Karlsruhe, Germany
Protease Inhibitor cocktail	Roche, Mannheim, Germany
Phosphatase Inhibitor Cocktail 2	Sigma-Aldrich, Steinheim, Germany
RNAse free water	Millipore corporation, MA, USA
Rotiphorese Gel (30% acrylamide mix)	Carl Roth, Karlsruhe, Germany
Rotiphorese 10X SDS-PAGE	Carl Roth, Karlsruhe, Germany
Roti fair HBS	Carl Roth, Karlsruhe, Germany
Sodiumdodecylsulfate (SDS)	Carl Roth, Karlsruhe, Germany
Sodium azid (NaN <sub>3</sub> )	Merck KGaA, Darmstadt, Germany
Sodium carboxymethyl cellulose	Sigma-Aldrich, St. Louis, Missouri, USA
Sodium chloride (NaCl)	Carl Roth, Karlsruhe, Germany
Sodium hydroxide (NaOH)	Merck KGaA, Darmstadt, Germany
TEMED	Carl Roth, Karlsruhe, Germany
Trishdroxymethyl aminomethan (Tris)	Carl Roth, Karlsruhe, Germany
Tris HCl	Carl Roth, Karlsruhe, Germany
Trypsin (2.5g/l)	Gibco, Invitrogen, Carlsbad, USA
Tween 20	Merck KGaA, Darmstadt, Germany
Xylazin 2%	CP-Pharma GmbH, Burgdorf, Germany

### 3.1.9 Laboratory consumables

Consumables	Manufacturer
Cellstar® 6 Well and 24 well Cell Culture Plate	GreinerBioOne, Frickenhausen, Germany
Cellstar® 75 cm <sup>2</sup> Cell cultur flasks	GreinerBioOne, Frickenhausen, Germany
Cell culture dish 60 x 15 mm	Sarstedt AG & Co, Nümbrecht, Germany
Cell scrapper	GreinerBioOne, Frickenhausen, Germany

Cryobox 136x136x50 mm	Ratiolab GmbH, Dreieich, Germany
CRYO.S cryo vials (2 ml)	GreinerBioOne, Frickenhausen, Germany
Eppendorf tubes 1,5 ml, 2 ml	Sarstedt AG & Co, Nümbrecht, Germany
Eppendorf tubes 1,5 ml, 2 ml (PCR clean-pyrogen & DNase free)	Nerbe Plus GmbH, Winsen (Luhe), Germany
Extra thick blot paper 19x18.5 cm	BioRad, München, Germany
Falcon tubes (15 ml, 50 ml)	GreinerBioOne, Frickenhausen, Germany
Glasswares (different sorts)	Fisherbrand; IDL; Schott&Gen; Simax
Glass Pasteur pipettes 150 mm	Brand, Wertheim, Germany
Ministart single use filter (0.2 µm)	Sartorius Stedim Biotech GmbH, Göttingen, Germany
Nitrocellulose membrane	GE Healthcare, Amersham™ Hybond ECL, Buckinghamshire, UK
Parafilm	Pechiney Plastic packaging, Menasha, WI
PCR Tube, cap-strips	Applied Biosystems, Darmstadt, Germany
Plastic feeding tubes, 22ga (black) x 25mm, sterile	Instech Laboratories, Inc. Pennsylvania, USA
Plastic pipettes (5 ml, 10 ml)	GreinerBioOne, Frickenhausen, Germany
Pipette tips without filter (10 µl, 100 µl, 1000 µl)	Sarstedt AG & Co, Nümbrecht, Germany
Sterile disposable cannula 26G	B. Braun Melsungen AG, Germany
Sterile PCR- clean pyrogen & DNase free tip with filter (10, 100, 200, 1000 µl)	Nerbe Plus GmbH, Winsen (Luhe), Germany
Syringe (1 ml, 25 ml)	B. Braun Melsungen AG, Germany
Vasco® Nitril powder free glove	B. Braun Melsungen AG, Germany

### 3.1.10 Laboratory instruments

<b>Instrument</b>	<b>Manufacturer</b>
Arpege 75, Liquid nitrogen tank	Air Liquide Medical GmbH, Düsseldorf, Germany
Axio Scan Z1 Microscope	Carl Zeiss Microscopy GmbH, Oberkochen, Germany
Centrifuge Universal 320 R (cooling)	Hettich GmbH, Kirchlengen, Germany
ECL ChemoCam Imager	INTAS Science Imaging Instruments GmbH, Göttingen, Germany
ELISA-Reader Multiscan EX	Thermo electron, Langenselbold, Germany
Magnetic stirrer	IKA® Werke GmbH, Staufen, Germany
Nanophotometer	Implen GmbH, München, Germany
Nikon Eclipse Ti-U microscope	Nikon GmbH, Düsseldorf, Germany
Peristaltic pump	Carl Roth, Karlsruhe, Germany
pH-Meter	Hanna Instruments, Vöhringen, Germany
Pipette boy	INTEGRA Biosciences, Fernwald, Germany
Power pack	Peqlab Biotechnologie, Erlangen, Germany
Refrigerators and freezers	Different companies
Roller RM5 Assistant 348	Karl Hechst GmbH, Sondheim, Germany
StepOne® Real-Time PCR system	Applied Biosystems, Darmstadt, Germany
Surgical instruments	Various companies
Table top centrifuge micro 120	Hettich GmbH, Kirchlengen, Germany
Thermomixer comfort	Eppendorf AG, Hamburg, Germany
TissueRuptor	Qiagen Instruments, Hombrechtikon, Switzerland
Trans-Blot® SD Semi-dry transfer cell	BioRad, München, Germany
Vortexer vortex-Genie2	Heidolph Instruments, Schwabach, Germany
Weighing balance	Sartorius Stedim Biotech GmbH, Göttingen, Germany
Western blotting system	BioRad, München, Germany

## 3.1.11 Buffers

Buffer	Components	Volume
1X SDS-PAGE Running Buffer	Rotiphorese® 10X SDS-PAGE Running Buffer	100 ml
	H <sub>2</sub> O	900 ml
10x PBS (1 Liter) pH 7.4	137 mM NaCl	80 g
	2 mM KH <sub>2</sub> PO <sub>4</sub>	2.4 g
	2.7 mM KCl	2 g
	10 mM Na <sub>2</sub> HPO <sub>4</sub>	14.4 g
	H <sub>2</sub> O	1000 ml
10x TBS (1 Liter) pH 7.2 to 7.6	Tris	24.2 g
	NaCl	87.7 g
	H <sub>2</sub> O	1000 ml
1x TBS-Tween (TBST) (1 Liter)	1x TBS	1000 ml
	0.1% Tween®20	1 ml
Lysis Buffer (250 ml) pH 7.4	NaCl	2.19 g
	Tris	0.61 g
	EDTA	0.07 g
	Glycerol	25 ml
	NP40	2.5 ml
	NaN <sub>3</sub>	0.025 g
6x SDS-PAGE Loading Buffer	60 mM Tris-HCl (pH 6.8)	36 ml
	2% SDS	60 ml
	0.01% Bromophenol blue	60 mg
	10% Glycerol	60 ml
	ddH <sub>2</sub> O	144 ml
	β-Mercaptoethanol	65 µl/ml
SDS-PAGE Transfer buffer (1 Liter)	10x Running buffer	100 ml
	Methanol	200 ml
	ddH <sub>2</sub> O	700 ml
Blocking buffer (5% BSA) Bovine Serum Albumin	BSA	5 g
	TBST	100 ml
10% Ammonium Persulfate (APS)	APS	1 g
	ddH <sub>2</sub> O	10 ml
10% Sodiumdodecylsulfate (SDS)	SDS	1 g
	ddH <sub>2</sub> O	10 ml
5% non-fat milk	Non-fat milk powder	5g
	TBST	100 ml

### **3.1.12 Software**

1. ZEN 3.2 (blue edition) software (Carl Zeiss Microscopy GmbH, Oberkochen, Germany).
2. Microsoft Office Professional Plus 2016 (Microsoft corporation, Washington, USA).
3. Image J software (Image J 1.53b, National Institute of Health, Maryland, USA).
4. StepOne Real Time PCR Software v2.1 (Applied Biosystems, Darmstadt, Germany).
5. Primer Blast online tool (<https://www.ncbi.nlm.nih.gov/tools/primer-blast/>, National Center for Biotechnology Information, Maryland USA).
6. GraphPad Prism Software Version 9 (GraphPad Software, Inc. CA, USA).

## 3.2 METHODS

### 3.2.1 Animal experiment procedures

#### 3.2.1.1 Ethics Statement

All scientific procedures on animals were approved by the regional council of Hesse, Giessen, Germany (Regierungspraesidium Giessen, reference number: GI 20/18-Nr. G38/2018) in accordance with the German animal welfare law and the European legislation for the protection of animals used for scientific purposes (2010/63/EU). All animal experiments were performed in accordance with the German animal welfare law and had been declared to the Animal Welfare Officer of Justus Liebig University (Registration No.: 891\_GP). The animal housing facility was licensed by the local authorities (Az: IV44-53r 30.03 UGI118.11.03). The methods used to euthanize the animals humanely were consistent with the recommendations of the AVMA Guidelines for the Euthanasia of Animals.

#### 3.2.1.2 Mice

Seven-week-old wild-type female C57BL/6J mice were purchased from Charles River (Charles River Laboratories, Sulzfeld, Germany). Mice were maintained in temperature, and light-controlled environment at the JLU animal facility, Schubert Strasse 81, 35392 Giessen, for a week to acclimatize themselves and were eight weeks old at the time of the experiment. Mice were free to access standard diet pellet (Altromin Spezialfultur GmbH, Lage, Germany) and autoclaved water *ad libitum*. The paralysed mice were housed in a cage with cellulose bedding and diet enrichment, including diet gel boost (ClearH2O<sup>®</sup> Westbrook, Portland, USA), wet food, and hydrogel (ClearH2O<sup>®</sup> Westbrook, Portland, USA).

#### 3.2.1.3 Induction of MOG<sub>35-55</sub>-induced EAE

Eight-week-old female C57BL/6J were immunized under inhalant anaesthetic isoflurane. The immunization induced by subcutaneous injections of 300 µg of myelin oligodendrocyte glycoprotein peptide (MOG<sub>35-55</sub> peptide; MEVGWYRSPFSRVVHLYRNGK, Institute for Medical Immunology, Charité University Hospital, Berlin, Germany) emulsified in complete

Freund's adjuvant (Sigma, Steinheim, Germany) containing 10 mg/ml heat inactivated *Mycobacterium tuberculosis* (Difco, Michigan, USA) in four ventral flanks. Mice have received an intraperitoneal injection of 100 µl PBS containing 300 ng *Bordetella pertussis* toxin (Merck KGaA, Darmstadt, Germany) twice at 0 and 48 hours post-immunization to facilitate the activated immune cells to cross the BBB and reach CNS. Mice were weighed and the neurological disability assessed after blinding for treatment groups until the end of the experiment. These mice were scored as 0 = normal, 0.5 = distal tail weakness, 1 = complete tail weakness, 1.5 = mild hind limb weakness, 2 = ascending hind limb weakness, 2.5 = severe hind limb weakness, 3 = hind limb paralysis, 3.5 = hind limb paralysis and forelimb weakness, 4 = tetraparesis, 4.5 = tetraplegia and incontinence, to 5 = moribund/death. The sample size was predefined as at least n = 8 in a minimum of three independent experiments.

#### **3.2.1.4 Selective FGFR inhibitor infigratinib treatment**

To investigate the effect of the selective FGFR inhibitor infigratinib, EAE was induced as described in the previous paragraph (3.2.1.3). FGFR inhibitor infigratinib (Selleckchem, Houston, TX, USA) was dissolved in 1% sodium carboxymethyl cellulose (Sigma-Aldrich, St. Louis, Missouri, USA) according to the manufacturer's recommendation. Mice received 100 µl infigratinib (30 mg/kg of body weight) orally using a plastic feeding tube (FTP-22-25; Linton Instrumentation, Palgrave, UK). Furthermore, placebo mice received 100 µl vehicle (1% sodium carboxymethyl cellulose) from day 0 till day 9 p.i. or from day 10 till day 19 post-immunization with MOG<sub>35-55</sub>-peptide. The study dose of 30 mg/kg of infigratinib was chosen based on recent pharmacokinetics/pharmacodynamics (PK/PD) studies that indicated 30 mg/kg of oral infigratinib efficiently inhibited the FGFR in a mouse model (Guagnano et al. 2011). Mice were sacrificed (prevention; acute phase day 17 p.i., chronic phase day 41 p.i.: suppression; acute phase day 20 p.i., chronic phase day 42 p.i.), and spinal cord tissue was collected for further analysis (Figure 12).



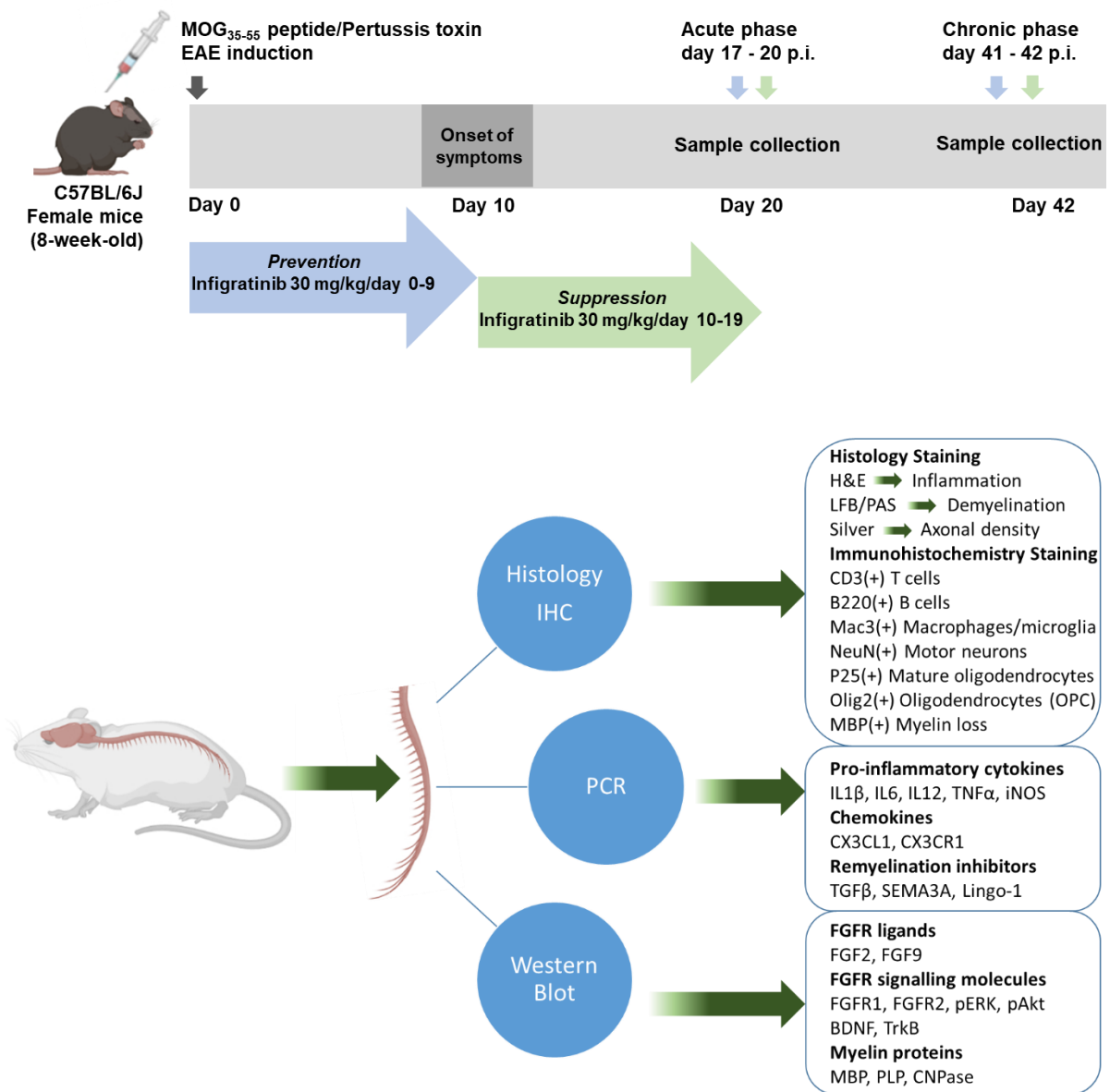


**Figure 12. Experimental design illustrating the timeline of EAE induction, infigratinib treatment, clinical scoring and tissue analysis till acute and chronic phase of EAE.**

### **3.2.2 Molecular biology methods**

#### **3.2.2.1 RNA isolation**

Spinal cord tissues of placebo and infingratinib treated mice were dissected after mice were euthanized with CO<sub>2</sub> at the respective time point of the acute and chronic phase of EAE (Figure 12). Total RNA was isolated from the frozen spinal cord tissue using the peqlab Total RNA kit (Peqlab Biotechnologie GmbH, Erlangen, Germany) according to manufacturer instructions. Depending on each spinal cord tissue's weight, the volume of RNA lysis buffer T was added, and tissues were homogenized with a tissue ruptor (Qiagen Instruments, Hombrechtikon, Switzerland). The tissue lysates were transferred to DNA removing columns in a collection tube and centrifuged at 14000 rpm for 1 min at room temperature. The lysates were mixed with equal volumes of 70% ethanol, vortexed, and then added to PerfectBind RNA columns followed by 14000 rpm for 1 min centrifugation. PerfectBind RNA columns were washed with Wash buffer I and Wash buffer II then total RNA was eluted with 60 µl RNase free water. The total RNA concentration was determined using the IMPLEN Nanophotometer® (Implen GmbH, München, Germany).

#### **3.2.2.2 Reverse transcription and cDNA synthesis**

cDNA was synthesized using the QuantiTect® Reverse Transcription Kit (Qiagen GmbH, Hilden, Germany). The prepared reaction mixture consists of 20 µl of diluted 1 µg/ml of total RNA and 3 µl genomic DNA wipeout buffer and then reaction mixtures were incubated at 42°C for 2 minutes. Then 4 µl 5x RT buffer, 1 µl RT Primer, 1 µl RT master mix are added to the reaction mixture and then incubated at 42 °C for 30 minutes and at 95 °C for 3 minutes. The synthesized cDNA was used for RT-PCR.

#### **3.2.2.3 Relative real time-PCR quantification**

Relative mRNA expression of specific genes in the spinal cord of placebo and infingratinib treated mice were measured by quantitative PCR. The gene expression was determined by 40 cycles at an annealing temperature of 60 °C in the StepOne® Real-Time PCR system (Applied Biosystems, Germany) using iTaq™ Universal SYBR® Green qPCR Master Mix (Bio-Rad,

CA, USA). Primers were designed by the NCBI nucleotide Primer designing tool and primers were purchased at Eurofins-Genomics (Eurofins MWG Synthesis GmbH, Ebersberg, Germany) (Table 3.1.7). The PCR was carried out using a composition of 10 µl Mastermix (iTaq™ Universal SYBR® Green), 1 µl forward primer, 1 µl reverse primer, 7 µl H<sub>2</sub>O, and 1 µl of cDNA. Relative mRNA expression was evaluated using the comparative  $\Delta\Delta CT$  method ( $\Delta CT = \text{target gene} - \text{housekeeping gene}$ ;  $\Delta\Delta CT = 2^{-\Delta CT}$ ) and GAPDH was used as the housekeeping gene.

### **3.2.3 Protein biochemistry**

#### **3.2.3.1 Protein extraction and quantification**

Spinal cord tissues were dissected after mice were euthanized with CO<sub>2</sub>. The spinal cord tissues were homogenized with ice cold cell lysis buffer (150 mM NaCl, 10% glycerol, 20 mM Tris HCl, 1% NP40, 1 mM EDTA, 0.01% sodium azide) using a tissue ruptor (Qiagen Instruments, Hombrechtikon, Switzerland). The spinal cord homogenate was centrifuged at 14,000 rpm for 30 minutes at 4 °C and then the supernatant was collected and transferred to a new microtube. According to manufacturer instructions, total protein concentration in the supernatant was measured by BCA assay (Pierce® BCA Protein Assay Kit, Thermo Scientific, IL, USA). Briefly, the protein was diluted with lysis buffer as 1:10 ratio and 10 µl protein was taken in triplicates in a 96 well flat bottom ELISA plate. Then 200 µl of reaction reagent (Pierce) was added to each well and incubated for 30 min at 37 °C. The protein and reaction reagent was mixed by shaking and the absorbance at 540 nm were measured using an ELISA reader (Thermo electron corporation, Langensfeld, Germany). The final protein concentration was adjusted to 1 µg/µl with cold lysis buffer and stored at -20 °C for further use.

#### **3.2.3.2 SDS-PAGE and western blot**

The 6x protein loading buffer was added to the normalized protein lysate 30 µl (1 µg/µl) and incubated for 5 min at 95 °C to denature the protein. Twenty to thirty micrograms of proteins were fractionated by denaturing gel electrophoresis (10% SDS-PAGE; polyacrylamide gel (Rotiphorese® 10x SDS-PAGE, Carl Roth GmbH, Karlsruhe, Germany)). The fractionated proteins were transferred (Trans Blot®, semi dry transfer cell, Bio Rad, California, USA) to a

nitrocellulose membrane (Amersham™ Protran™, GE Healthcare Life Science, Buckinghamshire, UK). The membranes were blocked with 5% BSA (Capricorn Scientific GmbH, Ebsdorfergrund, Germany) for 1 hour at 4 °C, then treated with protein-specific primary antibodies (Table 3.1.4) diluted in 5% BSA for overnight at 4 °C. Membranes were washed 3 times with 10 ml TBST for 5 min and treated with the respective secondary antibodies (Table 3.1.5) diluted in 5% non-fat milk (Cell Signaling Technology, Inc. MA, USA) for 1 hour and 40 minutes at RT, then washed 3 times with 10 ml TBST for 5 min. The protein-antibody reactive bands were detected with Super Signal West Pico chemiluminescent substrate (Thermo Scientific, Rockford, IL, USA) using ECL ChemoCam Imager (INTAS Science Imaging Instruments GmbH, Göttingen, Germany). Depending on the efficiency of antibodies, the exposure time was adjusted. GAPDH (Santa Cruz Biotechnology, CA, USA) was used as a loading control. Protein density ratios were analyzed by ImageJ 1.53b software (National Institute of Health, Maryland, USA).

### **3.2.4 Histopathology and immunohistochemistry (IHC)**

#### **3.2.4.1 Mice perfusion**

At the respective day of the acute and chronic phase of EAE (Figure 12), placebo and infingratinib treated mice were anesthetized with an intraperitoneal injection of ketamine (150 - 200 mg/kg) and xylazine (10 - 16 mg/kg). Then, anesthetized mice underwent transcardial perfusion for 10 minutes with phosphate-buffered saline (PBS, pH 7.4) and 4% paraformaldehyde (PFA). The perfused mice were post-fixed in 4% PFA for at least 7 days, then spinal cord tissues were dissected and embedded in paraffin blocks. Embedded paraffin blocks were serially sectioned into 1 µm thickness for histopathological and immunohistochemical analysis.

#### **3.2.4.2 Hematoxylin and Eosin staining (H&E)**

The spinal cord tissue sections of placebo and infingratinib treated mice were stained with hematoxylin and eosin (H&E) to examine the inflammatory immune cell accumulation that led to inflammation. The spinal cord tissue sections were dewaxed in xylene reagent and

rehydrated with ethanol. Then the slides were stained with hematoxylin for 5 minutes and washed with water. Further, the slides were stained with eosin for 5 minutes and dehydrated. Finally, slides were mounted with a mounting medium and coverslip.

#### **3.2.4.3 Luxol fast blue/periodic acid-schiff stain (LFB/PAS)**

LFB/PAS staining was performed to assess demyelination in the spinal cord of placebo and infingratinib treated mice. The tissue sections were dewaxed in xylene reagent and rehydrated with ethanol. Subsequently, the sections were incubated overnight with luxol fast blue stain at 56 °C. Then slides were stained in crystal violet for 30-40 seconds. The slides were rinsed and dehydrated, then mounted with mounting medium and coverslip. The demyelination area (%) was calculated by the equation shown below.

Demyelinated area (%) = (Demyelinated area in white matter / Total white matter area) × 100

#### **3.2.4.4 Bielschowsky (Silver staining)**

Axonal densities in the spinal cord of placebo and infingratinib treated mice were determined by histological Bielschowsky-silver staining. The spinal cord sections were dewaxed and rehydrated, further incubated with 20% silver nitrate (AgNO<sub>3</sub>) in the dark for 20 minutes, and then washed with water. Subsequently, the tissue sections were incubated with 2% Na-Thiosulfate for two minutes and then washed with water. Finally, the tissue sections were dehydrated, mounted with mounting medium and coverslip.

#### **3.2.4.5 Immunohistochemistry**

Immunohistochemistry staining was performed to assess the inflammatory immune cell infiltration in the spinal cord of placebo and infingratinib treated mice. The spinal cord sections were dewaxed and rehydrated. The sections were boiling with citrate buffer (10 mM, pH 6) over three times for 5 minutes to induce antigen retrieval and then endogenous peroxidases were blocked with 3% hydrogen peroxide for 10 minutes. Subsequently, sections were incubated with 10% FCS for 1 hour and incubated overnight with primary antibodies. Primary

antibodies used against the following targets, activated microglia-macrophage (Mac3, clone M3/84, Pharmingen, San Diego, CA, USA), B cells (B220, clone RA3-6B2, Pharmingen, San Diego, CA, USA), T cells (CD3, clone CD3-12, Serotec, Oxford, UK), MBP (Dako, Jena, Germany), OPCs (Olig2, clone 211F1.1, MerckMillipore, Darmstadt, Germany), mature oligodendrocytes (P25, Abcam, Cambridge, UK), neurons (NeuN, Abcam, Cambridge, UK). The sections were then incubated with biotinylated secondary antibodies for 1 hour (goat anti-rabbit and horse anti mouse). Immunoreactivity were detected with the avidin-biotin complex. For histology and immunohistochemistry, microscopic images were captured with Axio Scan Z1 Microscope and analyzed using the ZEN 3.2 (blue edition) software (Carl Zeiss Microscopy GmbH, Oberkochen, Germany). Immunohistochemically positive stained inflammatory infiltrates (CD3(+) T cells, B220(+) B cells and Mac3(+) macrophages/microglia), Olig2(+) OPCs, P25(+) mature oligodendrocytes and NeuN(+) motor neurons were semi-quantitatively determined in a minimum of 6 inflammatory lesions per mouse from the entire spinal cord and were normalized to an area of 1 mm<sup>2</sup>.

### **3.2.5 Cell culture experiments**

Oligodendroglial cell line OLN93 is an adherent cell kindly provided by Prof. Markus Kipp (Rostock, Germany). OLN93 cells were derived from spontaneously transformed cells in primary rat brain glial cultures used in this study (Richter-Landsberg and Heinrich, 1996). Cells were cultured in Dulbecco's modified Eagle medium (DMEM) (Life Technologies Limited, UK) with 10% fetal bovine serum (PAA Laboratories GmbH, Pasching, Austria) and 100 U/ml penicillin, and 100 µg/ml streptomycin (Life Technologies Limited, Renfrew, UK) in polystyrene 75 cm<sup>2</sup> culture flask with filter screw cap (Greiner Bio-One GmbH, Germany) at 37 °C in a humidified incubator 5% CO<sub>2</sub>. Confluent cultures were passaged by 1x PBS wash followed by 1% Trypsin was used for cell detachment from culture flask grounds and incubated at 37 °C for 1 minute. Experiments were performed at passages 10 - 20.

### 3.2.5.1 DAPI staining

OLN93 oligodendrocyte cells were seeded at 1.5 ml/well ( $2 \times 10^5$  cells/ml) in 24 well flat bottom plate. The cells were incubated for 24 hours at 37 °C with culture medium containing bFGF (25 ng/ml), infigratinib (1  $\mu$ M), bFGF + infigratinib (25 ng/ml, 1  $\mu$ M) and DMSO (1  $\mu$ l/ml). The culture medium was removed and 100  $\mu$ l 4% paraformaldehyde was added to fix the cells at room temperature for 10 min. The fixed cells were subsequently subjected to a 100  $\mu$ l PBS wash three times. 50  $\mu$ l of nuclear dye DAPI was added to each well and incubated 20 minutes in the dark at room temperature. The staining solution was removed and washed with 100  $\mu$ l of PBS for three times. After washing, fluorescent images of the OLN93 cells proliferation were captured using Nikon Eclipse Ti-U fluorescence microscope (Nikon GmbH, Düsseldorf, Germany).

### 3.2.5.2 Protein extraction

OLN93 cells were grown in 75 cm<sup>2</sup> culture flask with 80% confluence. Culture medium was added with respective treatments bFGF (25 ng/ml), infigratinib (1  $\mu$ M), bFGF + infigratinib (25 ng/ml, 1  $\mu$ M) and DMSO (1  $\mu$ l/ml) for 24 hours at 37 °C. Then the medium was removed and washed with cold PBS. Cells were scraped from the flask and centrifuged for 3500 rpm, 4 minutes at 4 °C. The supernatant was discarded and the cell pellet was lysed with 150  $\mu$ l of cell lysis buffer with protease and phosphatase inhibitors in 2 ml eppendorf tubes and incubated in ice for 1 hour. The cell lysate was centrifuged at 14000 rpm in 4 °C for 25 minutes; the supernatant was collected and stored at -20 °C until analysis.

### 3.2.5.3 Protein quantification and western blot

Protein quantification and western blot procedure were followed as described in sections 3.2.3.1 and 3.2.3.2.

### 3.2.6 Statistical analysis

All analyses were performed in a blinded manner and all mice and samples were included in the analysis. The statistical significance of EAE clinical scores between placebo and infliximab groups (three independent experiments) was analyzed using a Mann-Whitney U test. For immunohistochemical analyses, positively labelled cells were counted in a minimum of six spinal cord sections. Histological, immunohistochemical, western blot, and RT-PCR data analyses were evaluated using a Student's t test. GraphPad Prism 9 was used for statistical analyses and graph preparation. All data are presented as mean  $\pm$  SEM and  $P < 0.05$  was considered statistically significant (\*  $P < 0.05$ ; \*\*  $P < 0.01$ ; \*\*\*  $P < 0.001$ ).



## 4 RESULTS

### 4.1 Efficacy of fingratinib in MOG<sub>35-55</sub>-induced EAE

#### 4.1.1 EAE clinical scoring

EAE was induced with MOG<sub>35-55</sub> peptide in C57BL/6J mice. All placebo and fingratinib treated mice underwent daily EAE clinical scoring as mentioned in the method section.

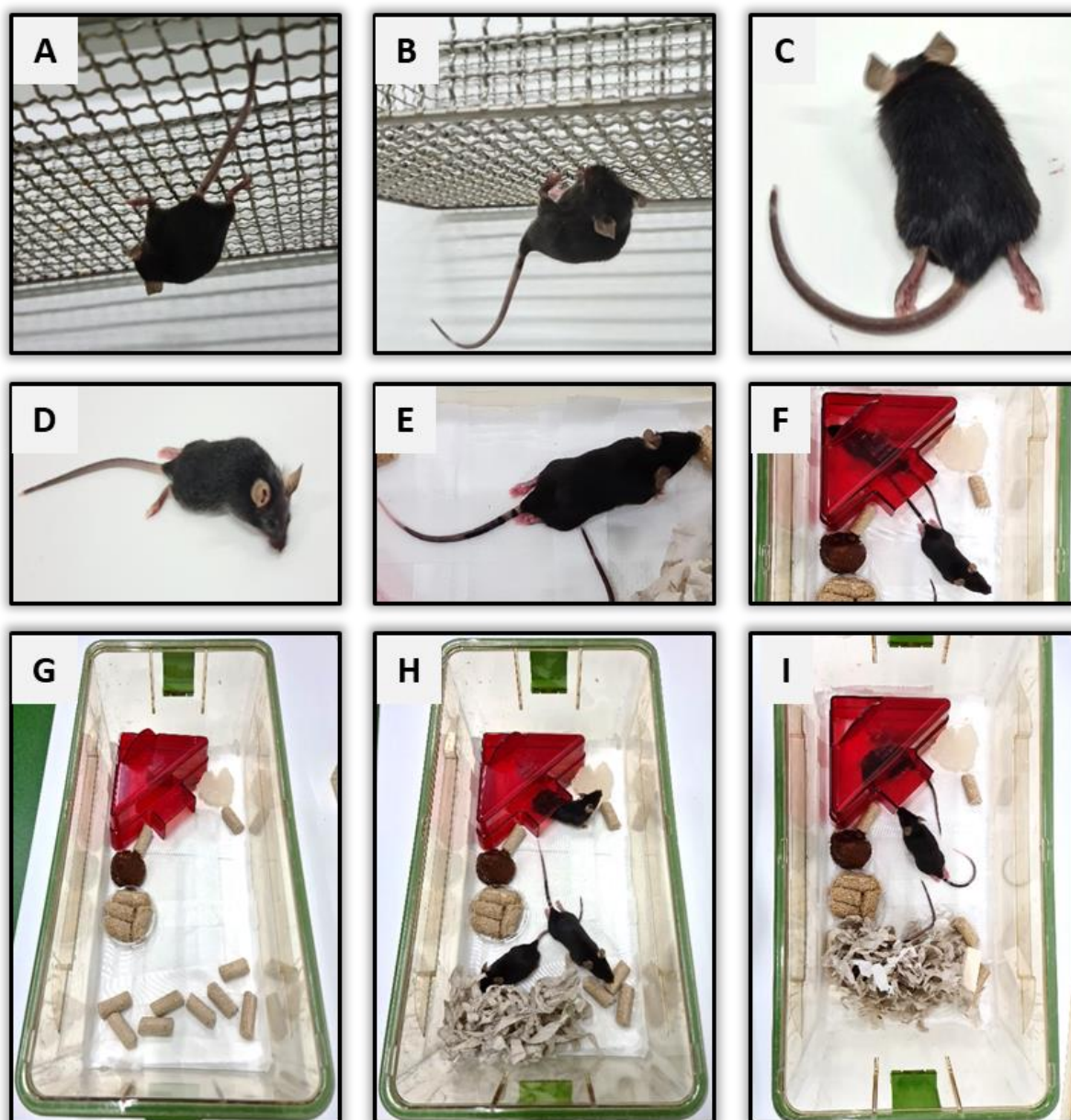


**Figure 13. Clinical symptoms of MOG<sub>35-55</sub>-induced EAE (placebo arm).** Healthy mice (A), tail paralysis (B), tail and hind limb paralysis (C-E). The hind limb paralyzed mice were housed in a cage with cellulose bedding and diet enrichment (F-I).

## 4.2 Infigratinib applied from the time of EAE induction (Preventive protocol)

### 4.2.1 Infigratinib given from day 0-9 p.i. reduces the severity and relapses in MOG<sub>35-55</sub>-induced EAE

Previous studies have shown that oligodendroglial specific *FGFR1* and *FGFR2* deletion reduces the severity of chronic EAE (Rajendran et al., 2018; Kamali et al., 2021). These prior studies were elucidating the pathological role of oligodendroglial FGFR in a chronic EAE model. Therefore, we examined the selective FGFR inhibitor infigratinib that could inhibit or prevent the onset of symptoms and relapses of MOG<sub>35-55</sub>-induced EAE. EAE was induced in 8 weeks old C57BL/6J female mice which received either infigratinib or placebo from day 0 - 9 p.i. as described in paragraph (3.2.1.3 and 3.2.1.4) (Figure 12). Mice treated with placebo showed a mean onset of symptoms of  $10.7 \pm 0.3$  days, whereas infigratinib treated mice showed a delayed onset of symptoms by 2 days ( $12.7 \pm 0.3$  days) ( $P < 0.001$ ) (Figure 15 A). The maximum EAE scores were less in mice treated with infigratinib ( $1.12 \pm 0.17$ ) compared to mice on placebo ( $2.45 \pm 0.19$ ) ( $P < 0.001$ ) (Figure 15 B). At day 18 p.i. (peak of disease), 54.5% of mice on placebo exhibited severe weakness of hindlimbs (EAE scores of  $\geq 2.5$ ), whereas only 14.3% mice treated with infigratinib showed severe symptoms. Infigratinib treatment significantly ameliorated the EAE disease severity from day 8 to the end of the study ( $P < 0.001$ ) (Figure 14 A) and lowered cumulative EAE scores ( $P < 0.001$ ) (Figure 14 B). At the end of the experiment, no mice on infigratinib showed severe symptoms, whereas 43.7% mice on placebo exhibited severe weakness or paralysis of hindlimbs. No effect of infigratinib on the bodyweight of mice were observed (Figure 15 C). Figure 14 A and Table 4 show the summary of the EAE clinical score in placebo and infigratinib treated mice.

**Table 4. Disease severity (Prevention protocol)**

Treatment	No. of mice	EAE clinical scores		
		Disease onset (day)	Maximum score	End of study
Placebo	46	$10.7 \pm 0.3$	3.5	$2.45 \pm 0.19$
Infigratinib	41	$12.7 \pm 0.3$	3	$1.12 \pm 0.17$

The efficacy of infigratinib to prevent severity and relapses in MOG<sub>35-55</sub>-induced EAE. Mice showed delayed onset of EAE clinical sign. Whereas from day 8 p.i. infigratinib treated mice showed a milder disease course till the end of the experiment.

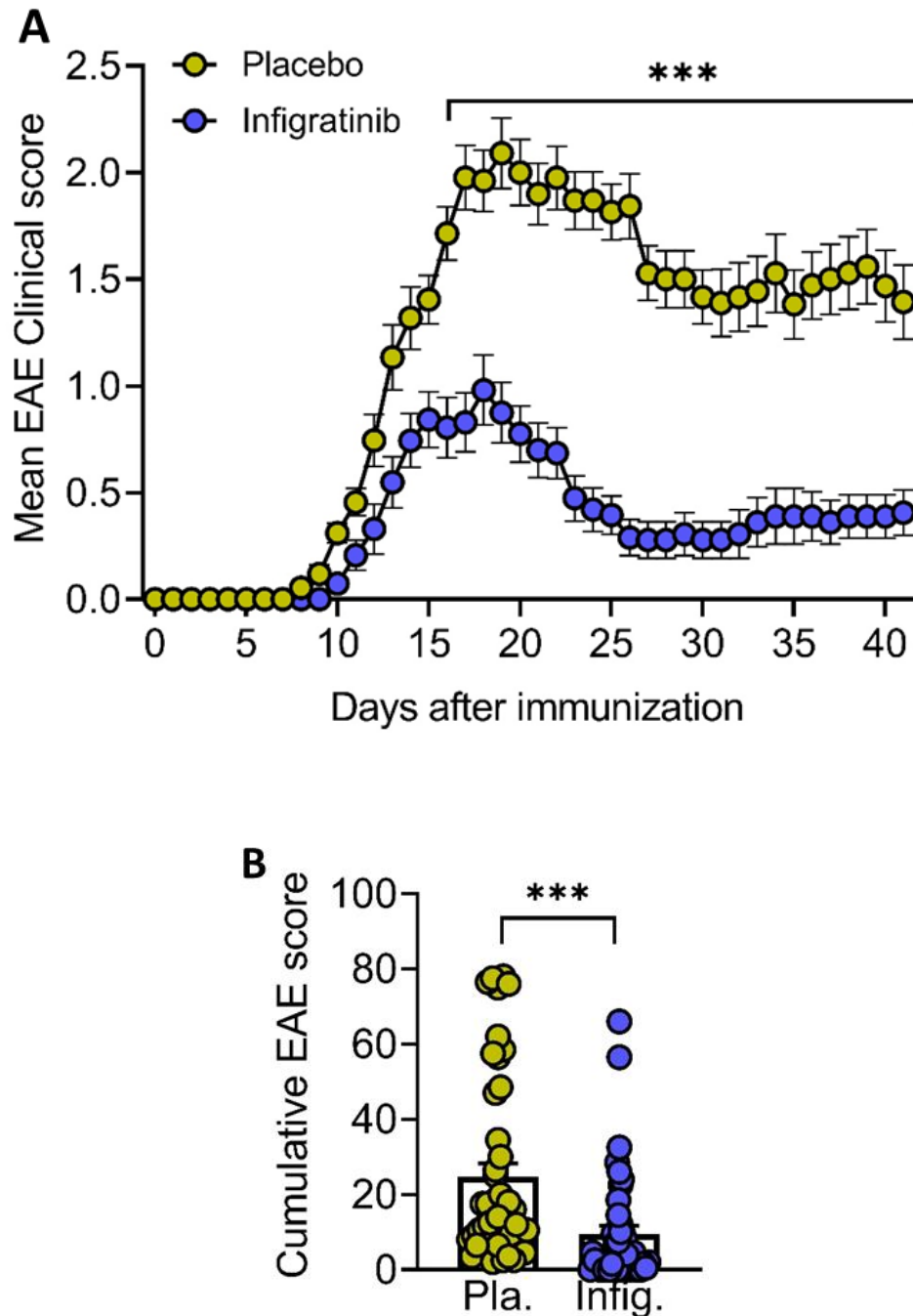


**Figure 14. Infigratinib reduces the severity of relapses in MOG<sub>35-55</sub>-induced EAE.** A) Infigratinib treated mice showed a milder disease course from day 8 until day 41 p.i. ( $P < 0.001$ ). B) Cumulative scores of chronic EAE until day 41 p.i. were less in mice treated with infigratinib ( $P < 0.0001$ ). Infigratinib ( $n = 41$ ) or placebo ( $n = 46$ ), data are presented as mean  $\pm$  SEM. ( $*P < 0.05$ ,  $**P < 0.01$ ,  $***P < 0.001$ ).

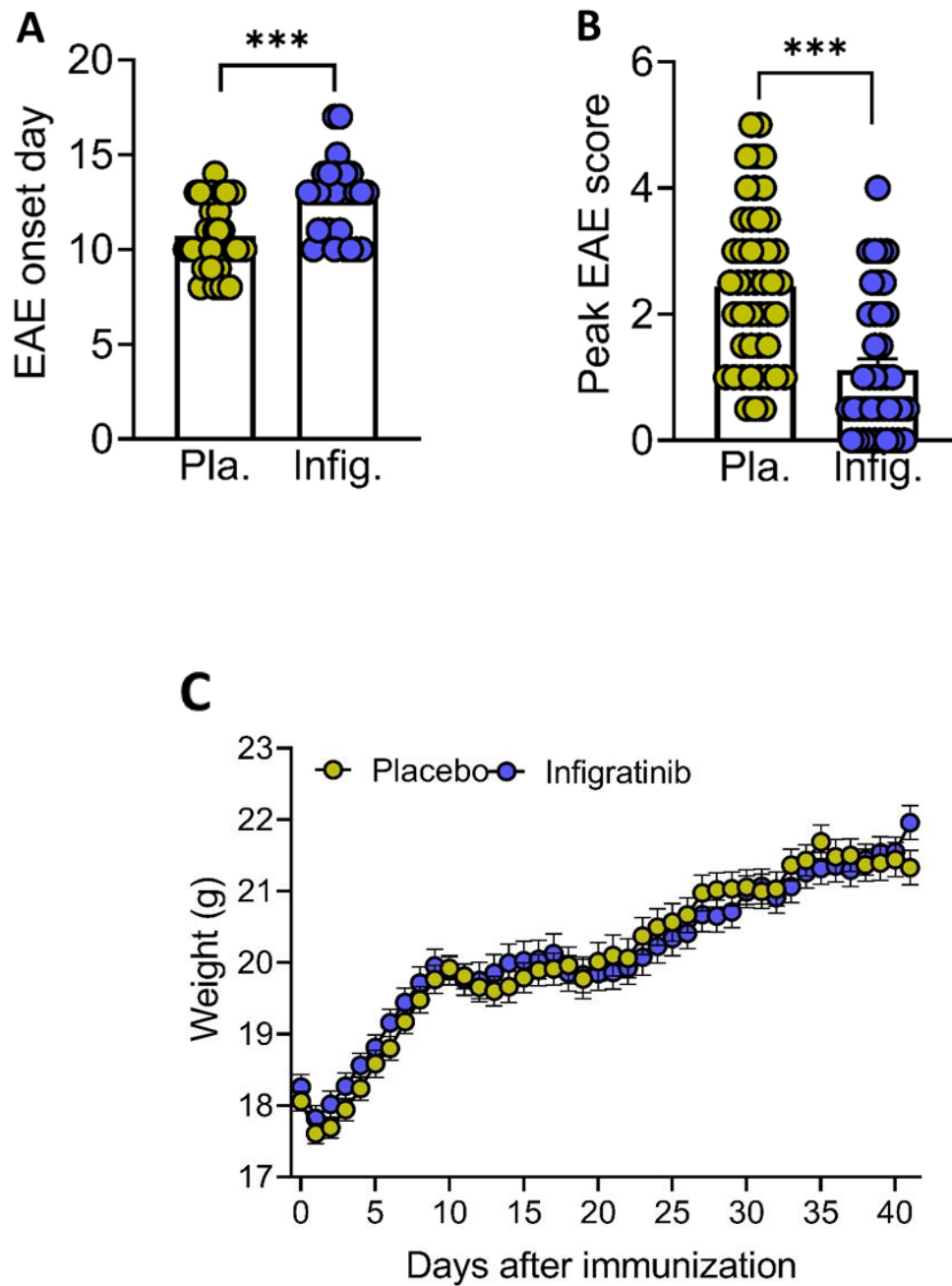


**Figure 15. Effect of infigratinib on EAE onset and body weight.** A) The onset of EAE disease was delayed ( $P < 0.0001$ ), B) peak EAE scores were less in infigratinib treated mice ( $P < 0.0001$ ). C) There was no difference in body weight between the groups. Infigratinib ( $n = 41$ ) and placebo ( $n = 46$ ), data are presented as mean  $\pm$  SEM ( $*P < 0.05$ ,  $**P < 0.01$ ,  $***P < 0.001$ ).

#### 4.2.2 Immune cells infiltration was reduced by infigratinib

The effects of infigratinib administered on days 0-9 p.i. on inflammation and inflammatory immune cell infiltration in spinal cord WML were determined by histological hematoxylin/eosin and immunostainings. Histological analyses of spinal cord sections on day 17 p.i./acute phase of the disease showed that infigratinib decreased infiltrated immune cell accumulation compared to placebo ( $P < 0.0001$ ; Figure 16). Further immunostainings confirmed that infigratinib treatment reduces infiltrating inflammatory CD3(+) T cells ( $P < 0.0001$ ), B220(+) B cells ( $P < 0.0001$ ), and Mac3(+) macrophages/microglia ( $P < 0.0001$ ) in WML (Figure 16).

Further, we investigated the spinal cord sections on day 41 p.i., the chronic phase of the disease. Consistent with the acute phase, the immune cell accumulation ( $P = 0.0013$ ), infiltration of CD3(+) T cells ( $P = 0.0140$ ), B220(+) B cells ( $P = 0.0008$ ), and Mac3(+) macrophages/microglia ( $P < 0.0001$ ) were less in WML in infigratinib treated mice (Figure 17). These data indicate that infigratinib treatment reduces immune cell infiltration into the CNS during EAE.

**Table 5. Immune cell infiltrations (Prevention protocol)**

Pathology	Day 17 p.i.		<i>P</i> -value	Day 41 p.i.		<i>P</i> -value
	Placebo	Infigratinib		Placebo	Infigratinib	
Inflammatory index	2.44 ± 0.26	0.69 ± 0.06	< 0.0001	1.99 ± 0.33	0.52 ± 0.06	0.0013
CD3(+) T cells	524.5 ± 60.77	90.85 ± 18.34	< 0.0001	265.8 ± 68.63	60.29 ± 8.34	0.0140
B220(+) B cells	823.1 ± 104.0	85.57 ± 16.83	< 0.0001	387.7 ± 71.63	47.35 ± 9.71	0.0008
Mac3(+) macrophages/microglia	1303 ± 101.4	238.7 ± 36.07	< 0.0001	633.2 ± 76.25	119.7 ± 5.02	< 0.0001

Quantification of immune cell infiltration of T cells, B cells and macrophages into the spinal cord WML of placebo or infigratinib treated mice in acute (day 17 p.i.) and chronic phase of EAE (day 41 p.i.). Data are presented as mean ± SEM. Histology and IHC analysis were performed blinded to the treatment group.



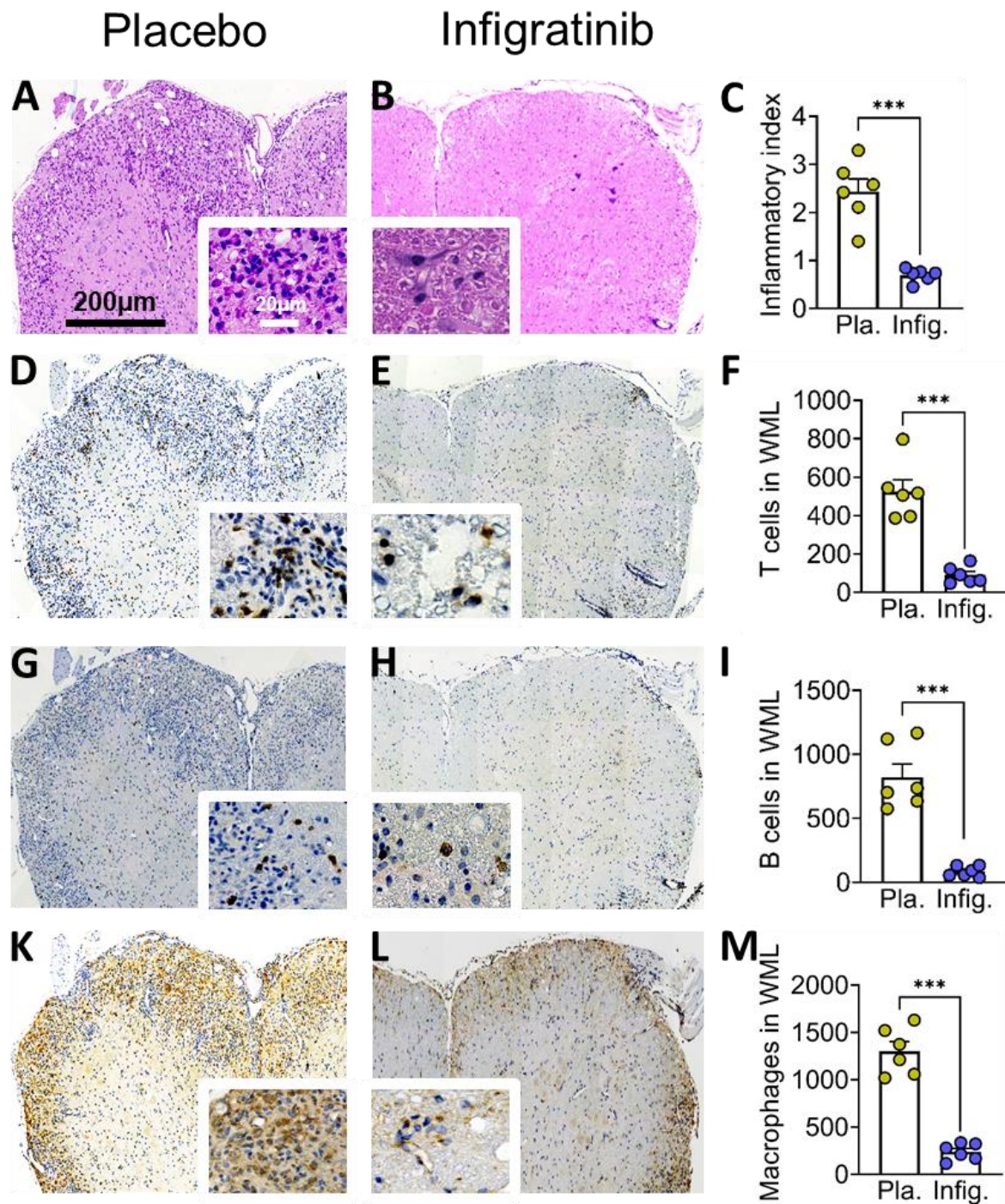


**Figure 16. Inflammation and immune cell infiltration in spinal cord WML at day 17 p.i.** The inflammatory index (A - C) was less in infigratinib treated mice compared to placebo ( $P < 0.0001$ ). The number of CD3(+) T cells ( $P < 0.0001$ ) (D - F), B220(+) B cells ( $P < 0.0001$ ) (G - I) and Mac3(+) macrophages/microglia ( $P < 0.0001$ ) (K - M) per mm<sup>2</sup> were reduced by infigratinib. Representative images of spinal cord sections are shown. Bar: 200 µm, 20 µm (insert).  $n = 6$ /group, data are presented as mean  $\pm$  SEM (\* $P < 0.05$ , \*\* $P < 0.01$ , \*\*\* $P < 0.001$ ).



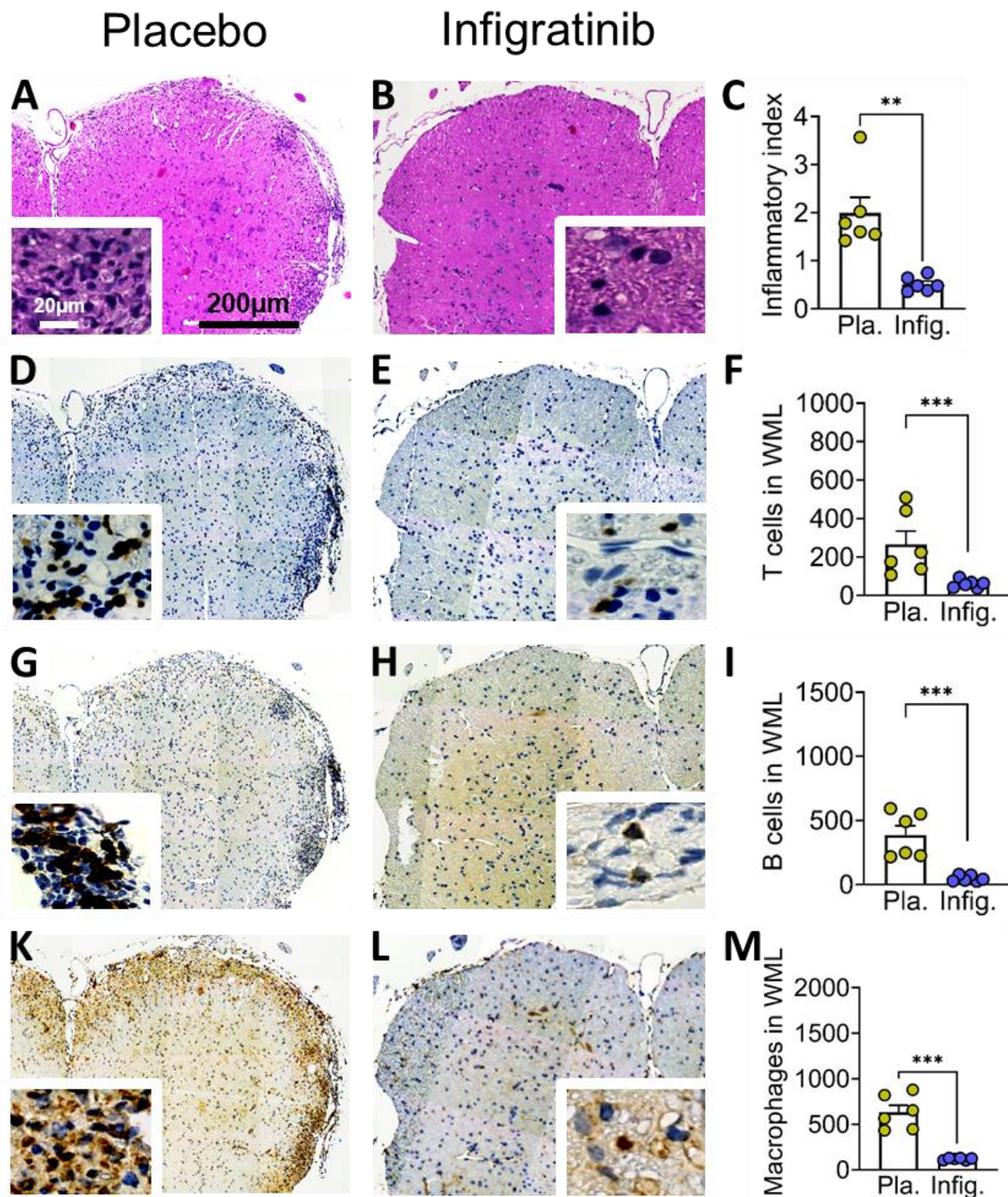


**Figure 17. Inflammation and immune cell infiltration spinal cord WML at day 41 p.i.** (A - C) The inflammatory index was less in infigratinib treated mice compared to placebo ( $P = 0.0013$ ). The number of CD3(+) T cells ( $P = 0.0140$ ) (D - F), B220(+) B cells ( $P < 0.0008$ ) (G - I) and Mac3(+) macrophages/microglia ( $P < 0.0001$ ) (K - M) per  $\text{mm}^2$  were reduced by infigratinib. Representative images of spinal cord sections are shown. Bar: 200  $\mu\text{m}$ , 20  $\mu\text{m}$  (insert).  $n = 6/\text{group}$ , data are presented as mean  $\pm$  SEM ( $*P < 0.05$ ,  $**P < 0.01$ ,  $***P < 0.001$ ).

### 4.2.3 Regulation of inflammatory mediators in the whole spinal cord during EAE

To investigate whether inhibition of FGFR with infigratinib can control the inflammatory processes mediated by pro-inflammatory cytokines (IL1 $\beta$ , IL6, IL12, TNF $\alpha$  and iNOS) and chemokines (CX3CL1 and CX3CR1) in the spinal cord of acute and chronic EAE, we analyzed mRNA expression of pro-inflammatory cytokines and chemokines by RT-PCR. In acute phase of EAE (day 17 p.i.), infigratinib treatment did not regulate the mRNA expression of IL1 $\beta$  ( $P = 0.8198$ ), IL6 ( $P = 0.2911$ ), IL12 ( $P = 0.5994$ ), TNF $\alpha$  ( $P = 0.8319$ ) and iNOS ( $P = 0.8126$ ) compared to placebo; no changes in chemokine CX3CL1 ( $P = 0.1232$ ) and CX3CR1 ( $P = 0.6604$ ) expression were observed (Figure 18 A).

In contrast to the acute phase, mRNA expression levels of IL1 $\beta$  ( $P = 0.0011$ ), IL6 ( $P = 0.0319$ ), IL12 ( $P = 0.001$ ) and TNF $\alpha$  ( $P = 0.001$ ) were significantly downregulated by infigratinib in the chronic phase of EAE (day 41 p.i.). There was no effect on the regulation of iNOS ( $P = 0.0692$ ), chemokine CX3CL1 ( $P = 0.4240$ ) and CX3CR1 ( $P = 0.3488$ ) expression (Figure 18 B).



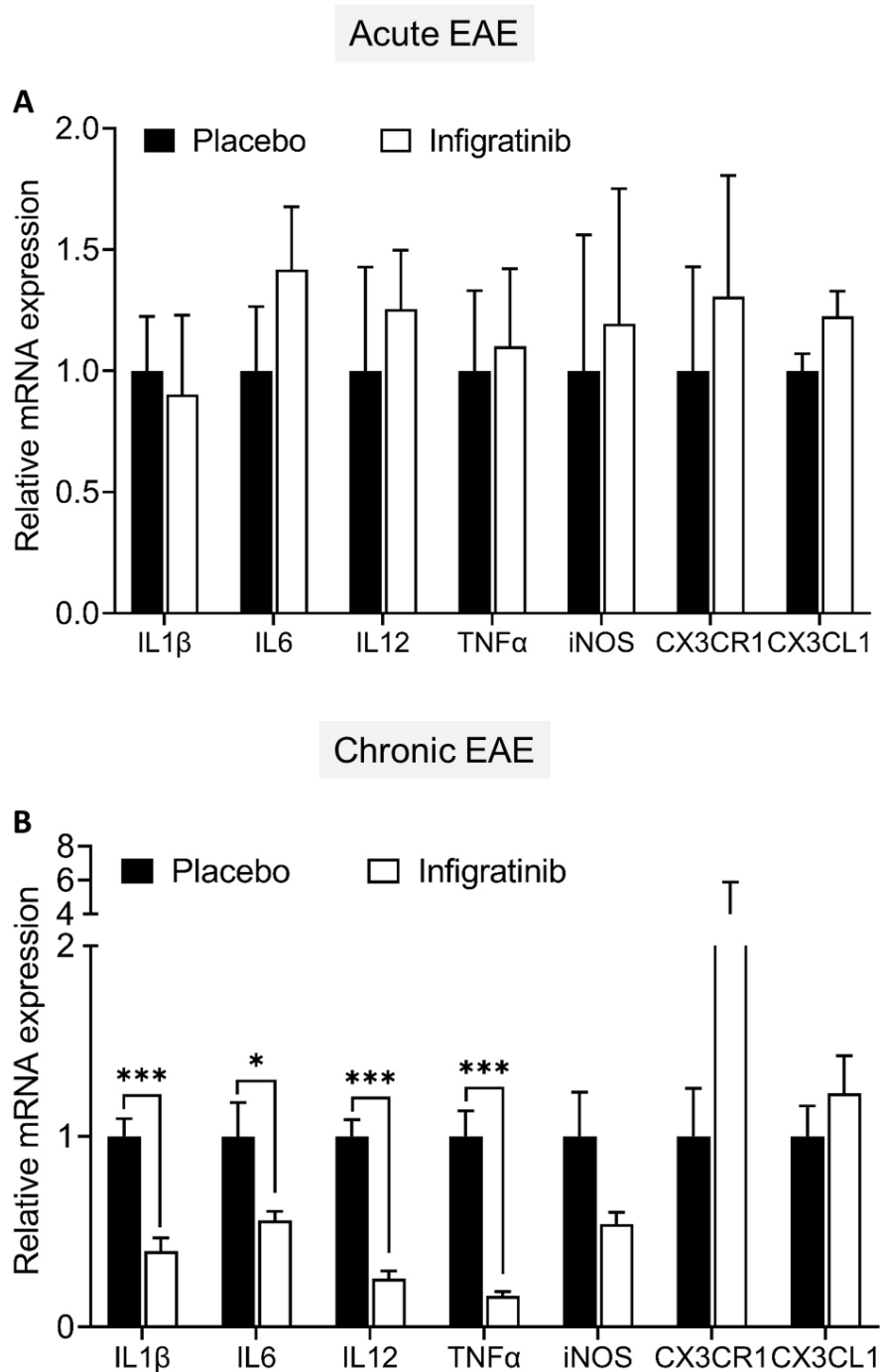


**Figure 18. Effects of infigratinib on pro-inflammatory cytokines and chemokines in spinal cord at day 17/41 p.i.** Findings at the acute (A) and the chronic EAE (B) are shown. In acute EAE (day 17 p.i.), the pro-inflammatory cytokines (IL1 $\beta$ , IL6, IL12, TNF $\alpha$  and iNOS) and chemokines (CX3CL1 and CX3CR1) were not different between infigratinib and placebo. In chronic EAE (day 41 p.i.), decreased mRNA expression of IL1 $\beta$ , IL6, IL12 and TNF $\alpha$  was observed in mice treated with infigratinib compared with placebo. No difference of iNOS and chemokines (CX3CL1 and CX3CR1) mRNA levels in the chronic EAE (day 41 p.i.) were detected. Acute EAE  $n = 5-6$ /group and chronic EAE  $n = 4-5$ /group). Data are presented as mean  $\pm$  SEM (\* $P < 0.05$ , \*\* $P < 0.01$ , \*\*\* $P < 0.001$ ).

#### 4.2.4 Treatment with infigratinib decreases demyelination and increases axonal density

Based on the H&E results (Figure 16 A-C, 17 A-C), the degree of demyelination and axonal density in spinal cord WML was detected by histological LFB/PAS and Bielschowsky stainings. We conducted a MBP immunostaining to confirm the findings obtained by the LFB/PAS staining. Consistent with disease severity, mice treated with placebo exhibited extensive demyelination and axonal loss in the acute (day 17 p.i.) and chronic phases of EAE (day 41 p.i.). In contrast to the placebo group, the infigratinib treated mice exhibited a significantly reduced demyelination, parallel with increased axonal density in both acute (Figure 19) and chronic phases of EAE (Figure 20). Figure 19-20 and Table 6 show the summary of demyelination and axonal density in placebo and infigratinib treated mice.

**Table 6. Demyelination and axonal density (Prevention protocol)**

Pathology	Day 17 p.i.		<i>P</i> -value	Day 41 p.i.		<i>P</i> -value
	Placebo	Infigratinib		Placebo	Infigratinib	
Demyelination (%) (LFB/PAS)	38.28 ± 4.87	13.77 ± 3.20	0.0018	31.12 ± 6.17	8.63 ± 2.53	0.0071
Demyelination (%) (MBP)	21.30 ± 2.27	10.04 ± 1.47	0.0019	12.58 ± 2.41	5.67 ± 0.96	0.0236
Axonal density %	31.50 ± 3.82	69.70 ± 4.42	< 0.0001	38.77 ± 4.49	84.98 ± 7.94	0.0005

Quantification of demyelination (LFB/PAS and MBP) and axonal density (Bielschowsky staining) in the spinal cord of placebo and infigratinib treated mice in acute (day 17 p.i.) and chronic phase of EAE (day 41 p.i.). Data are presented as mean ± SEM. Histology and IHC analysis was performed blinded to the treatment group.

#### 4.2.5 Myelin inhibitor expression is modulated by infigratinib

The effects of infigratinib on myelin inhibitor genes such as Lingo-1, TGFβ and SEMA3A were analyzed by RT-PCR. In the acute phase of EAE (day 17 p.i.), mRNA expression levels of Lingo-1 was decreased by infigratinib ( $P = 0.0096$ ). There were no differences in mRNA expression levels of TGFβ and SEMA3A (Figure 21 A). In the chronic phase of EAE (day 41 p.i.), SEMA3A ( $P = 0.0078$ ) mRNA expression was downregulated by infigratinib, but there was no difference in the expression of Lingo-1 and TGFβ (Figure 21 B).

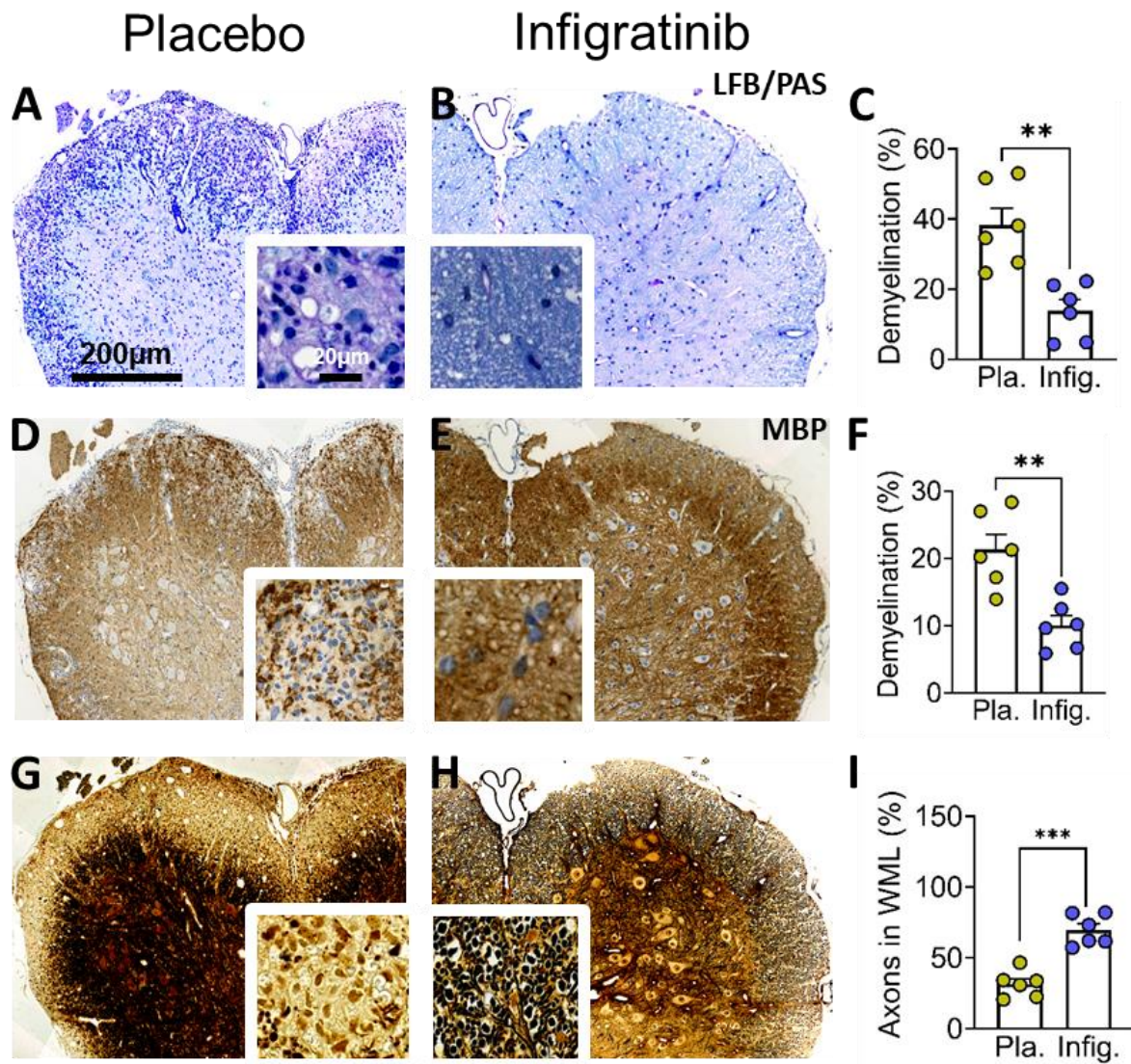


**Figure 19. Effects of infigratinib on demyelination and axonal density in the spinal cord at day 17 p.i.** The percentage of demyelination (LFB/PAS staining (A - C):  $P = 0.0018$ ; MBP staining (D - F):  $P = 0.0019$ ) was less in spinal cord WML in mice treated with infigratinib than placebo. The percentage of axonal density in spinal cord WML (G - I) was higher in infigratinib treated mice than in placebo ( $P < 0.0001$ ). Representative images of spinal cord sections are shown. Bar: 200  $\mu\text{m}$ , 20  $\mu\text{m}$  (insert).  $n = 6/\text{group}$ , data are presented as mean  $\pm$  SEM ( $*P < 0.05$ ,  $**P < 0.01$ ,  $***P < 0.001$ ).



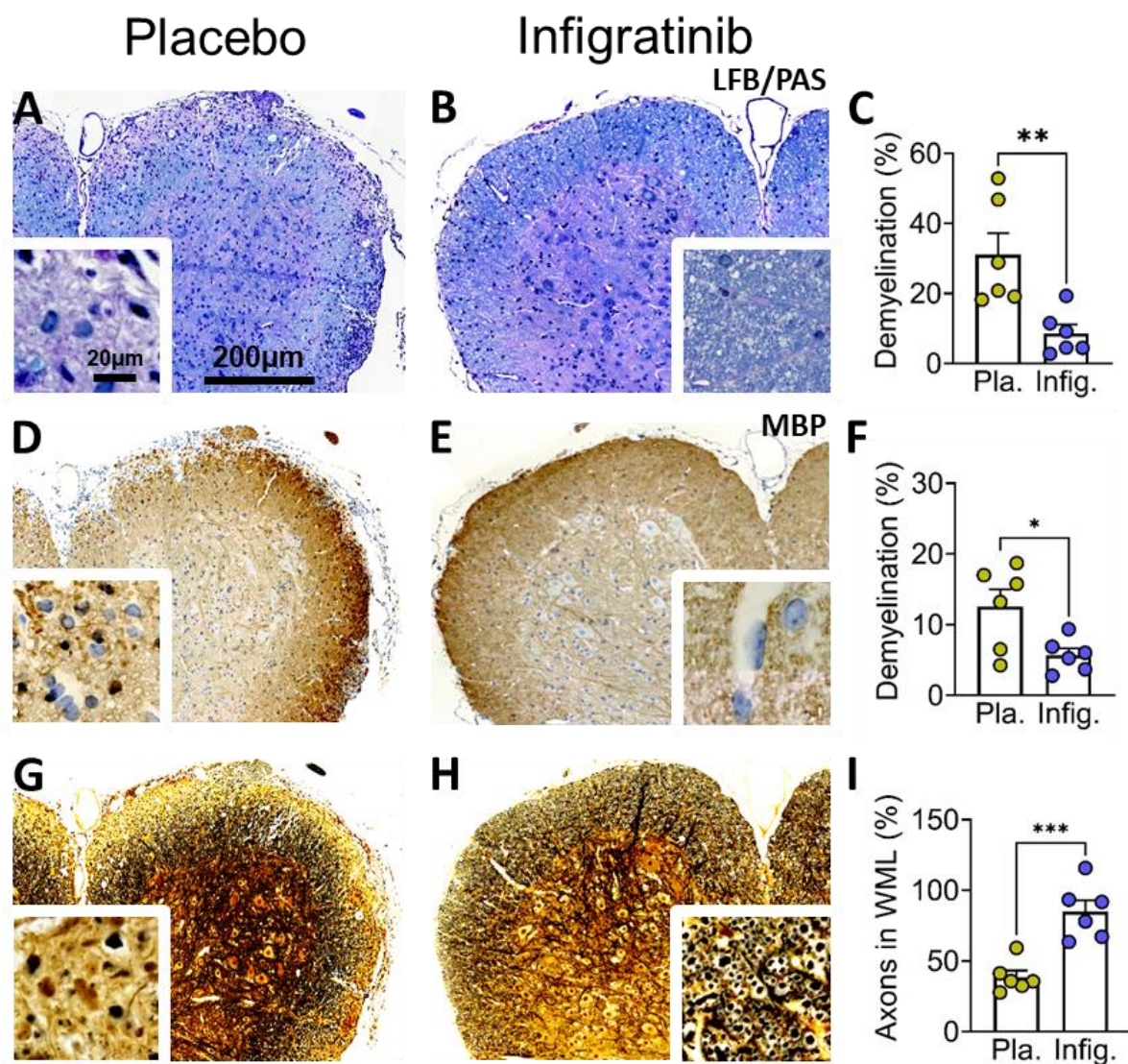


**Figure 20. Effect of infigratinib on demyelination and axonal density in the spinal cord at day 41 p.i.** The percentage of demyelination (LFB/PAS staining (A - C):  $P = 0.0071$ ; MBP staining (D - F):  $P = 0.0236$ ) was less in spinal cord WML in mice treated with infigratinib than placebo. The percentage of axonal density in spinal cord WML (G - I) was higher in infigratinib treated mice than in placebo ( $P = 0.0005$ ). Representative images of spinal cord sections are shown. Bar: 200  $\mu\text{m}$ , 20  $\mu\text{m}$  (insert).  $n = 6/\text{group}$ , data are presented as mean  $\pm$  SEM ( $*P < 0.05$ ,  $**P < 0.01$ ,  $***P < 0.001$ ).

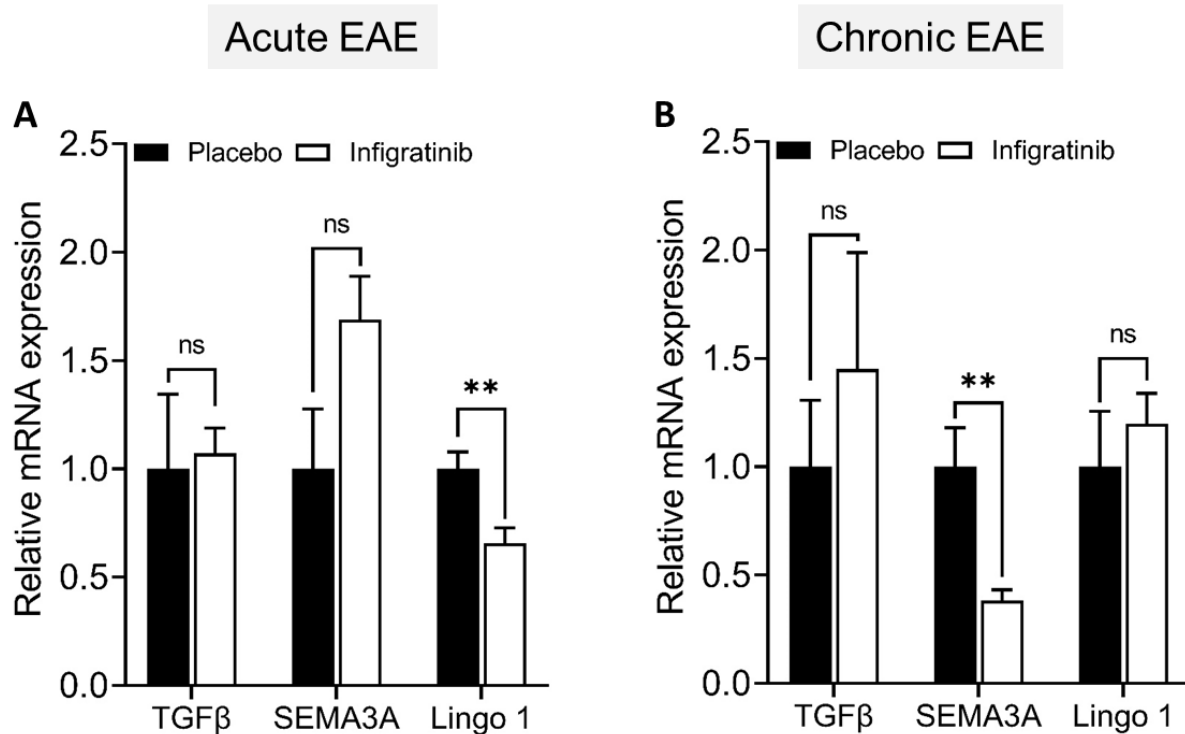


**Figure 21. Expression of remyelination inhibitors in the whole spinal cord at day 17/41 p.i.** A) In acute EAE (day 17 p.i.), Lingo-1 mRNA expression ( $P = 0.0096$ ) was reduced in mice treated with infigratinib, there was no regulation in TGFβ ( $P = 0.8340$ ) and SEMA3A mRNA expression ( $P = 0.0681$ ). B) In chronic EAE (day 17 p.i.), mRNA expression of SEMA3A was reduced ( $P = 0.0078$ ) by infigratinib treatment, there was no regulation in TGFβ ( $P = 0.5204$ ) and Lingo-1 mRNA expression ( $P = 0.4913$ ). Acute EAE  $n = 5-6$ /group and chronic EAE  $n = 4-5$ /group. Data are presented as mean  $\pm$  SEM. ns = not significant ( $*P < 0.05$ ,  $**P < 0.01$ ,  $***P < 0.001$ ).

#### 4.2.6 Infigratinib enhances the number of OPCs, mature oligodendrocytes, and motor neurons, and myelin protein expression

We next assessed the effects of infigratinib administered on days 0-9 p.i. on oligodendroglial lineage cells in spinal cord WML, NAMW and the motor neuron population in the spinal cord grey matter was analyzed by immunostaining. In the acute phase (day 17 p.i.), a significant increase of P25(+) mature oligodendrocyte density in normal-appearing white matter (NAWM;  $P = 0.0040$ ) and white matter lesion (WML;  $P = 0.0001$ ) areas in the spinal cord of infigratinib treated mice was detected (Figure 24-25). Furthermore, there was no difference in OPCs numbers in NAWM and WML between placebo and infigratinib treated mice (Figure 22-23). A significant increase of NeuN(+) motor neuron numbers was observed in spinal cord grey

matter of mice treated with fingertinib ( $P = 0.0378$ ; Figure 26). Western blot analyses of myelin protein MBP ( $P = 0.9702$ ), PLP ( $P = 0.7001$ ) and CNPase ( $P = 0.8196$ ) in spinal cord lysates showed that fingertinib did not change myelin protein expression (Figure 27 A-B).

In the chronic phase of EAE (day 41 p.i.), fingertinib treated mice showed a higher number of P25(+) mature oligodendrocytes in WML in the spinal cord ( $P = 0.0051$ ) but no difference in NAWM ( $P = 0.1666$ ) (Figure 24-25). The Olig2(+) OPC density was increased in WML ( $P = 0.0072$ ) but did not alter in NAWM of fingertinib treated mice spinal cord ( $P = 0.6496$ ) (Figure 22-23). There were no differences in NeuN(+) motor neuron numbers between the groups ( $P = 0.0881$ ; Figure 26). Fingertinib treatment significantly increased the expression of the myelin proteins MBP ( $P = 0.0056$ ), PLP ( $P = 0.0041$ ), and CNPase ( $P = 0.0048$ ) over placebo (Figure 27 C-D).

**Table 7. Oligodendrocyte population (Prevention protocol)**

Cell types	Day 17 p.i.		P-value	Day 41 p.i.		P-value
	Placebo	Fingertinib		Placebo	Fingertinib	
Olig2(+) cells NAWM	473.7 ± 23.02	514.3 ± 9.979	0.1361	554.0 ± 11.04	544.3 ± 17.44	0.6496
Olig2(+) cells WML	395.7 ± 32.79	430.0 ± 37.03	0.5034	442.3 ± 20.63	557.0 ± 27.16	0.0072
P25(+) cells NAWM	532.5 ± 28.98	736.7 ± 46.78	0.0040	606.7 ± 52.54	688.7 ± 16.15	0.1666
P25(+) cells WML	90.33 ± 4.318	130.5 ± 5.136	0.0001	142.0 ± 8.517	195.2 ± 12.22	0.0051
NeuN(+) motor neurons in grey matter	408.7 ± 34.43	520.7 ± 31.74	0.0378	492.0 ± 66.00	645.3 ± 47.20	0.0881

Quantification of Olig2(+) OPCs, P25(+) mature oligodendrocytes in the spinal cord WML and NAWM of placebo or fingertinib treated mice in acute and chronic phases of EAE. NeuN(+) motor neurons in the spinal cord grey matter of placebo or fingertinib treated mice in acute and chronic phase of EAE. Data are presented as mean ± SEM. IHC analysis was performed blinded to the treatment group.



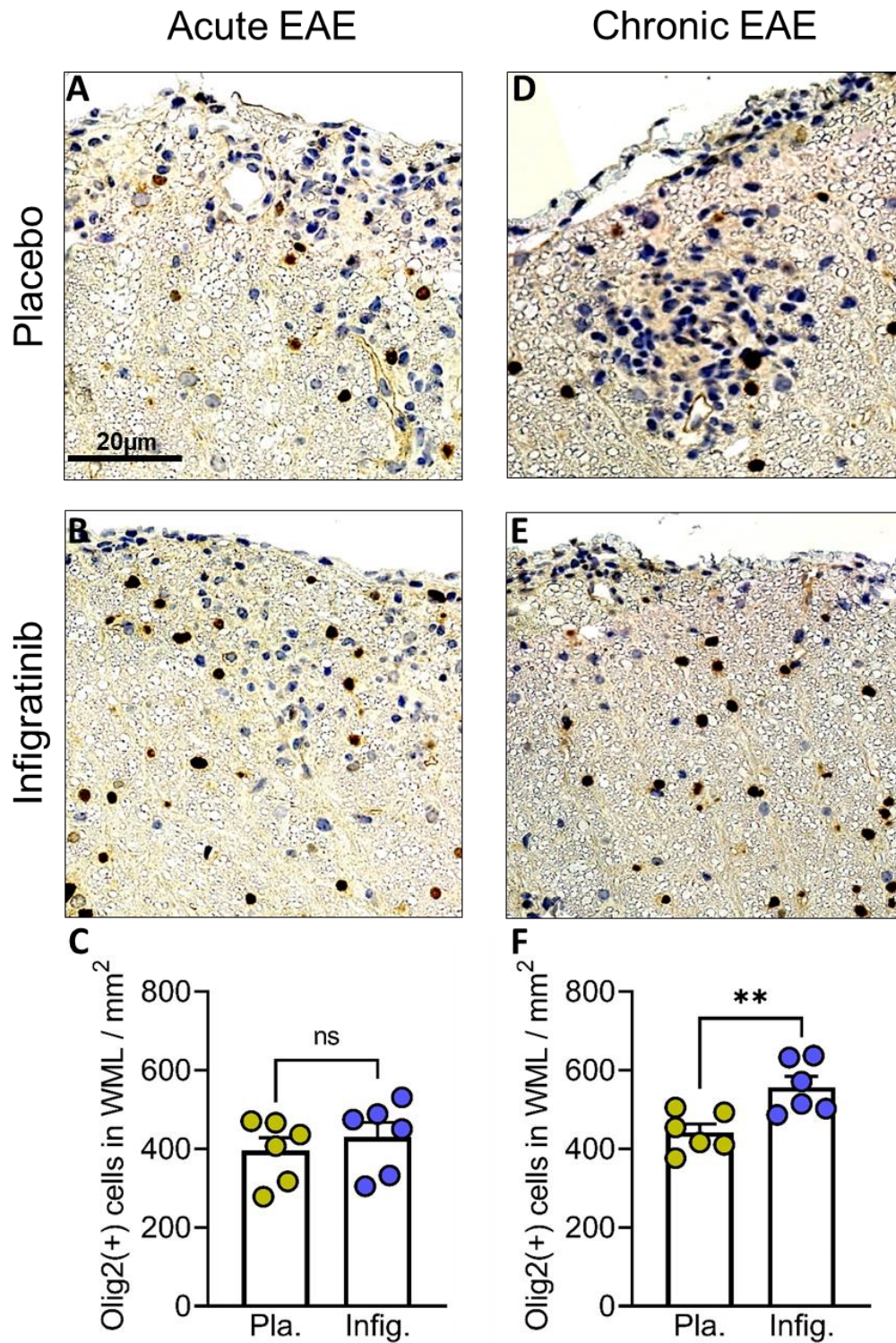


**Figure 22. Oligodendrocyte precursor cell populations in spinal cord WML at day 17/41 p.i.** (A - C) In acute EAE (day 17 p.i.), Olig2(+) OPCs ( $P = 0.5034$ ) populations in spinal cord WML were not different between infigratinib and placebo groups. (D - F) In chronic EAE (day 41 p.i.), higher number of OPCs in spinal cord WML ( $P = 0.0072$ ) were observed in infigratinib treated mice. Representative images of spinal cord sections are shown. Bar: 20  $\mu\text{m}$ .  $n = 6/\text{group}$ , data are presented as mean  $\pm$  SEM. ns = not significant ( $*P < 0.05$ ,  $**P < 0.01$ ,  $***P < 0.001$ ).

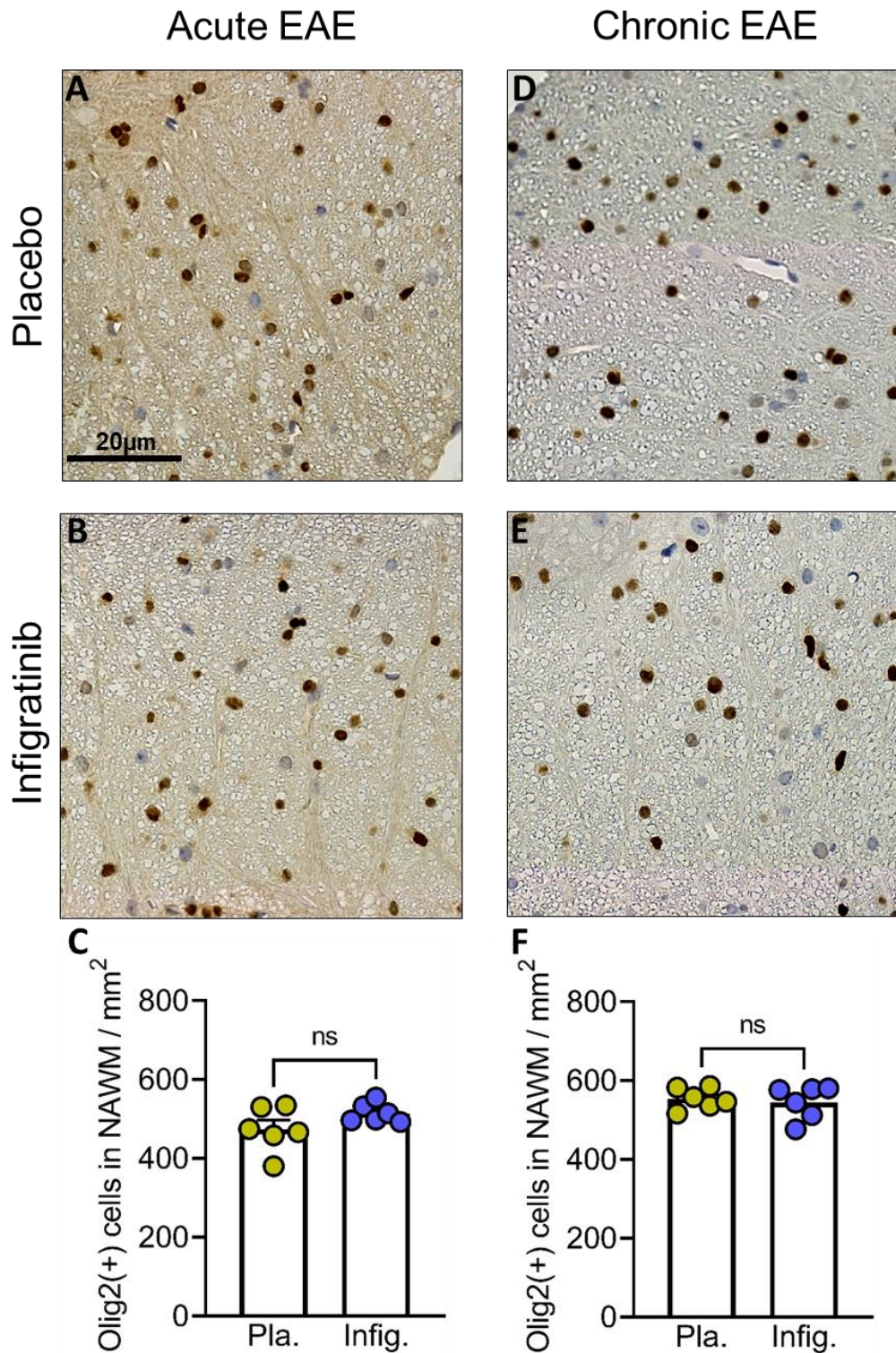


**Figure 23. Oligodendrocyte precursor cell populations in spinal cord NAWM at day 17/41 p.i.** In both acute (A - C) and chronic (D - F) EAE, there was no difference in Olig2(+) OPCs populations in spinal cord NAWM in infiguratinib treated mice compared with the placebo group. (Acute EAE ( $P = 0.1361$ ) (day 17 p.i.), Chronic EAE ( $P = 0.6496$ ) (day 41 p.i.)). Representative images of spinal cord sections are shown. Bar: 20  $\mu\text{m}$ .  $n = 6/\text{group}$ , data are presented as mean  $\pm$  SEM. ns = not significant.



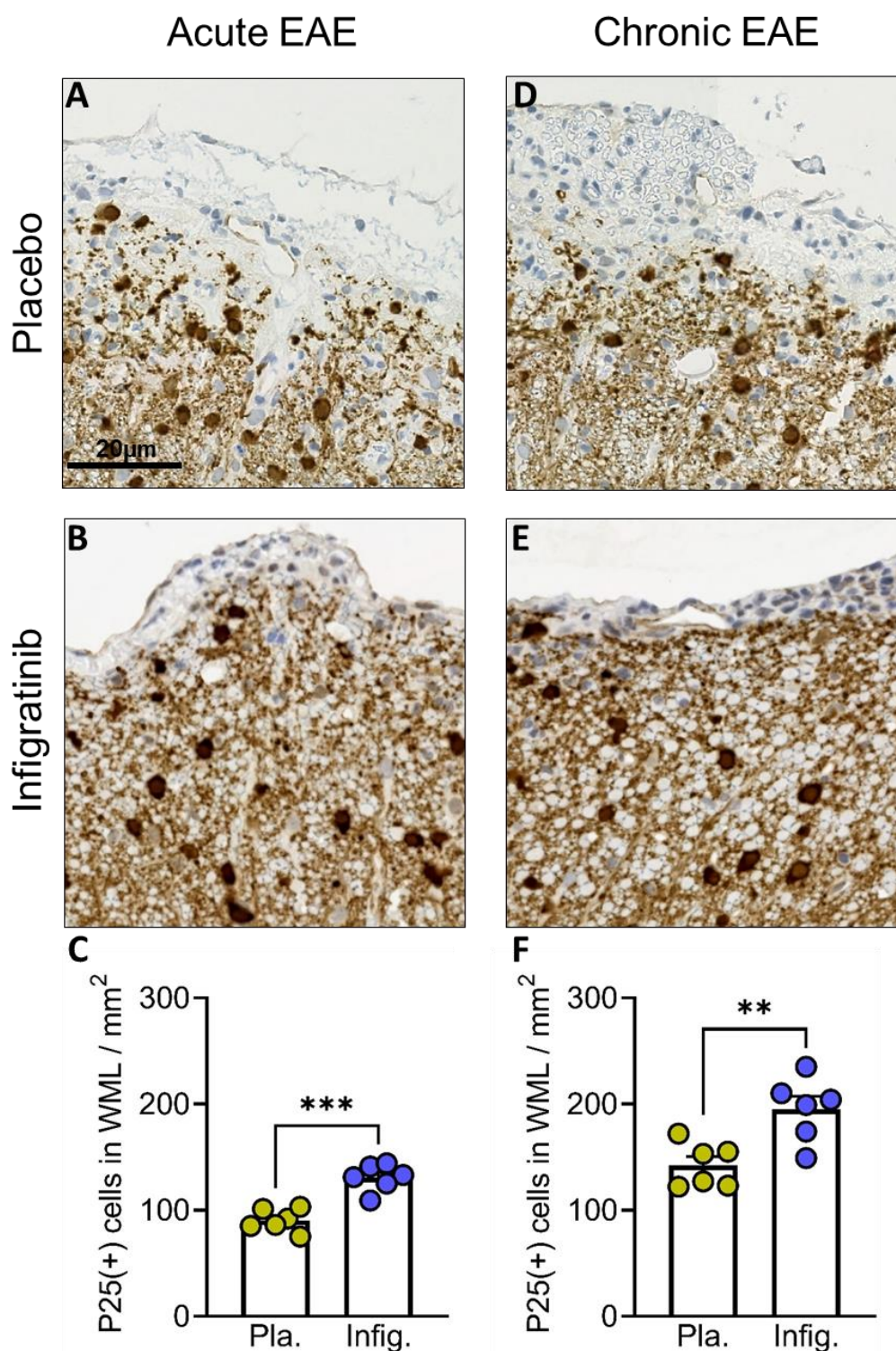


**Figure 24. Mature oligodendrocyte populations in spinal cord WML at day 17/41 p.i.** In both acute (A - C) and chronic (D - F) EAE, increased P25(+) mature oligodendrocytes were observed in spinal cord WML in mice treated with infigratinib (Acute EAE ( $P = 0.0001$ ) (day 17 p.i.), Chronic EAE ( $P = 0.0051$ ) (day 41 p.i.)). Representative images of spinal cord sections are shown. Bar: 20  $\mu\text{m}$ .  $n = 6/\text{group}$ , data are presented as mean  $\pm$  SEM ( $*P < 0.05$ ,  $**P < 0.01$ ,  $***P < 0.001$ ).

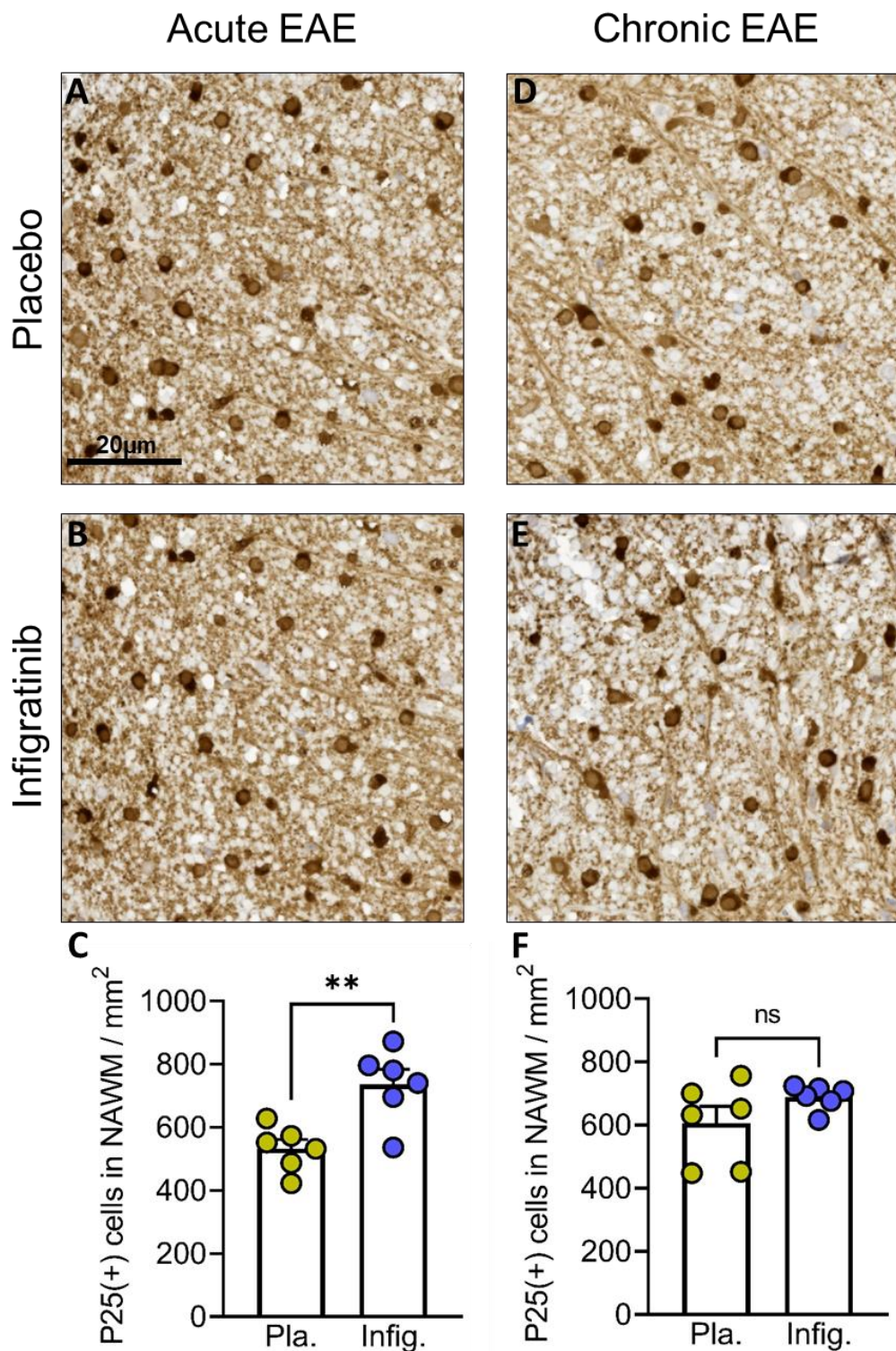


**Figure 25. Mature oligodendrocyte populations in spinal cord NAWM at day 17/41 p.i.** (A - C) In acute EAE (day 17 p.i.), higher P25(+) mature oligodendrocytes ( $P = 0.0040$ ) were observed in spinal cord NAWM in mice treated with infigratinib. (D - F) In chronic EAE (day 41 p.i.), P25(+) mature oligodendrocytes ( $P = 0.1666$ ) populations in spinal cord NAWM were not different between infigratinib and placebo groups. Representative images of spinal cord sections are shown. Bar: 20  $\mu\text{m}$ .  $n = 6/\text{group}$ , data are presented as mean  $\pm$  SEM. ns = not significant ( $*P < 0.05$ ,  $**P < 0.01$ ,  $***P < 0.001$ ).



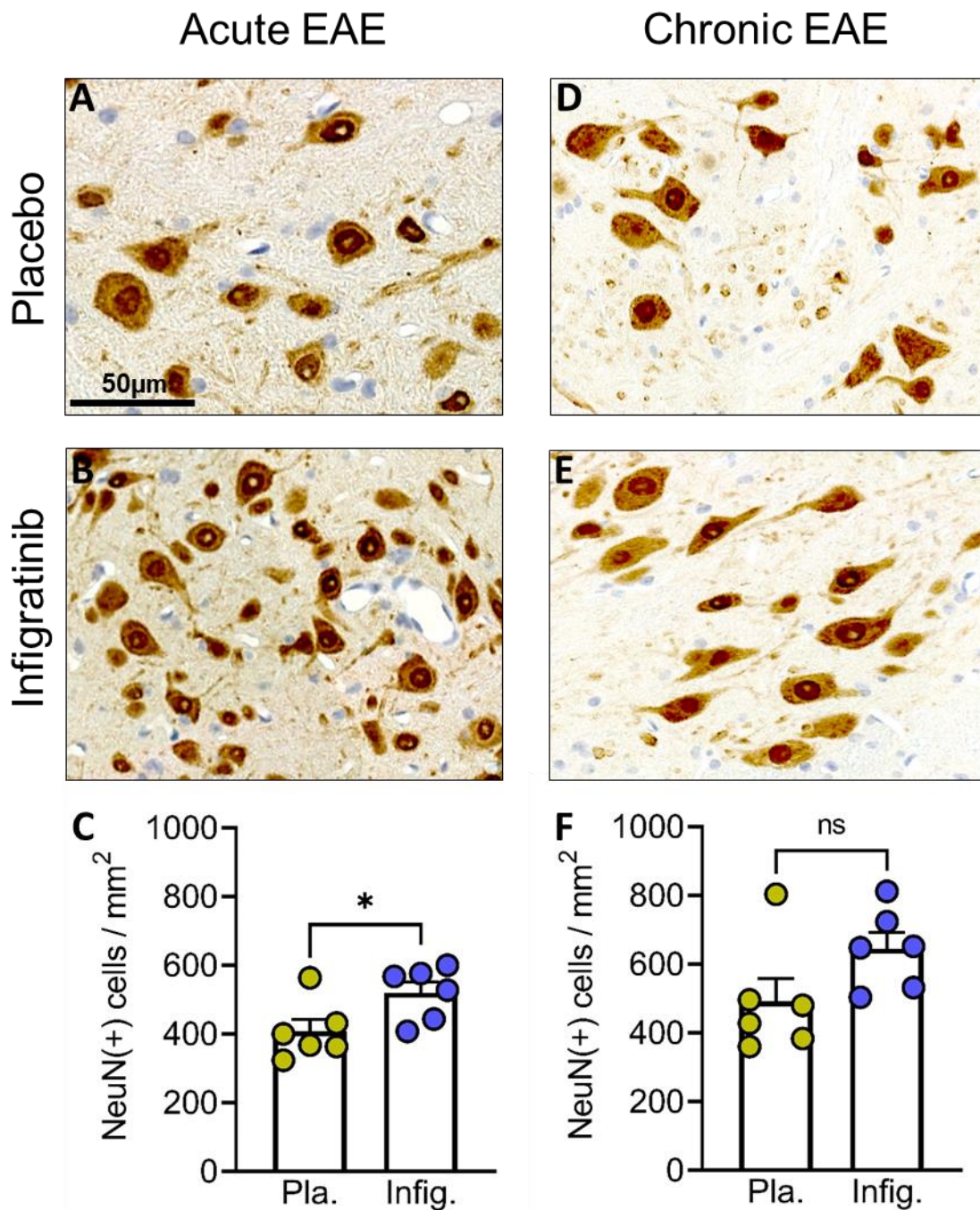


**Figure 26. Motor neuron populations in spinal cord grey matter at day 17/41 p.i.** (A - C) In acute EAE (day 17 p.i.), NeuN(+) motor neuron population ( $P = 0.0378$ ) was higher in spinal cord grey matter in mice treated with infigratinib. (D - F) In chronic EAE (day 41 p.i.), NeuN(+) motor neuron population ( $P = 0.0881$ ) in spinal cord grey matter were not different between infigratinib and placebo groups. Representative images of spinal cord sections are shown. Bar: 50  $\mu\text{m}$ .  $n = 6/\text{group}$ , data are presented as mean  $\pm$  SEM. ns = not significant ( $*P < 0.05$ ,  $**P < 0.01$ ,  $***P < 0.001$ ).

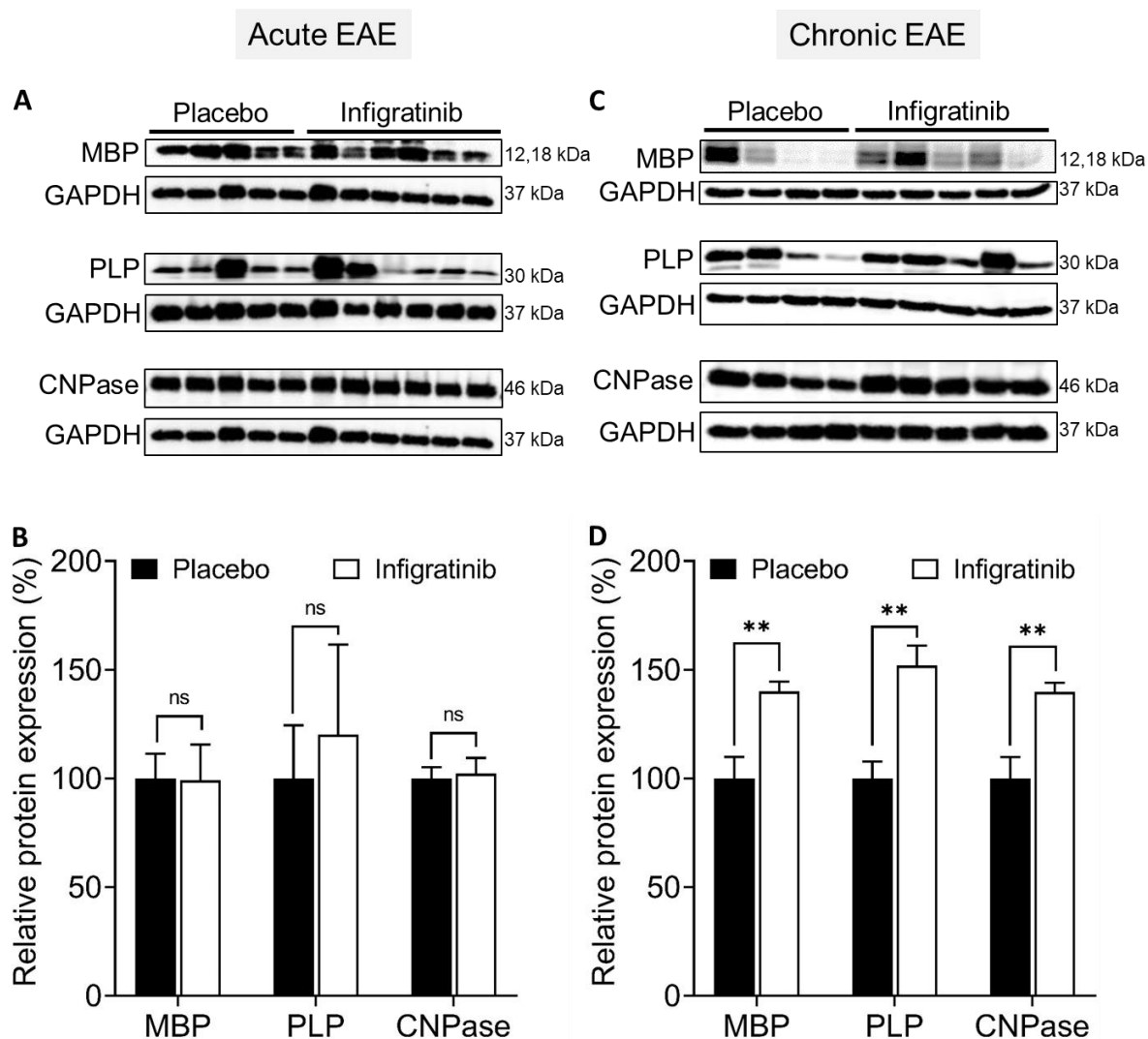


**Figure 27. Myelin protein expression in the spinal cord at at day 17/41 p.i.** (A - B) In acute EAE (day 17 p.i.), MBP ( $P = 0.9702$ ), PLP ( $P = 0.7001$ ), CNPase ( $P = 0.8196$ ) protein expression was not altered in spinal cord of mice treated with infigratinib. (C - D) In chronic EAE (day 41 p.i.), MBP ( $P = 0.0056$ ), PLP ( $P = 0.0041$ ), CNPase ( $P = 0.0048$ ) protein expression was significantly increased in spinal cord of mice treated with infigratinib. Representative western blots for MBP, PLP and CNPase are shown. Acute EAE  $n = 5-6$ /group and chronic EAE  $n = 4-5$ /group. Data are presented as mean  $\pm$  SEM (\* $P < 0.05$ , \*\* $P < 0.01$ , \*\*\* $P < 0.001$ ).

#### **4.2.7 Infigratinib modifies FGFR-dependent signalling and BDNF/ TrkB receptors expression**

To investigate the effects of infigratinib administered on days 0-9 p.i. on FGFR-dependent signalling proteins, BDNF and TrkB receptor in the spinal cord were analyzed by western blot. In the acute phase of EAE (day 17 p.i.) FGFR1 ( $P = 0.0013$ ) and FGFR2 protein expression was downregulated by infigratinib ( $P = 0.0219$ ). There were no effects of infigratinib on expression of FGF2 ( $P = 0.8696$ ), FGF9 ( $P = 0.9554$ ), FGFR downstream molecules pERK ( $P = 0.8295$ ), Akt phosphorylation ( $P = 0.6771$ ) and TrkB receptor ( $P = 0.3959$ ). Expression of BDNF was increased in infigratinib treated mice ( $P = 0.0366$ ) (Figure 28 A-B).

In the chronic phase of EAE (day 41 p.i.), a reduction of FGFR1 ( $P = 0.0432$ ) and FGFR2 protein expression by infigratinib was observed ( $P = 0.0334$ ). Furthermore, infigratinib treatment decreased the expression of FGF2 ( $P = 0.0169$ ), but did not alter FGF9 expression ( $P = 0.8335$ ). MAPK phosphorylation of ERK ( $P = 0.0286$ ) and Akt were increased in infigratinib treated mice ( $P = 0.0301$ ). Whereas BDNF expression was decreased ( $P = 0.0068$ ), TrkB protein expression was increased by infigratinib ( $P = 0.0205$ ) (Figure 29 A-B).

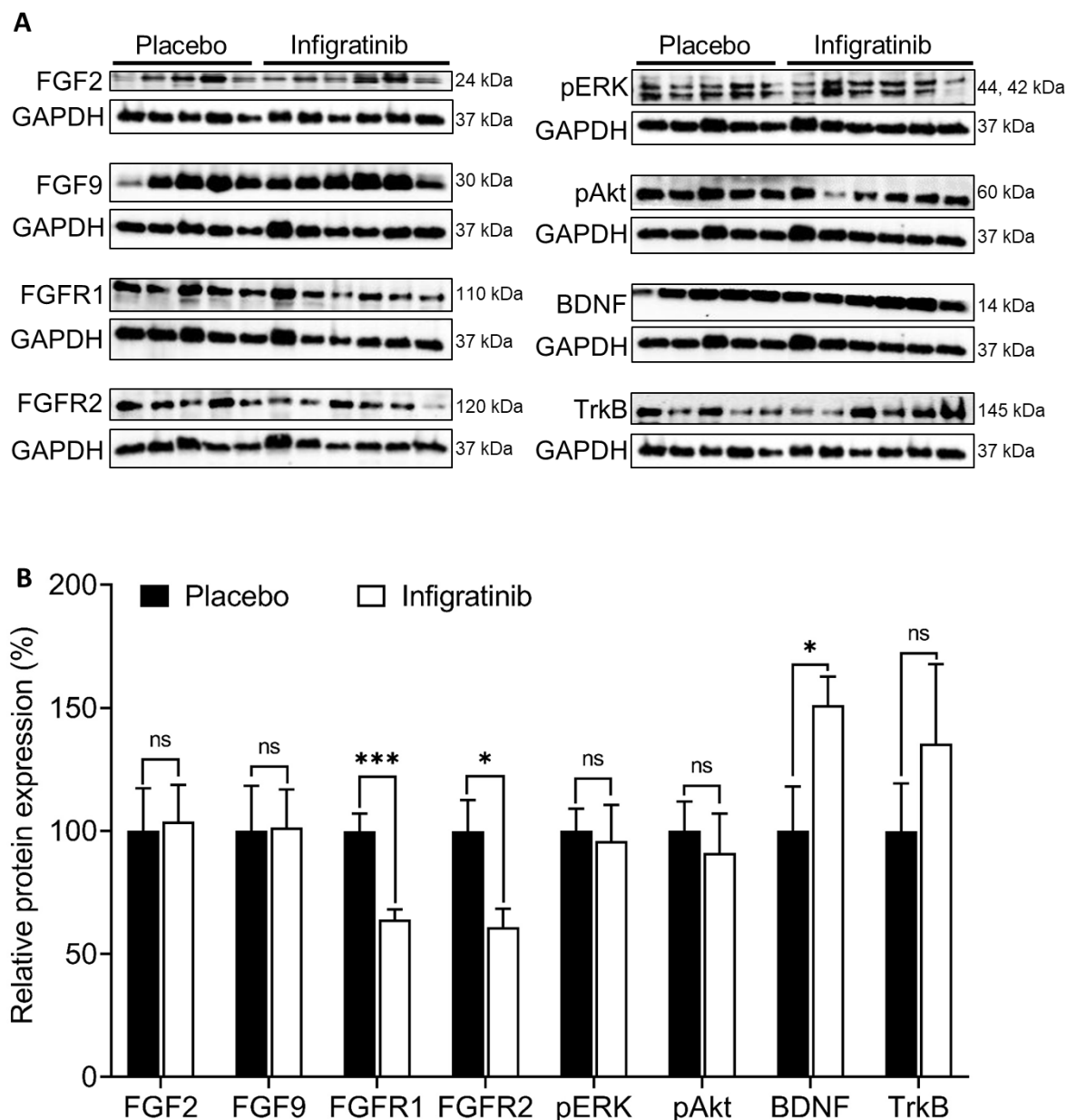


**Figure 28. FGF/FGFR and BDNF/TrkB expression in the spinal cord at day 17 p.i.** (A - B) FGFR1 ( $P = 0.0013$ ) and FGFR2 ( $P = 0.0219$ ) protein expression was downregulated, BDNF ( $P = 0.0366$ ) expression was upregulated in spinal cord of mice treated with infigratinib. There was no regulation of FGF2 ( $P = 0.8696$ ), FGF9 ( $P = 0.9554$ ), pERK ( $P = 0.8295$ ) and pAkt ( $P = 0.6771$ ) and TrkB ( $P = 0.3959$ ). Representative western blots images are shown.  $n = 5-6/\text{group}$ . Data are presented as mean  $\pm$  SEM. ns = not significant ( $*P < 0.05$ ,  $**P < 0.01$ ,  $***P < 0.001$ ).

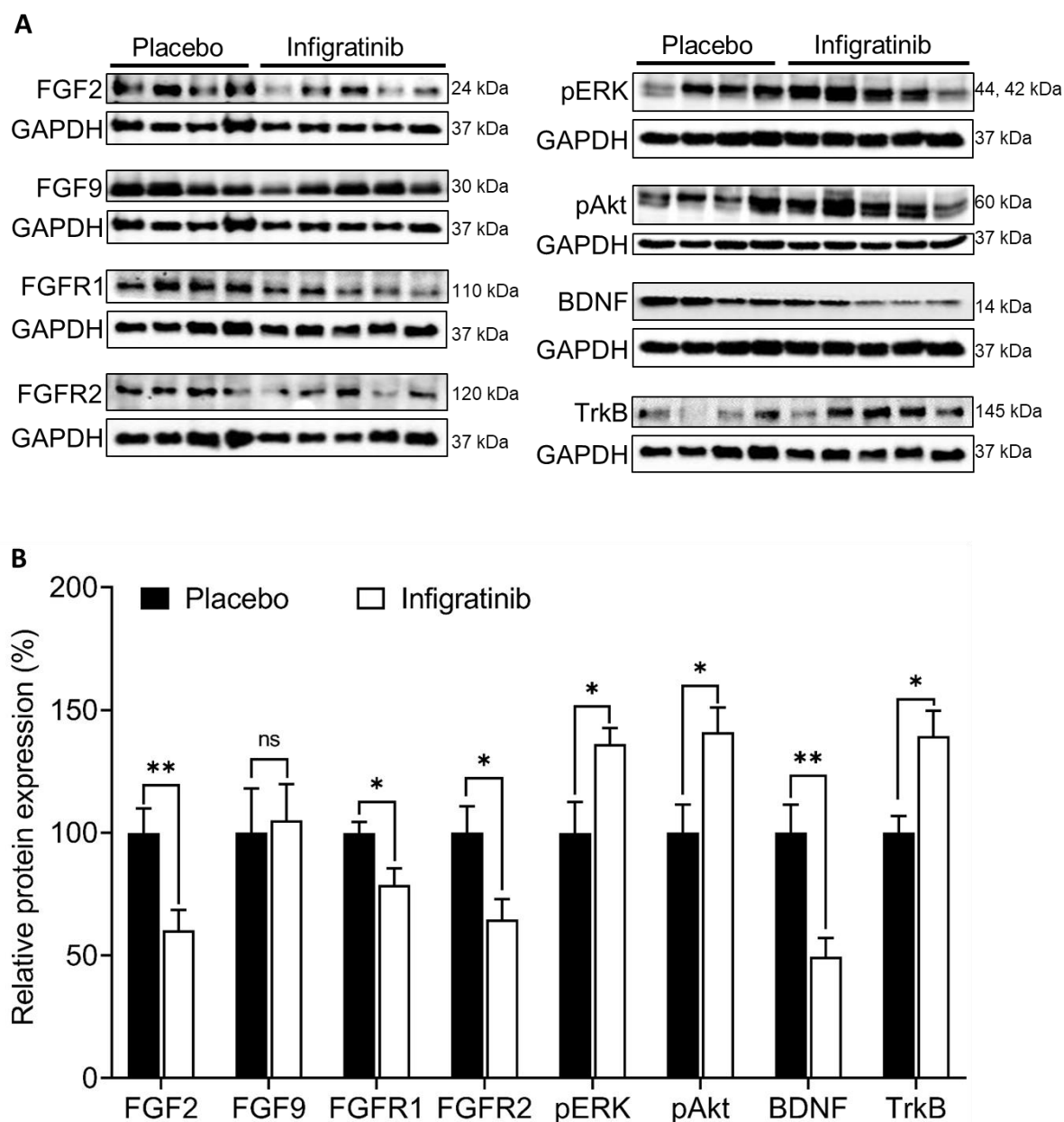


**Figure 29. FGF/FGFR and BDNF/TrkB expression in the spinal cord at day 41 p.i.** (A - B) Protein expression of FGF2 ( $P = 0.0169$ ), FGFR1 ( $P = 0.0432$ ), FGFR2 ( $P = 0.0334$ ), BDNF were downregulated and phosphorylation ERK ( $P = 0.0286$ ), pAkt ( $P = 0.0301$ ) were upregulated in spinal cord of mice treated with infigratinib. There was no regulation of FGF9 ( $P = 0.8335$ ). Representative western blots images are shown.  $n = 4-5$ /group. Data are presented as mean  $\pm$  SEM. ns = not significant (\* $P < 0.05$ , \*\* $P < 0.01$ , \*\*\* $P < 0.001$ ).

### 4.3 Infigratinib applied from the time of onset of EAE disease (Suppressive protocol)

#### 4.3.1 Infigratinib given from day 10-19 p.i. suppresses severity and relapses of MOG<sub>35-55</sub>-induced EAE

To investigate the *in vivo* efficacy of infigratinib in suppressing the severity and relapses of MOG<sub>35-55</sub>-induced EAE, infigratinib was administered from the onset of symptoms (days 10 to 19 p.i.) (Figure 12). Infigratinib treatment resulted in a substantial reduction of severity and relapses from day 12 p.i. to the end of the experiment ( $P < 0.001$ ) (Figure 30 A) and a lower cumulative EAE score ( $P < 0.001$ ) (Figure 30 B). Mean EAE clinical score revealed that application of infigratinib from days 10 to 19 p.i. suppresses the EAE progression with higher efficiency than administered at the time of immunization (days 0 to 9 p.i.). The onset of diseases has not differed between groups ( $P = 0.7716$ , Figure 31 A). Peak EAE scores were less in mice, which had received infigratinib ( $0.79 \pm 0.10$ ) compared to mice on placebo ( $2.52 \pm 0.14$ ) ( $P < 0.001$ , Figure 31 B). At the day 20 p.i. (peak of the disease), 65% of mice on placebo exhibited severe weakness of hindlimbs (EAE scores of  $\geq 2.5$ ), whereas no severe symptoms were observed in mice on infigratinib. At day 42 p.i., 5.3% of mice treated with infigratinib showed mild weakness of hind limbs, whereas 22.2% of mice on placebo exhibited severe weakness of hindlimbs. No differences in body weight were seen between groups (Figure 31 C). Taken together, the results obtained in mice treated infigratinib showed significant amelioration of EAE until the end of the experiment, indicating the sustained effect of infigratinib after treatment termination. Figure 30 A and Table 8 show the summary of the EAE clinical score in placebo and infigratinib treated mice.

**Table 8. Disease severity (Suppression protocol)**

Treatment	No. of mice	EAE clinical scores		
		Disease onset (day)	Maximum score	End of study
Placebo	34	$9.74 \pm 0.20$	3.5	$2.52 \pm 0.14$
Infigratinib	34	$10.06 \pm 0.49$	2.5	$0.80 \pm 0.10$

The efficacy of infigratinib to suppress the severity and relapses in MOG<sub>35-55</sub>-induced EAE, from day 12 p.i. infigratinib treated mice showed a milder disease course till the end of the experiment.



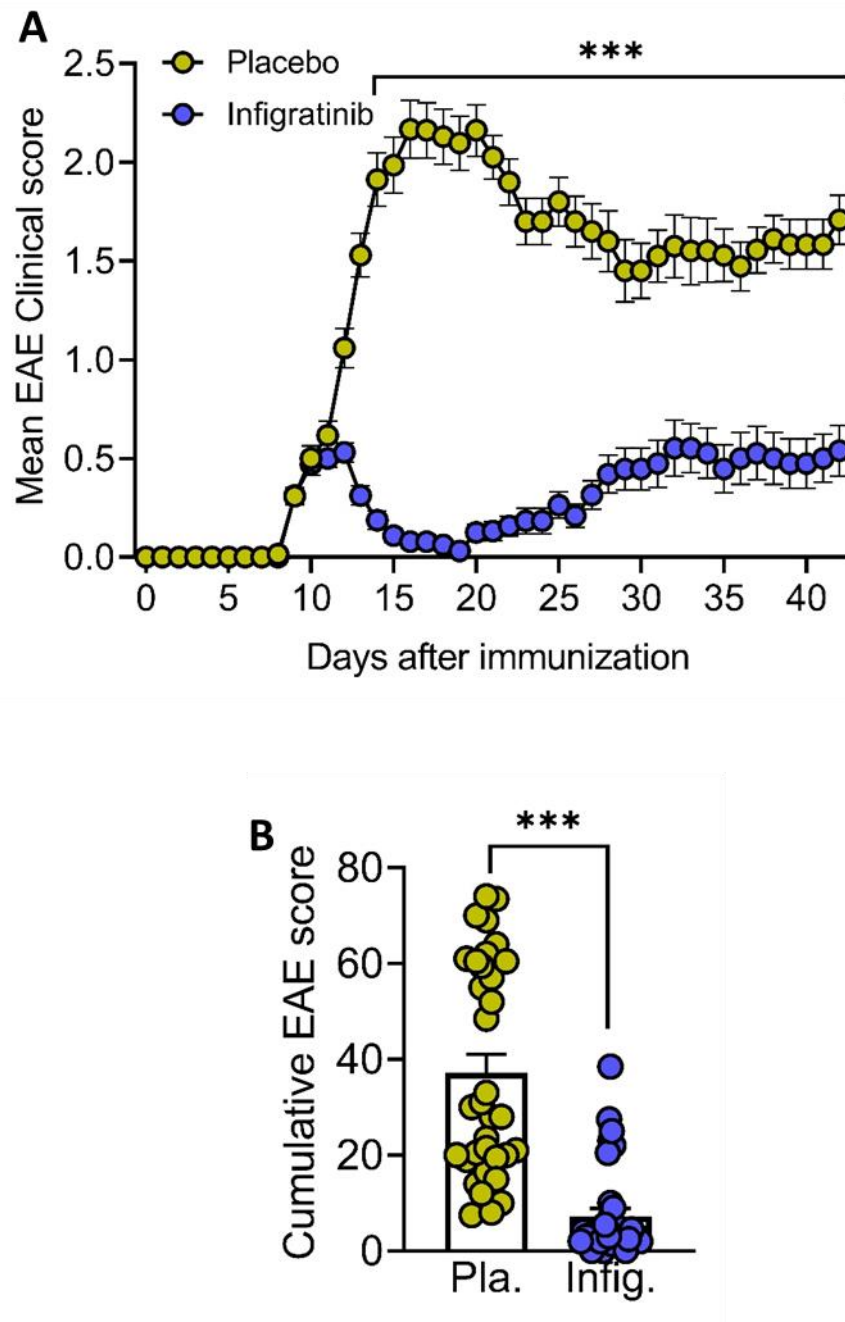


**Figure 30. Infigratinib suppresses the severity of relapses in MOG<sub>35-55</sub>-induced EAE.** A) Infigratinib treated mice exhibited a milder disease course from day 12 until day 42 p.i. B) Cumulative score of chronic EAE until day 42 p.i. was less in infigratinib treated mice ( $P < 0.0001$ ). Infigratinib ( $n = 34$ ) or placebo ( $n = 34$ ), data are presented as mean  $\pm$  SEM ( $*P < 0.05$ ,  $**P < 0.01$ ,  $***P < 0.001$ ).

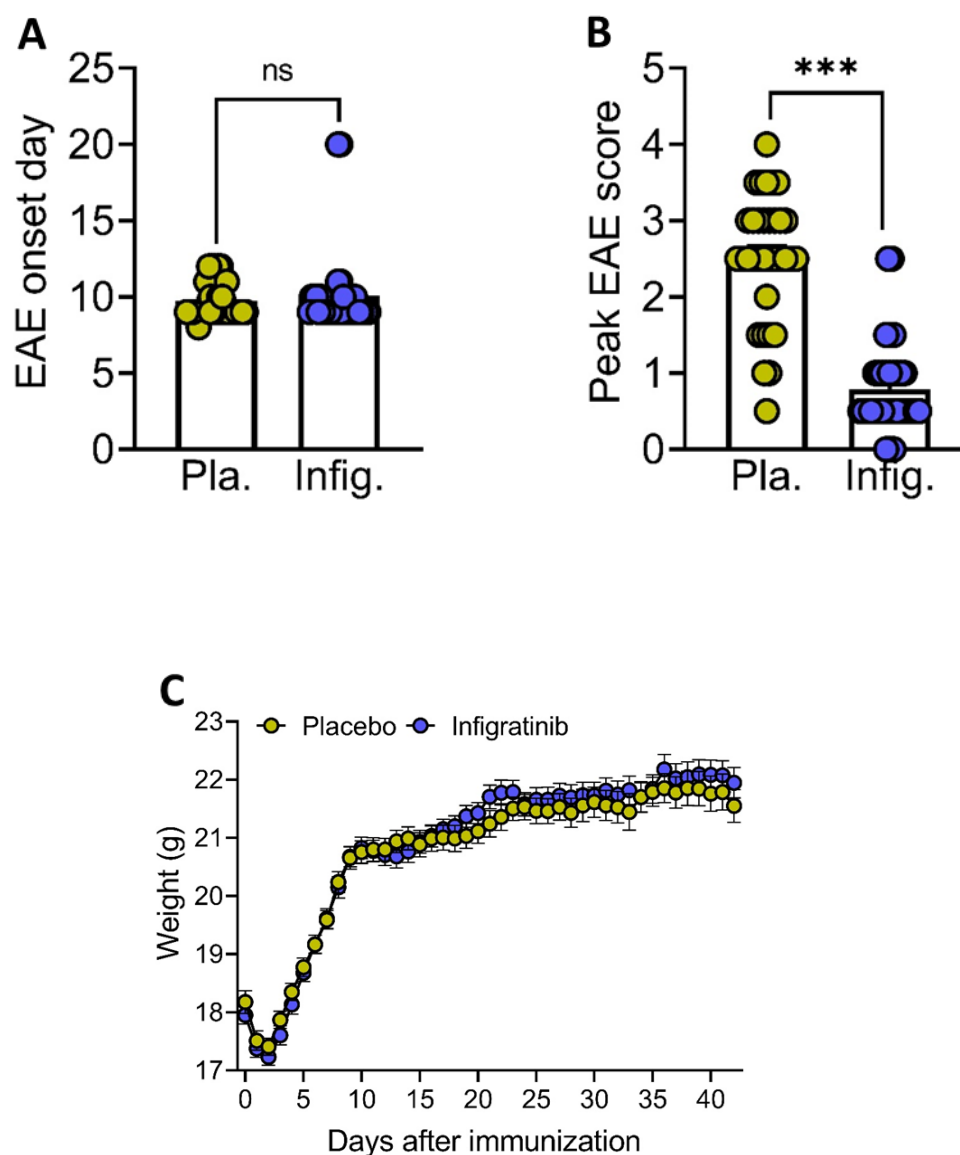


**Figure 31. Effect of infigratinib on EAE onset and body weight.** A) There was no difference in onset of disease between infigratinib and placebo group ( $P = 0.7716$ ). B) The peak EAE scores were less in infigratinib treated mice ( $P < 0.0001$ ). C) There was no difference in body weight between the groups. Infigratinib ( $n = 34$ ) or placebo ( $n = 34$ ), data are presented as mean  $\pm$  SEM ( $*P < 0.05$ ,  $**P < 0.01$ ,  $***P < 0.001$ ).

### 4.3.2 Migration of immune cells into the CNS was reduced by infigratinib

To investigate whether infigratinib administered on days 10-19 p.i. on the accumulation of inflammatory immune cells and composition of different immune cell populations in the spinal cord tissue was analyzed. In the both acute (day 20 p.i.) and chronic phases of EAE (day 42 p.i.), consistent with EAE clinical score infigratinib treated mice showed less inflammation in spinal cord WML (acute  $P < 0.0001$ ; chronic  $P < 0.0001$ ). The level of inflammatory infiltrates of CD3+ T cells (acute  $P < 0.0001$ ; chronic  $P = 0.0001$ ), B220+ B cells (acute  $P < 0.0001$ ; chronic  $P < 0.0001$ ) and activated macrophages/microglia (Mac3+ cells) (acute  $P = 0.0012$ ; chronic  $P < 0.0001$ ) were reduced in spinal cord WML by infigratinib (Figure 32-33).

**Table 9. Immune cell infiltrations (Suppression protocol)**

Pathology	Day 20 p.i.		<i>P</i> -value	Day 42 p.i.		<i>P</i> -value
	Placebo	Infigratinib		Placebo	Infigratinib	
Inflammatory index	2.682 ± 0.2309	0.1700 ± 0.008563	< 0.0001	2.325 ± 0.2746	0.4517 ± 0.08031	< 0.0001
CD3(+) T cells	606.1 ± 74.06	27.07 ± 8.891	< 0.0001	592.2 ± 87.32	56.58 ± 6.144	0.0001
B220(+) B cells	928.1 ± 121.9	31.13 ± 10.29	< 0.0001	478.2 ± 47.07	41.15 ± 5.001	< 0.0001
Mac3(+) macrophages/microglia	1429 ± 301.6	68.47 ± 32.91	0.0012	753.1 ± 33.75	144.7 ± 12.39	< 0.0001

Quantification of immune cell infiltration of T cells, B cells and macrophages in the spinal cord WML of placebo or infigratinib treated mice in acute (day 20 p.i.) and chronic phase of EAE (day 42 p.i.). Data are presented as mean ± SEM. Histology and IHC analysis was performed blinded to the treatment group.

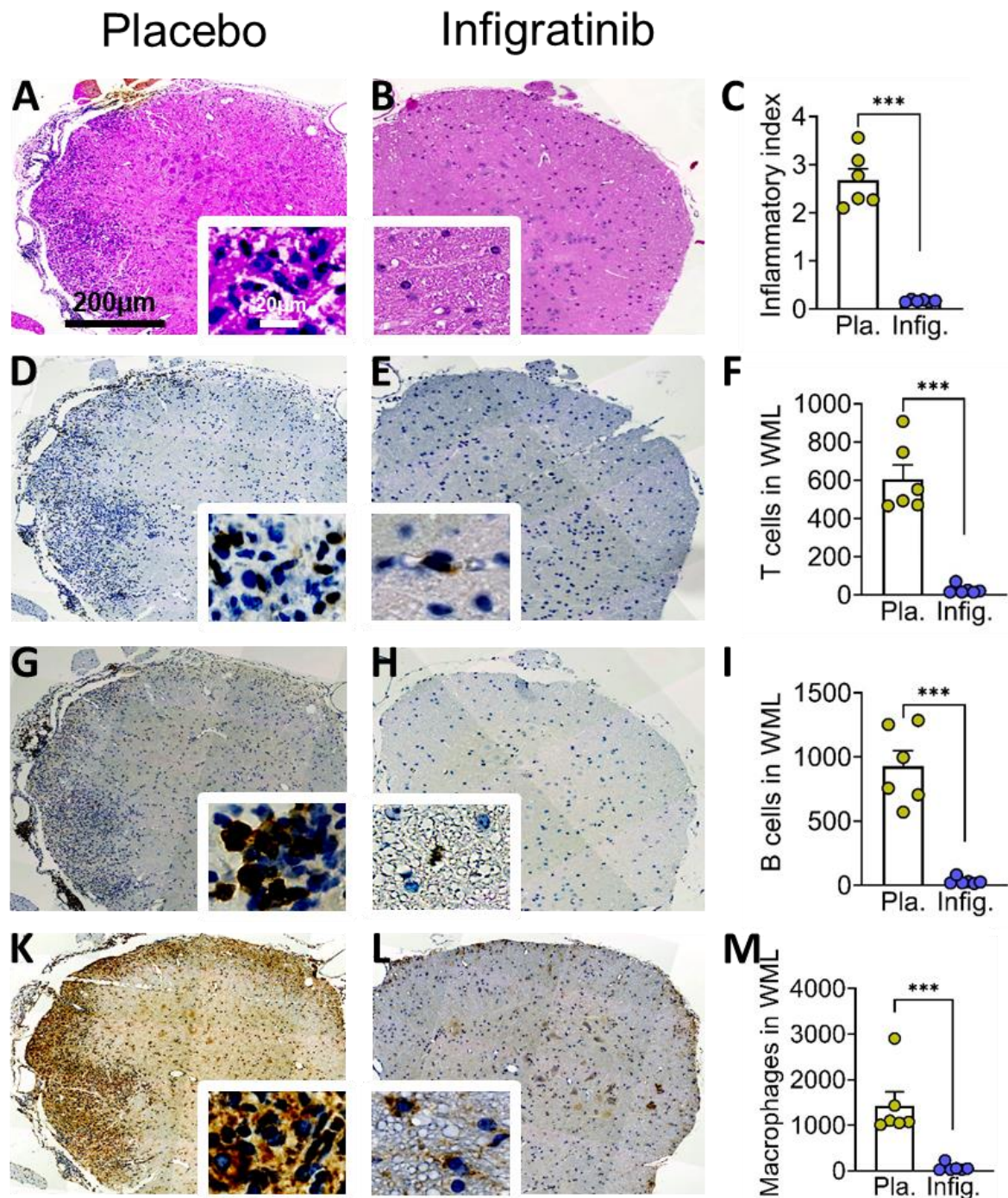


**Figure 32. Inflammation and immune cell infiltration in spinal cord WML at day 20 p.i.** The inflammatory index (A - C) was less in infigratinib treated mice compared to placebo ( $P < 0.0001$ ). The number of CD3(+) T cells ( $P < 0.0001$ ) (D - F), B220(+) B cells ( $P < 0.0001$ ) (G - I) and Mac3(+) macrophages ( $P = 0.0012$ ) (K - M) per  $\text{mm}^2$  were reduced by infigratinib. Representative images of spinal cord sections are shown. Bar: 200  $\mu\text{m}$ , 20  $\mu\text{m}$  (insert).  $n = 6/\text{group}$ , data are presented as mean  $\pm$  SEM (\* $P < 0.05$ , \*\* $P < 0.01$ , \*\*\* $P < 0.001$ ).



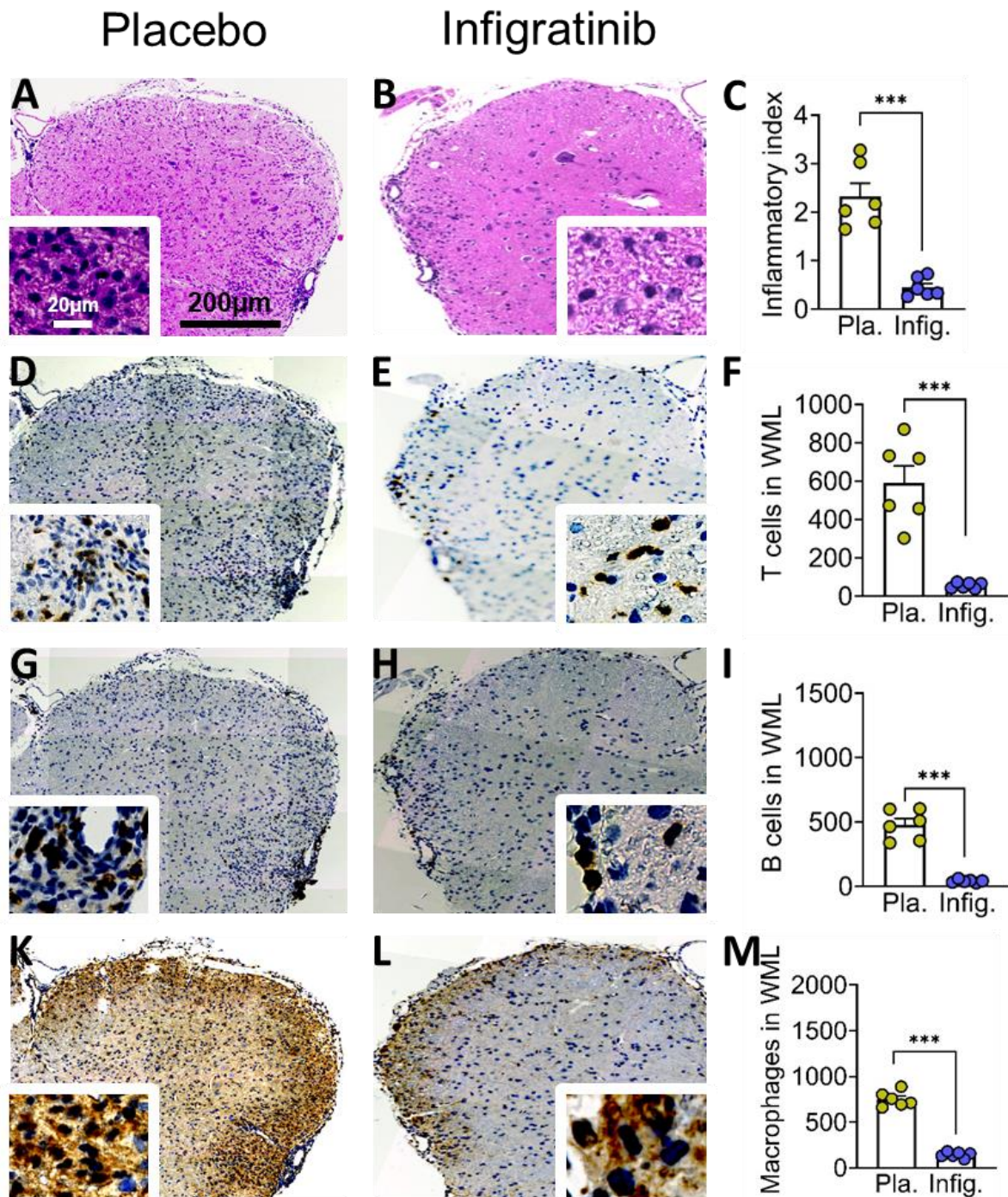


**Figure 33. Inflammation and immune cell infiltration in spinal cord WML at day 42 p.i.** The inflammatory index (A - C) was less in mice treated with infigratinib ( $P < 0.0001$ ). The number of CD3(+) T cells ( $P = 0.0001$ ) (D - F), B220(+) B cells ( $P < 0.0001$ ) (G - I) and Mac3(+) macrophages ( $P < 0.0001$ ) (K - M) per  $\text{mm}^2$  were reduced by infigratinib. Representative images of spinal cord sections are shown. Bar: 200  $\mu\text{m}$ , 20  $\mu\text{m}$  (insert).  $n = 6/\text{group}$ , data are presented as mean  $\pm$  SEM (\* $P < 0.05$ , \*\* $P < 0.01$ , \*\*\* $P < 0.001$ ).

### 4.3.3 Pro-inflammatory cytokine changes induced by infogratinib

To investigate whether inhibition of FGFR with infogratinib administered on days 10-19 p.i. could suppress the mRNA expression of pro-inflammatory cytokines and chemokines were analyzed in the spinal cord by RT-PCR. In the acute phase of EAE (day 20 p.i.), infogratinib treatment significantly downregulated pro-inflammatory cytokine IL1 $\beta$  ( $P = 0.0255$ ) and TNF $\alpha$  ( $P = 0.0322$ ) compared to placebo. Infogratinib did not affect the mRNA expression levels of IL6 ( $P = 0.7508$ ), IL12 ( $P = 0.2386$ ), iNOS ( $P = 0.0790$ ) and chemokine CX3CL1 ( $P = 0.4895$ ) and CXC3R1 ( $P = 0.7424$ ) expression were observed (Figure 34 A).

In the chronic phase of EAE (day 42 p.i.), the mRNA expression levels of IL12 ( $P = 0.0297$ ) and TNF $\alpha$  ( $P = 0.0384$ ) were downregulated by infogratinib and no effect of infogratinib on IL1 $\beta$  ( $P = 0.6854$ ), IL6 ( $P = 0.8340$ ), iNOS ( $P = 0.1523$ ) and chemokine CX3CL1 ( $P = 0.5265$ ) and CXC3R1 ( $P = 0.4601$ ) expression were observed (Figure 34 B).

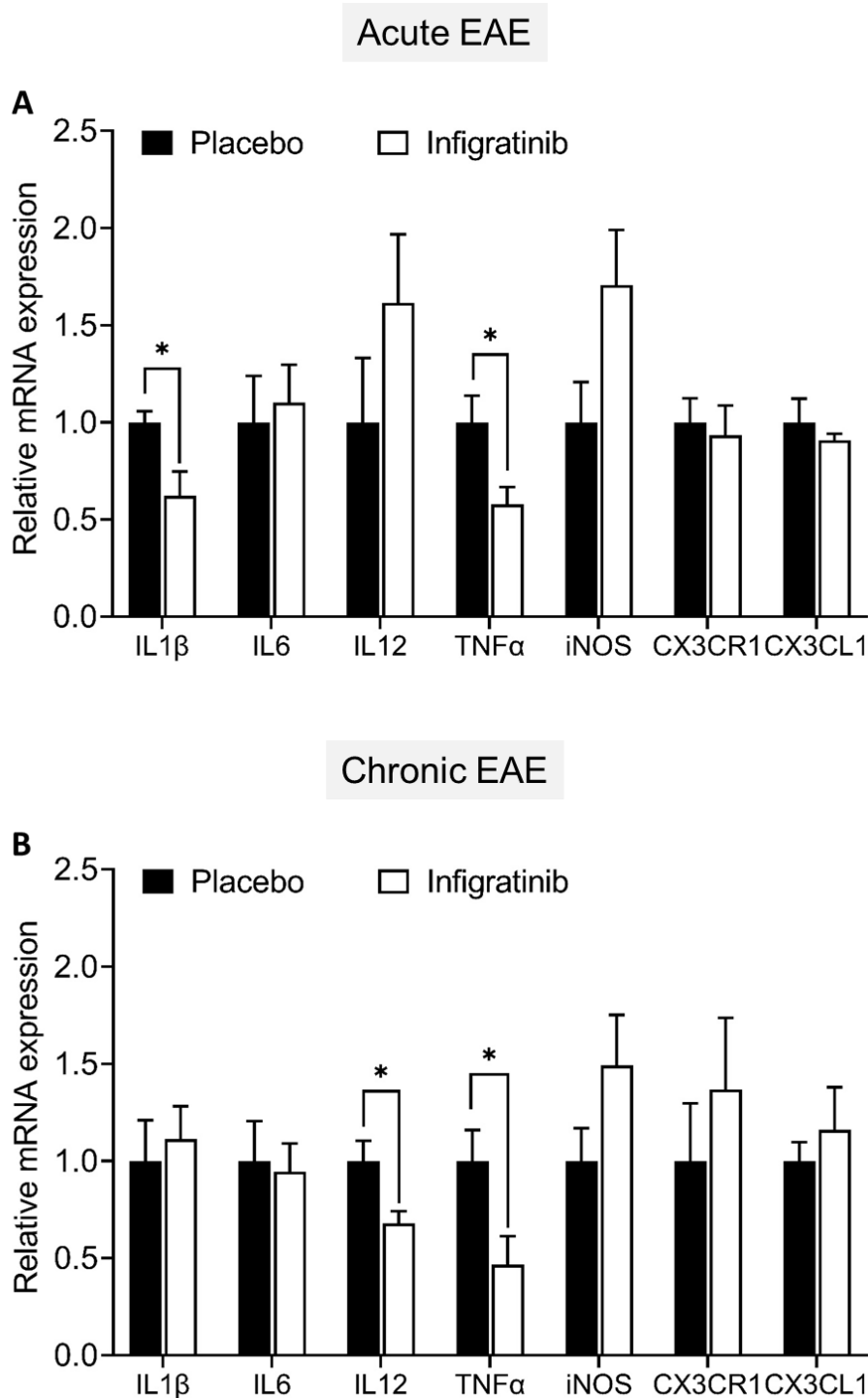


**Figure 34. Relative mRNA expression of pro-inflammatory cytokines/chemokines in spinal cord at day 20/42 p.i.** Findings at the acute EAE (A) and the chronic EAE (B) are shown. In acute EAE (day 20 p.i.), decreased mRNA expression of IL1 $\beta$  and TNF $\alpha$  was observed in mice treated with infigratinib. There were no differences in IL6, IL12, iNOS and chemokine (CX3CL1 and CX3CR1) levels in the acute EAE. In the chronic EAE (day 42 p.i.), decreased IL12 and TNF $\alpha$  mRNA expression were observed in infigratinib treated mice compared with placebo. There were no differences in IL1 $\beta$ , IL12, iNOS and chemokine (CX3CL1 and CX3CR1) levels in the chronic EAE. Acute and chronic EAE  $n = 5$ /group. Data are presented as mean  $\pm$  SEM (\* $P < 0.05$ , \*\* $P < 0.01$ , \*\*\* $P < 0.001$ ).

#### 4.3.4 Infigratinib decreases demyelination and increases axonal density

We investigated the administration of infigratinib on days 10-19 p.i. on demyelination and axonal density in the spinal cord by histological LFB/PAS and Bielschowsky staining. In both acute (day 20 p.i.) and chronic phases (day 42 p.i.) of EAE, histological staining revealed significantly less demyelination and higher axonal density in spinal cord WML in infigratinib treated mice compared to placebo (Figure 35-36). This demyelination and axonal density were observed at the same site of inflammation. We performed MBP immunostaining to confirm the results achieved with the LFB/PAS staining. Figure 35-36 and Table 10 show the summary of demyelination and axonal density in placebo and infigratinib treated mice.

**Table 10. Demyelination and axonal density (Suppression protocol)**

Pathology	Acute EAE		<i>P</i> -value	Chronic EAE		<i>P</i> -value
	Placebo	Infigratinib		Placebo	Infigratinib	
Demyelination (%) (LFB/PAS)	38.49 ± 3.95	3.56 ± 0.10	< 0.0001	34.60 ± 4.02	7.90 ± 0.75	< 0.0001
Demyelination (%) (MBP)	18.55 ± 1.17	3.25 ± 0.60	< 0.0001	14.43 ± 2.40	6.82 ± 1.46	0.0219
Axonal density %	34.32 ± 2.51	94.77 ± 6.92	< 0.0001	32.29 ± 5.20	87.64 ± 5.02	< 0.0001

Quantification of demyelination (LFB/PAS and MBP) and axonal density (Bielschowsky staining) in the spinal cord of placebo and infigratinib treated mice in acute (day 20 p.i.) and chronic phase of EAE (day 42 p.i.). Data are presented as mean ± SEM. Histology and IHC analysis was performed blinded to the treatment group.

#### 4.3.5 Expression of inhibitor of remyelination.

The effects of infigratinib on remyelination inhibitor in the spinal cord were identified by RT-PCR. Infigratinib didn't alter the remyelination inhibitor TGFβ, SEMA3A and Lingo-1 mRNA expression in both acute and chronic phases of EAE (Figure 37 A-B).



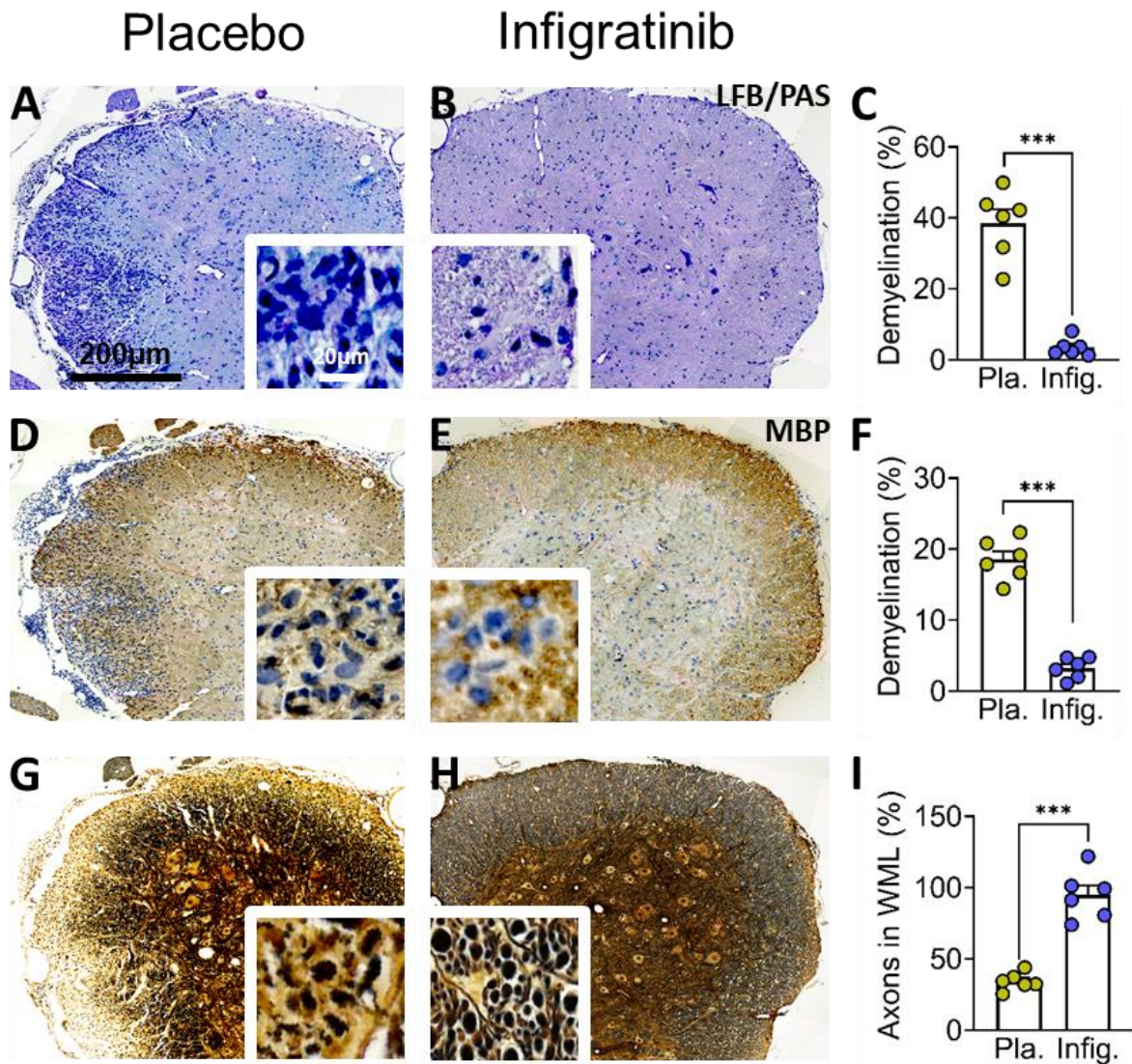


**Figure 35. Effects of infigratinib on demyelination and axonal density in the spinal cord at day 20 p.i.** The percentage of demyelination (LFB/PAS staining (A - C):  $P < 0.0001$ ; IHC MBP staining (D - F):  $P < 0.0001$ ) was less in spinal cord WML in mice treated with infigratinib than placebo. The percentage of axonal density in spinal cord WML (G - I) was higher in infigratinib treated mice than in placebo ( $P < 0.0001$ ). Representative images of spinal cord sections are shown. Bar: 200 µm.  $n = 6$ /group, data are presented as mean  $\pm$  SEM ( $*P < 0.05$ ,  $**P < 0.01$ ,  $***P < 0.001$ ).

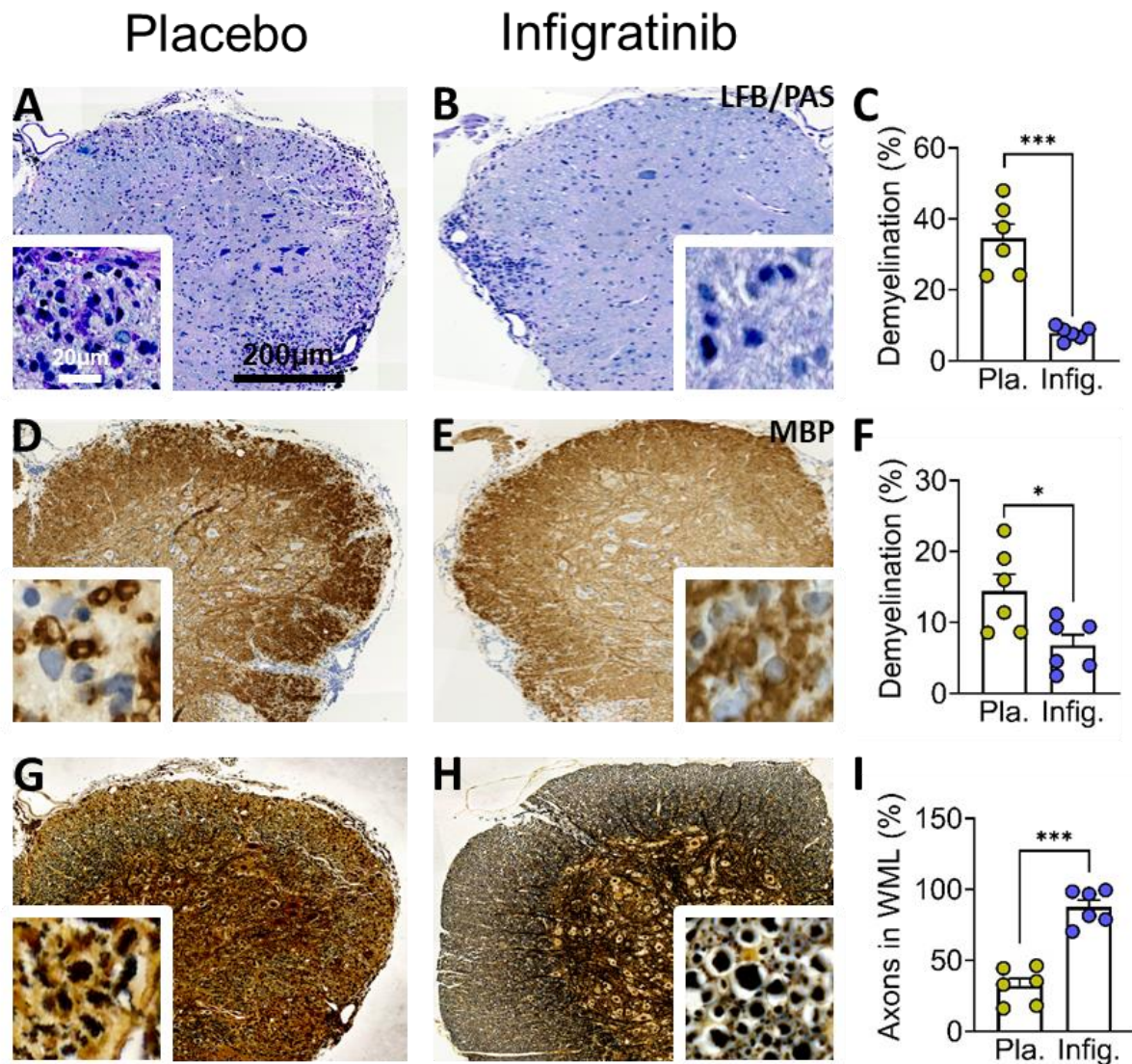


**Figure 36. Effect of infigratinib on demyelination and axonal density in the spinal cord at day 42 p.i.** The percentage of demyelination (LFB/PAS staining (A - C):  $P < 0.0001$ ; IHC MBP staining (D - F):  $P = 0.0219$ ) was less in spinal cord WML in mice treated with infigratinib. The percentage of axonal density in spinal cord WML (G - I) was higher in infigratinib treated mice than in placebo ( $P < 0.0001$ ). Representative images of spinal cord sections are shown. Bar: 200  $\mu\text{m}$ .  $n = 6/\text{group}$ , data are presented as mean  $\pm$  SEM ( $*P < 0.05$ ,  $**P < 0.01$ ,  $***P < 0.001$ ).

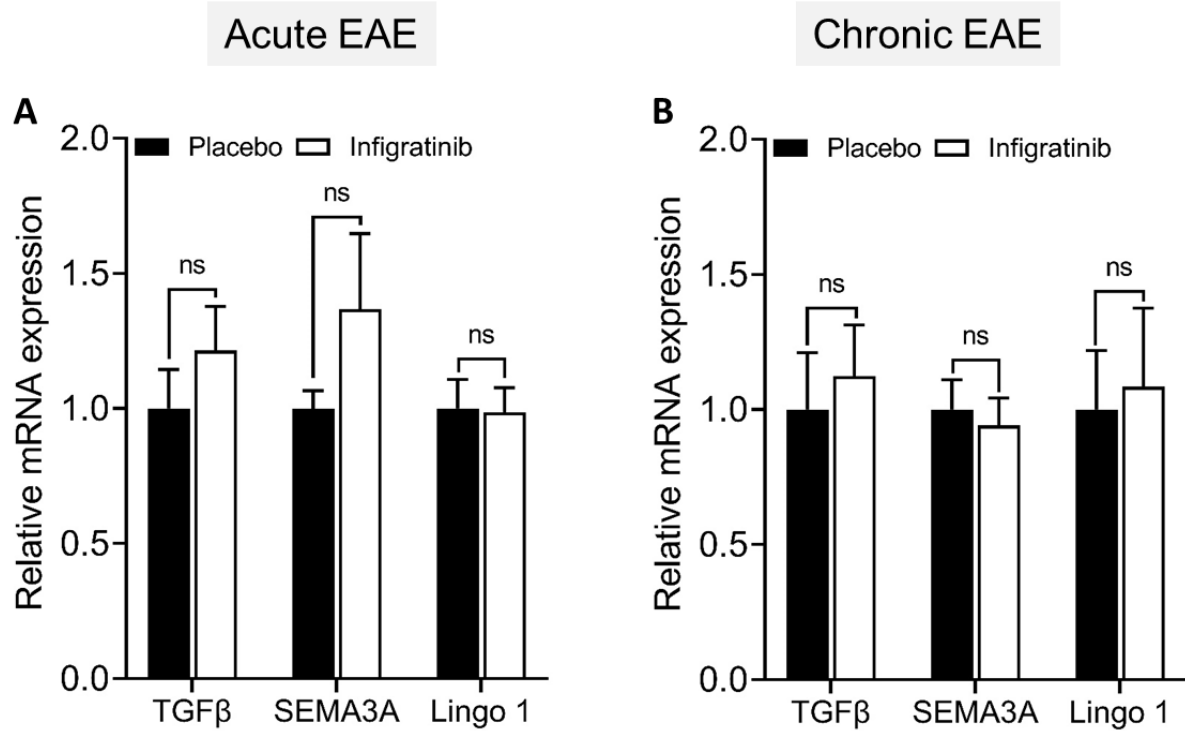


**Figure 37. Relative mRNA expression of remyelination inhibitors in spinal cord at day 20/42 p.i.** There was no regulation of remyelination inhibitors mRNA expression in both acute (A) and chronic EAE (B). (Acute EAE (day 20 p.i.): TGFβ ( $P = 0.3525$ ), SEMA3A ( $P = 0.2359$ ), Lingo-1 ( $P = 0.9246$ ); chronic EAE (day 42 p.i.): TGFβ ( $P = 0.6720$ ), SEMA3A ( $P = 0.7067$ )). Acute and chronic EAE  $n = 5$ /group, ns = not significant. Data are presented as mean  $\pm$  SEM.

### 4.3.6 Infigratinib enhances the number of mature oligodendrocytes, motor neurons and myelin protein expression

We next evaluated the consequences of infigratinib administered on days 10-19 p.i. on oligodendroglial lineage cells, motor neuron population in the spinal cord was analyzed by immunostaining. In both acute (day 20 p.i.) and chronic phase of EAE (day 42 p.i.), immunostaining showed a notable increase of P25(+) mature oligodendrocytes density in spinal cord normal-appearing white matter (NAWM) and white matter lesion (WML) area in the spinal cord of mice treated with infigratinib (Figure 40-41). There were no variation in OPCs numbers in spinal cord NAWM and WML between infigratinib treated mice and placebo (Figure 38-39). A significant increase of NeuN(+) motor neuron density was observed in infigratinib treated mice spinal cord grey matter (Figure 42).

In acute phase of EAE (day 20 p.i.), western blot analyses revealed that expression of myelin protein MBP ( $P = 0.0072$ ) and PLP ( $P = 0.0450$ ) were increased in spinal cord lysate of mice treated with infigratinib (Figure 43 A-B). Infigratinib treatment did not change the myelin protein expression over placebo in chronic phase of EAE (day 42 p.i.) (Figure 43 C-D).

**Table 11. Oligodendrocyte population (Suppression protocol)**

Cell types	Day 20 p.i.		<i>P</i> -value	Day 42 p.i.		<i>P</i> -value
	Placebo	Infigratinib		Placebo	Infigratinib	
Olig2(+) cells NAWM	457.7 ± 16.29	472.0 ± 31.85	0.6971	514.0 ± 16.46	514.5 ± 28.44	0.9882
Olig2(+) cells WML	372.5 ± 36.44	413.5 ± 56.82	0.5571	410.2 ± 27.75	422.8 ± 26.10	0.7464
P25(+) cells NAWM	462.7 ± 19.07	881.3 ± 49.17	< 0.0001	535.5 ± 28.62	684.3 ± 59.11	0.0469
P25(+) cells WML	73.00 ± 5.66	202.0 ± 14.56	< 0.0001	111.5 ± 4.48	192.0 ± 8.76	< 0.0001
NeuN(+) motor neurons in grey matter	440.7 ± 21.28	703.3 ± 66.32	0.0037	354.0 ± 23.64	549.3 ± 20.47	< 0.0001

Quantification of Olig2(+) OPCs, P25(+) mature oligodendrocytes in the spinal cord WML and NAWM of placebo or infigratinib treated mice in acute and chronic phases of EAE. NeuN(+) motor neurons in the spinal cord grey matter of placebo or infigratinib treated mice in acute and chronic phase of EAE. Data are presented as mean ± SEM. IHC analysis was performed blinded to the treatment group.



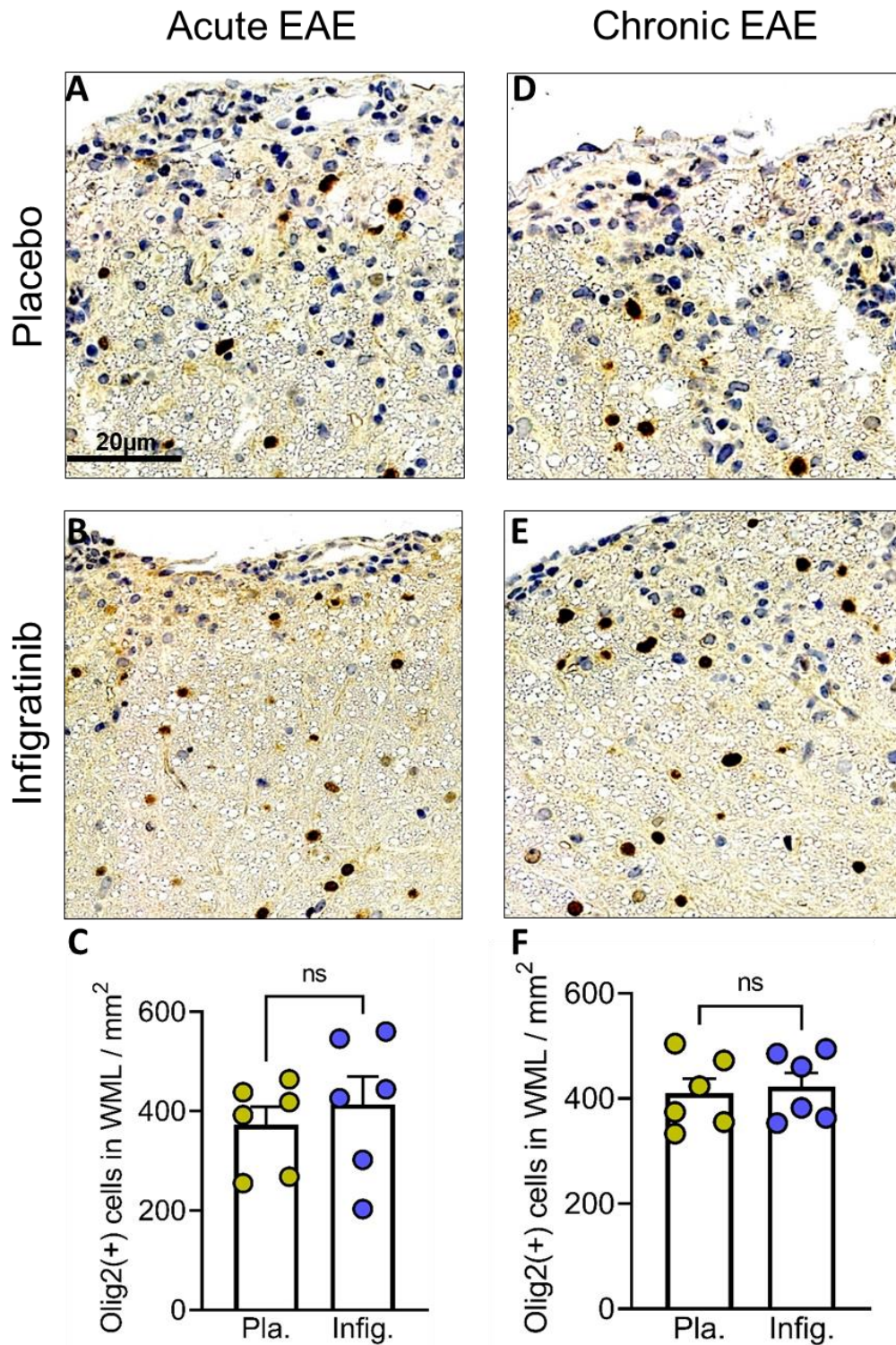


**Figure 38. Oligodendrocyte precursor cell populations in spinal cord WML at day 20/42 p.i.** In both acute (A - C) and chronic (D - F) EAE, no difference of Olig2(+) OPCs populations in infigratinib treated mice compared with placebo (Acute EAE (day 20 p.i.) ( $P = 0.5571$ ), Chronic EAE (day 20 p.i.) ( $P = 0.7464$ )). Representative images of spinal cord sections are shown. Bar: 20  $\mu$ m.  $n = 6$ /group, ns = not significant. Data are presented as mean  $\pm$  SEM.

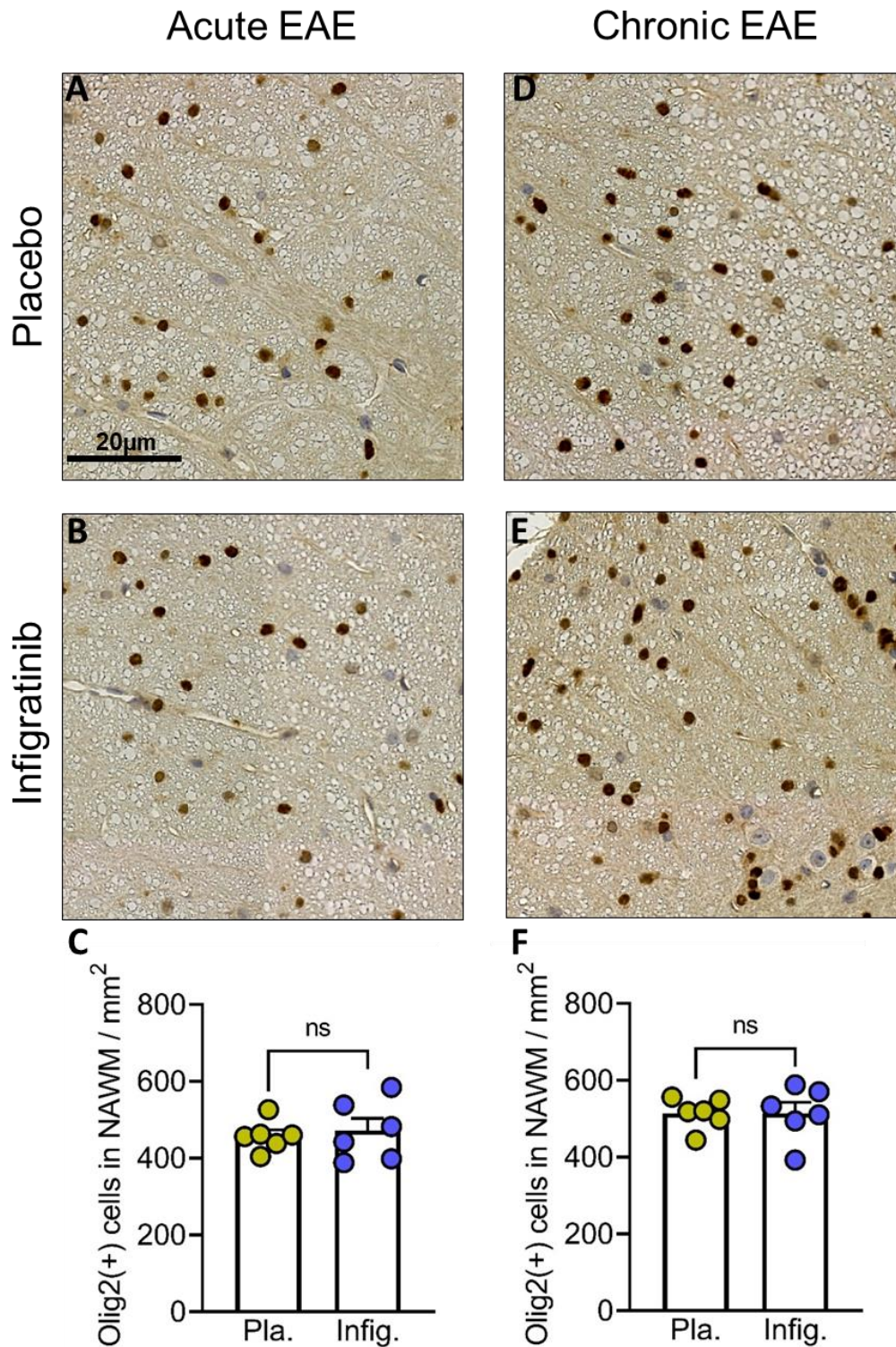


**Figure 39. Oligodendrocyte precursor cell populations in spinal cord NAWM at day 20/42 p.i.** In both acute (A - C) and chronic (D - F) EAE, no difference of Olig2(+) OPCs populations in infigratinib treated mice compared with placebo (acute EAE (day 20 p.i.) ( $P = 0.6971$ ), chronic EAE (day 42 p.i.) ( $P = 0.9882$ )). Representative images of spinal cord sections are shown. Bar: 20  $\mu$ m.  $n = 6$ /group, ns = not significant. Data are presented as mean  $\pm$  SEM.



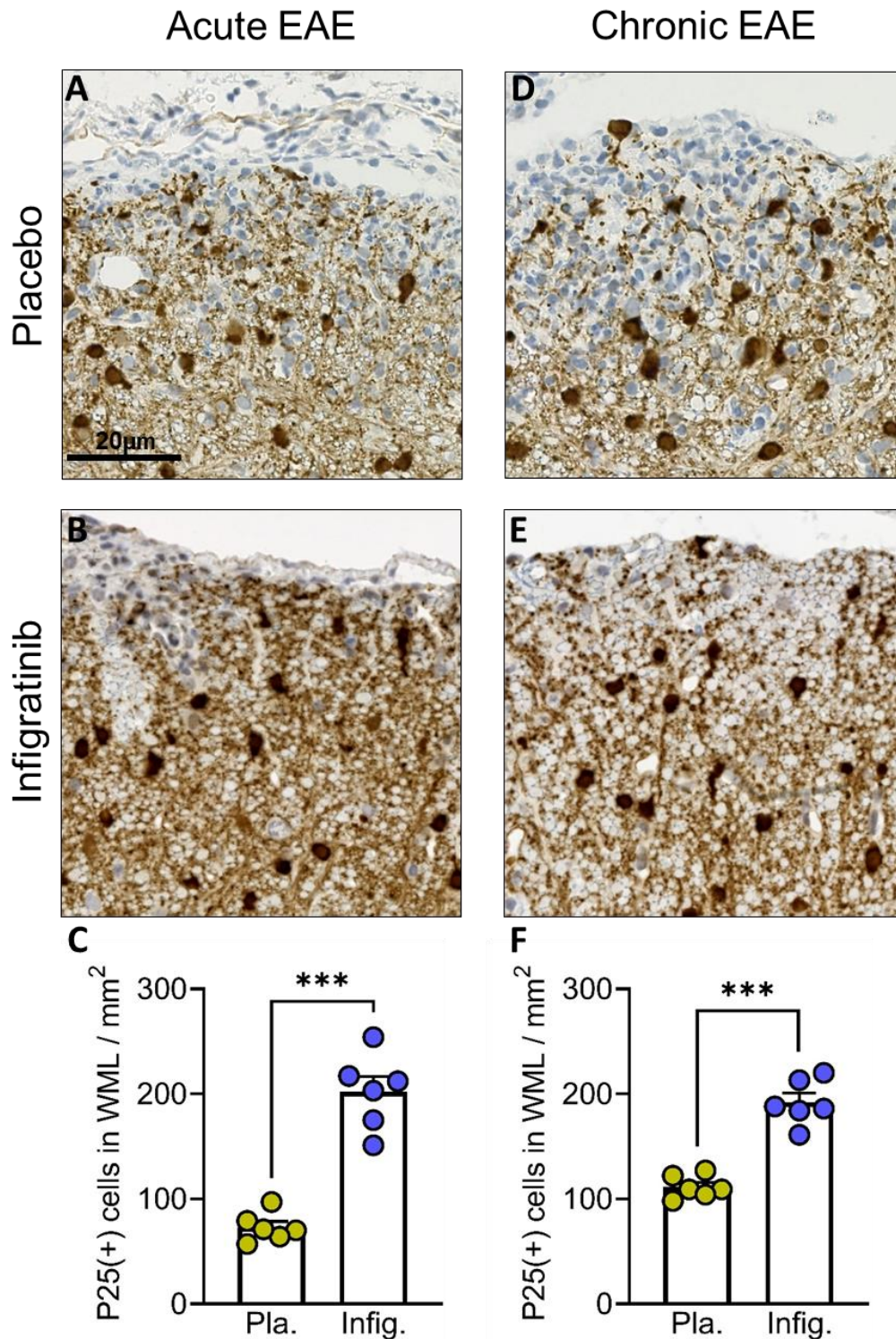


**Figure 40. Mature oligodendrocyte populations in spinal cord WML at day 20/42 p.i.** In both acute (A - C) and chronic (D - F) EAE, increased P25(+) mature oligodendrocytes were observed in spinal cord WML in mice treated with infigratinib (acute EAE (day 20 p.i.) ( $P < 0.0001$ ), chronic EAE (day 42 p.i.) ( $P < 0.0001$ )). Representative images of spinal cord sections are shown. Bar: 20  $\mu\text{m}$ .  $n = 6/\text{group}$ , data are presented as mean  $\pm$  SEM ( $*P < 0.05$ ,  $**P < 0.01$ ,  $***P < 0.001$ ).

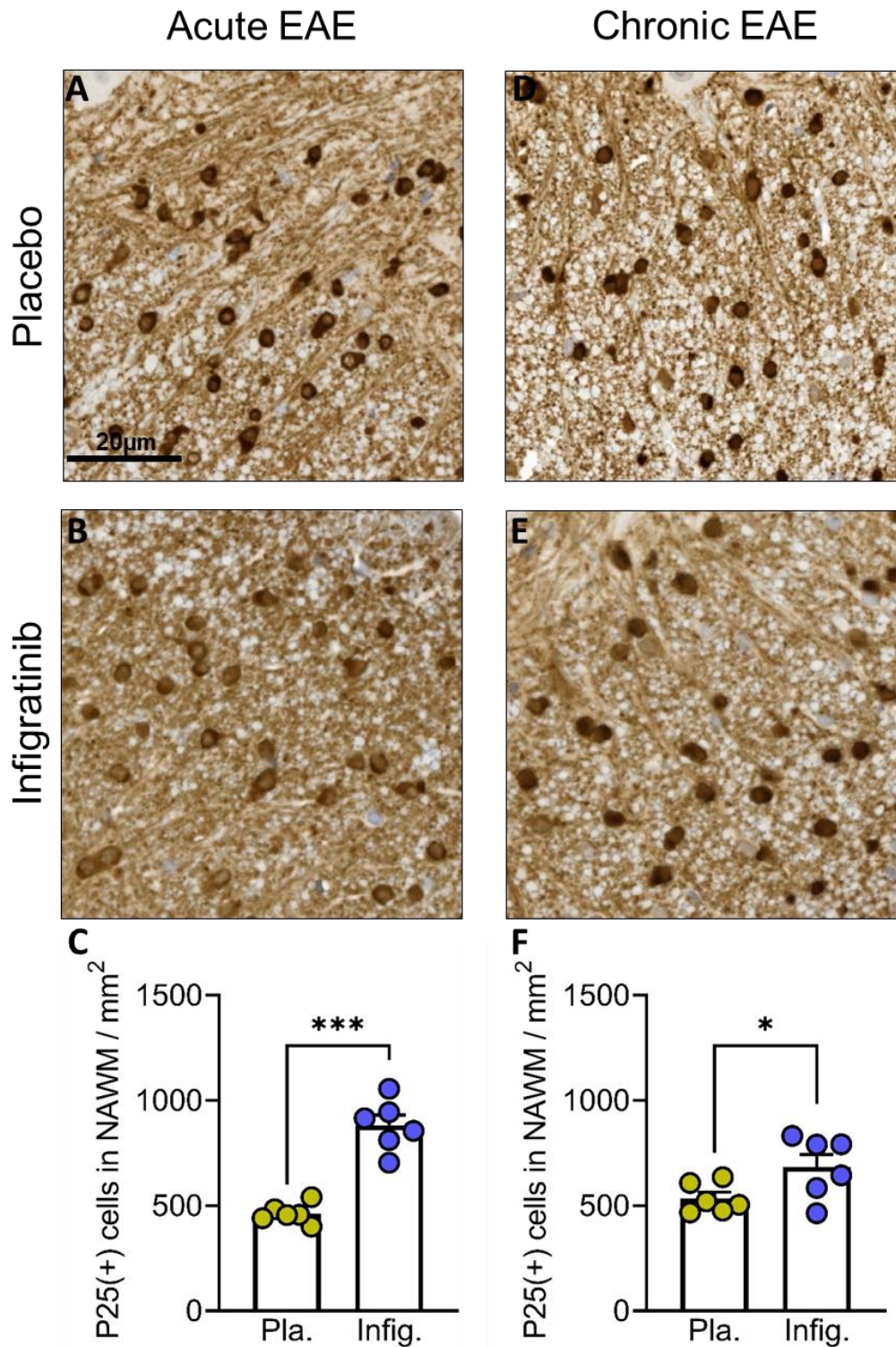


**Figure 41. Mature oligodendrocyte populations in spinal cord NAWM at day 20/42 p.i.** In both acute (A - C) and chronic EAE (D - F), increased P25(+) mature oligodendrocytes were observed in spinal cord NAWM in mice treated with infigratinib (acute EAE (day 20 p.i.) ( $P < 0.0001$ ), chronic EAE (day 42 p.i.) ( $P = 0.0469$ )). Representative images of spinal cord sections are shown. Bar: 20  $\mu\text{m}$ .  $n = 6/\text{group}$ , data are presented as mean  $\pm$  SEM (\* $P < 0.05$ , \*\* $P < 0.01$ , \*\*\* $P < 0.001$ ).



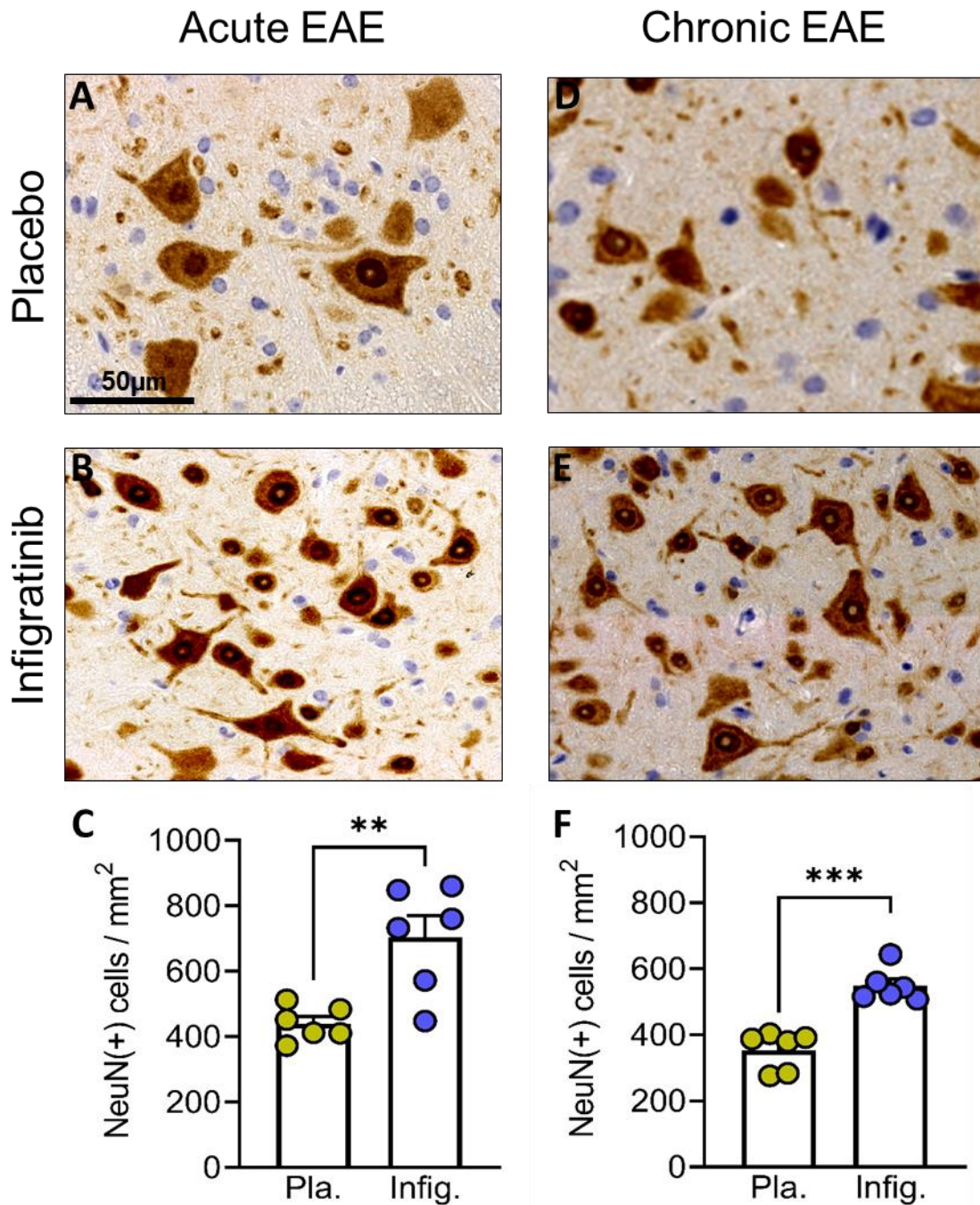


**Figure 42. Motor neuron populations in spinal cord grey matter at day 20/42 p.i.** In the acute (A - C) and chronic EAE (D - F), NeuN(+) motor neuron population was higher in spinal cord grey matter in mice treated with infigratinib (acute EAE (day 20 p.i.) ( $P = 0.0037$ ), chronic EAE (day 42 p.i.) ( $P < 0.0001$ )). Representative images of spinal cord sections are shown. Bar: 50  $\mu$ m.  $n = 5$ /group, data are presented as mean  $\pm$  SEM ( $*P < 0.05$ ,  $**P < 0.01$ ,  $***P < 0.001$ ).

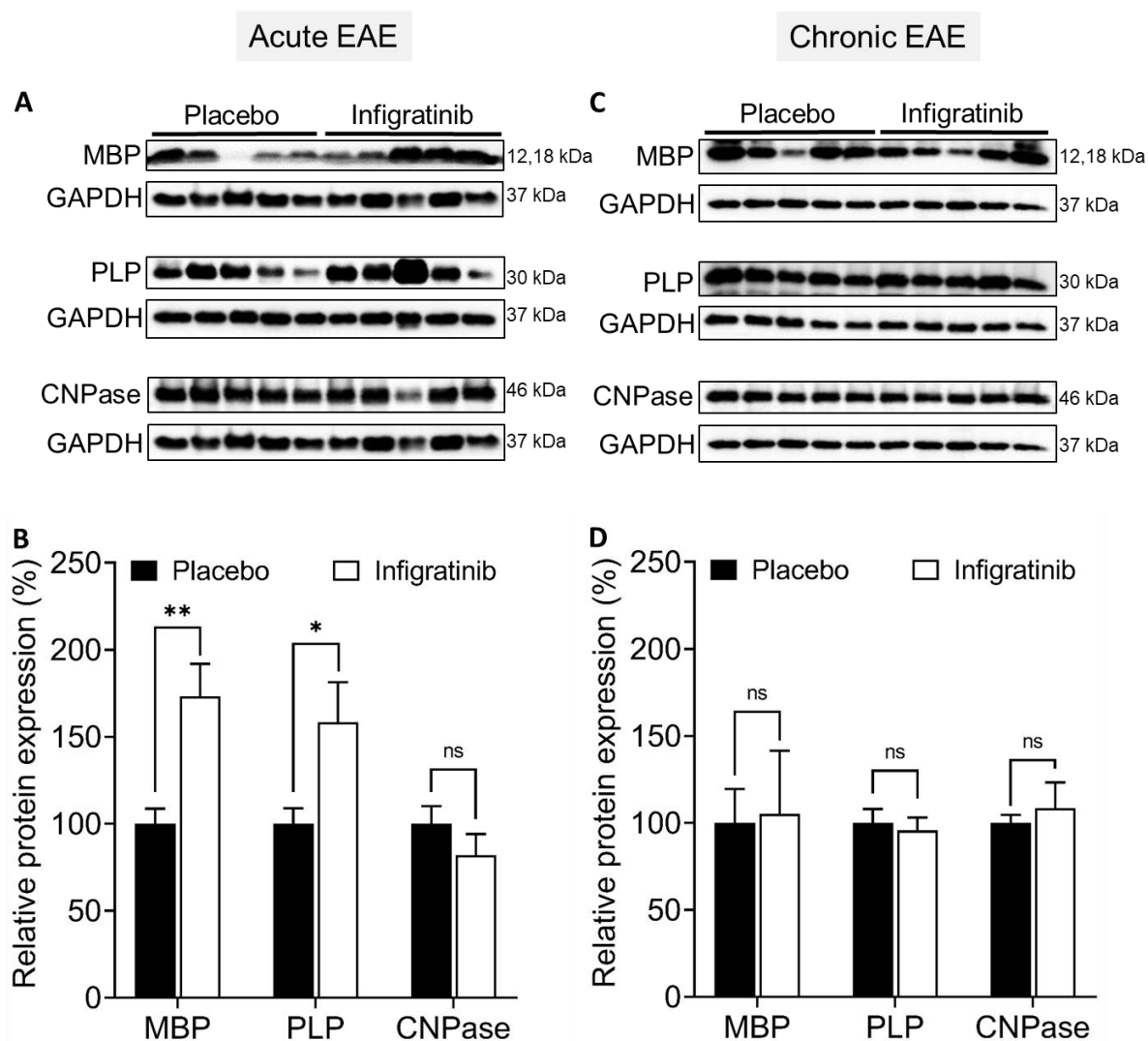


**Figure 43. Myelin protein expression in the spinal cord at day 20/42 p.i.** (A - B) In acute EAE (day 20 p.i.), MBP ( $P = 0.0072$ ) and PLP ( $P = 0.0450$ ) was significantly increased in infigratinib treated mice spinal cord. There was no regulation of CNPase ( $P = 0.2868$ ) protein expression. (C - D) In chronic EAE (day 42 p.i.), MBP ( $P = 0.9011$ ), PLP ( $P = 0.7018$ ), CNPase ( $P = 0.5984$ ) protein expression was not altered in infigratinib treated mice spinal cord. Representative western blots for MBP, PLP and CNPase are shown. Acute EAE  $n = 5$ /group and chronic EAE  $n = 5$ /group. Data are presented as mean  $\pm$  SEM ( $*P < 0.05$ ,  $**P < 0.01$ ,  $***P < 0.001$ ).

#### **4.3.7 Infigratinib on FGFR dependent signalling proteins and BDNF/TrkB receptors expression**

To investigate the effect of infigratinib administered on days 10-19 p.i. on FGFR signalling proteins, BDNF and TrkB receptors in the spinal cord lysate were analyzed by western blot. In the acute phase of EAE (day 20 p.i.), a reduction of FGFR1 ( $P = 0.0122$ ) and FGFR2 ( $P = 0.0211$ ) protein expression was observed in mice treated with infigratinib. Furthermore, infigratinib treatment decreased the expression of FGF2 ( $P = 0.0161$ ) and FGF9 expression ( $P = 0.0082$ ). MAPK phosphorylation of ERK ( $P = 0.0250$ ) was increased, but did not alter the phosphorylation of Akt ( $P = 0.6175$ ) in infigratinib treated mice. Infigratinib induces increases protein levels of BDNF ( $P = 0.0018$ ) and TrkB receptors ( $P = 0.0277$ ) (Figure 44 A-B).

In the chronic phase of EAE (day 42 p.i.), a decrease of FGFR1 ( $P = 0.0036$ ) and FGFR2 ( $P = 0.0288$ ) protein expression was observed in mice treated with infigratinib. Furthermore, infigratinib treatment did not alter the expression of FGF2 ( $P = 0.0929$ ), FGF9 ( $P = 0.7736$ ), phosphorylation of ERK ( $P = 0.9128$ ) and Akt ( $P = 0.1687$ ), BDNF ( $P = 0.0888$ ) and TrkB receptor expression ( $P = 0.5873$ ) (Figure 45 A-B).

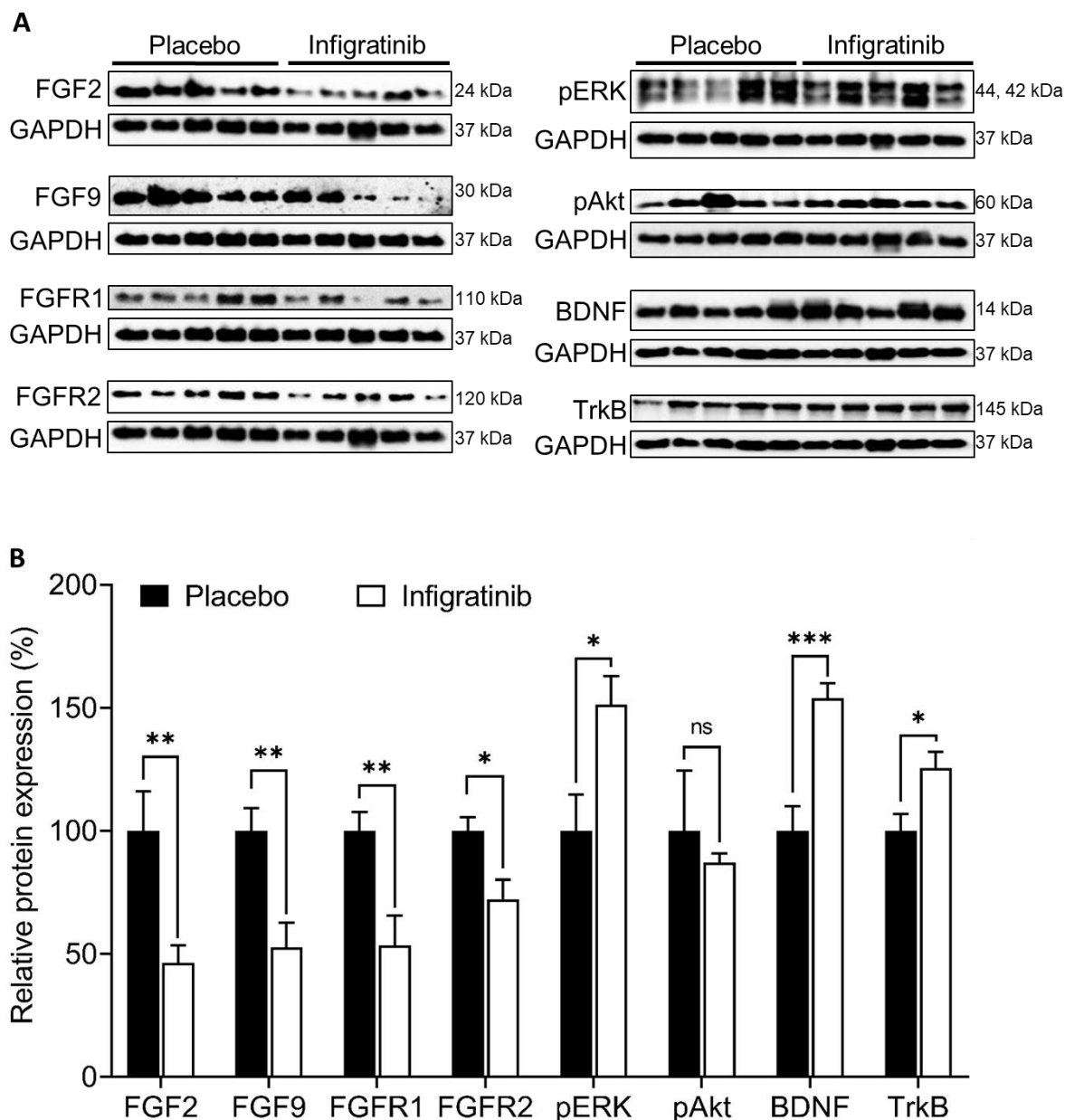


**Figure 44. FGF/FGFR and BDNF/TrkB expression in the spinal cord at day 20 p.i.** (A, B) FGF2 ( $P = 0.0161$ ), FGF9 ( $P = 0.0082$ ), FGFR1 ( $P = 0.0122$ ) and FGFR2 ( $P = 0.0211$ ) protein expression was downregulated and phosphorylation ERK ( $P = 0.0250$ ), BDNF ( $P = 0.0018$ ) and TrkB ( $P = 0.0277$ ) expression were upregulated in infigratinib treated mice spinal cord. There was no regulation of phosphorylation of Akt ( $P = 0.6175$ ). Representative western blots images are shown.  $n = 5$ /group. Data are presented as mean  $\pm$  SEM. ns = not significant ( $*P < 0.05$ ,  $**P < 0.01$ ,  $***P < 0.001$ ).

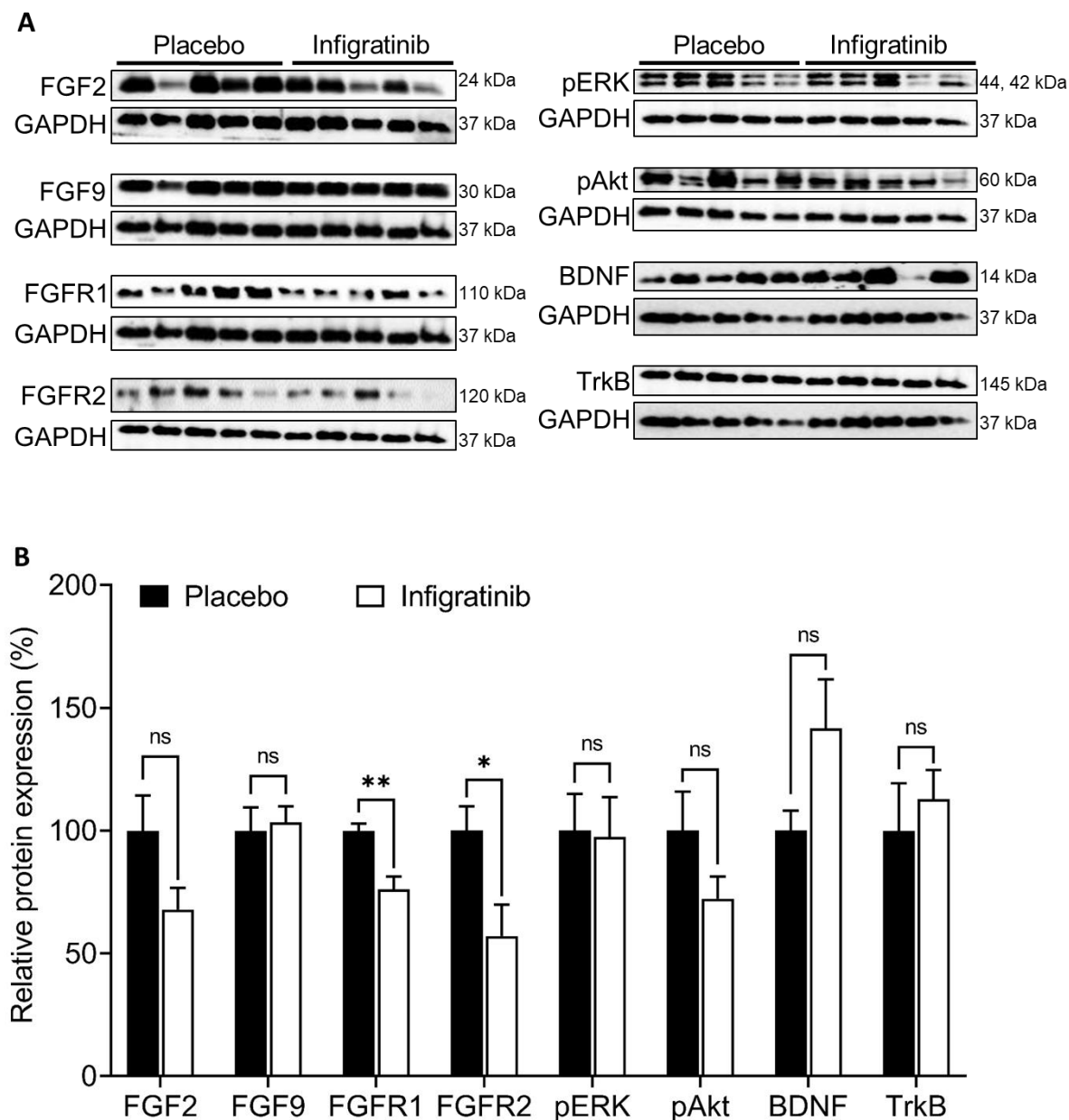


**Figure 45. FGF/FGFR and BDNF/TrkB expression in the spinal cord at day 42 p.i.** (A, B) FGFR1 ( $P = 0.0036$ ) and FGFR2 ( $P = 0.0288$ ) protein expression was downregulated in infigratinib treated mice spinal cord. There was no regulation of FGF2 ( $P = 0.0929$ ), FGF9 ( $P = 0.7736$ ), ERK ( $P = 0.9128$ ) and Akt phosphorylation ( $P = 0.1687$ ), BDNF ( $P = 0.0888$ ) and TrkB ( $P = 0.5873$ ) expression. Representative western blots images are shown.  $n = 5$ /group. Data are presented as mean  $\pm$  SEM. ns = not significant (\* $P < 0.05$ , \*\* $P < 0.01$ , \*\*\* $P < 0.001$ ).

Table 12. Summary of findings from EAE study

	Spinal cord	Infigratinib applied from day 0 - 9 p.i.		Infigratinib applied from day 10 - 19 p.i.	
		Acute phase day 17	Chronic phase day 41	Acute phase day 20	Chronic phase day 42
<b>Inflammation</b>	<b>Inflammatory Index</b>	↓	↓	↓	↓
<b>Immune cell infiltration</b>	CD3(+) T cell	↓	↓	↓	↓
	B220(+) B cell	↓	↓	↓	↓
	Mac3(+) Macrophages	↓	↓	↓	↓
<b>Proinflammatory cytokine expression</b>	IL1 $\beta$ mRNA	—	↓	↓	—
	IL6 mRNA	—	↓	—	—
	IL12 mRNA	—	↓	—	↓
	TNF $\alpha$ mRNA	—	↓	↓	↓
	iNOS mRNA	—	↓	—	—
<b>Chemokine expression</b>	CX3CR1 mRNA	—	—	—	—
	CX3Cl1 mRNA	—	—	—	—
	<b>Demyelination (%)</b>	↓	↓	↓	↓
	<b>Axonal density in WML (%)</b>	↑	↑	↑	↑
<b>Remyelination inhibitor expression</b>	TGF $\beta$ mRNA	—	—	—	—
	SEMA3A mRNA	—	↓	—	—
	Lingo1 mRNA	↓	—	—	—
<b>OPC</b>	Olig2(+) cells in WML	—	↑	—	—
	Olig2(+) cells in NAWM	—	—	—	—
<b>Mature oligodendrocytes</b>	P25(+) cells in WML	↑	↑	↑	↑
	P25(+) cells in NAWM	↑	—	↑	↑
<b>Motor neurons</b>	NeuN(+) cells	↑	—	↑	↑
<b>FGFR signalling protein expression</b>	FGF2	—	↓	↓	—
	FGF9	—	—	↓	—
	FGFR1	↓	↓	↓	↓
	FGFR2	↓	↓	↓	↓
	pERK	—	↑	↑	—
	pAkt	—	↑	—	—
	<b>BDNF</b>	↑	↓	↑	—
	<b>TrkB</b>	—	↑	↑	—
<b>Myelin protein expression</b>	MBP	—	↑	↑	—
	PLP	—	↑	↑	—
	CNPase	—	↑	—	—

↑ Significant increase

↓ Significant decrease

— Not regulated

#### 4.4 *In vitro* experiments

##### 4.4.1 The effects of FGFR inhibition with infigratinib in OLN93 oligodendrocytes

To study whether infigratinib alters the proliferation of oligodendrocytes, OLN93 cells were treated with infigratinib. Infigratinib resulted in less proliferation of OLN93 cells compared to untreated or bFGF stimulated cells (Figure 46 A-B). In contrast, the application of bFGF (FGF2) did not affect the proliferation of OLN93 cells (Figure 46 A-B). There was a strong trend to lower FGFR1/2 protein expression by infigratinib. FGFR1 protein expression was lower in cells treated with infigratinib compared to bFGF treated cells; phosphorylation of ERK/Akt was not altered by infigratinib. Treatment with infigratinib caused an upregulation of BDNF, TrkB, and PLP compared to untreated cells (Figure 47 A-B).

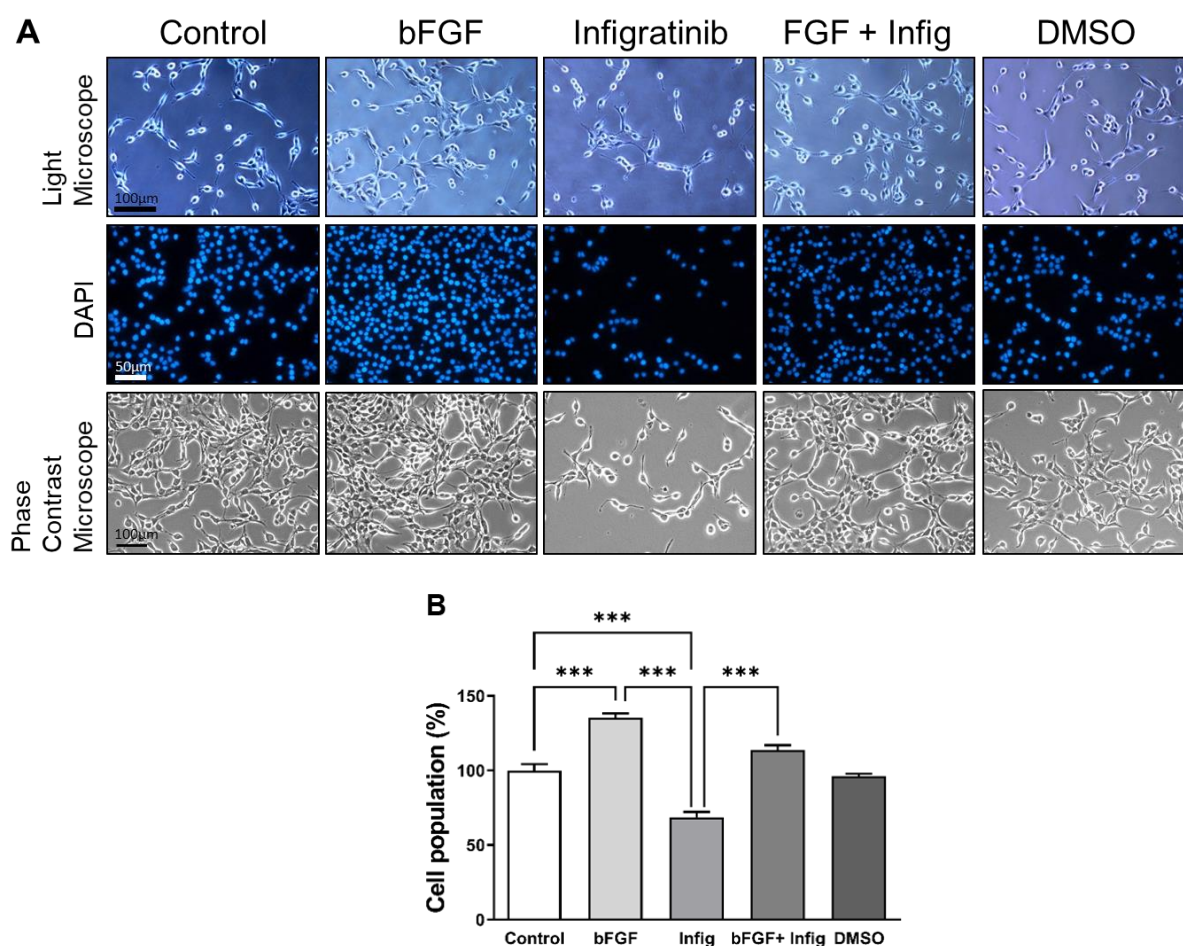


**Figure 46. Proliferation effects of infigratinib on OLN93 cells.** FGFR inhibition with infigratinib decreases the proliferation of OLN93 oligodendrocytes ( $P < 0.001$ ). \*\*\* represent  $< 0.001$ .



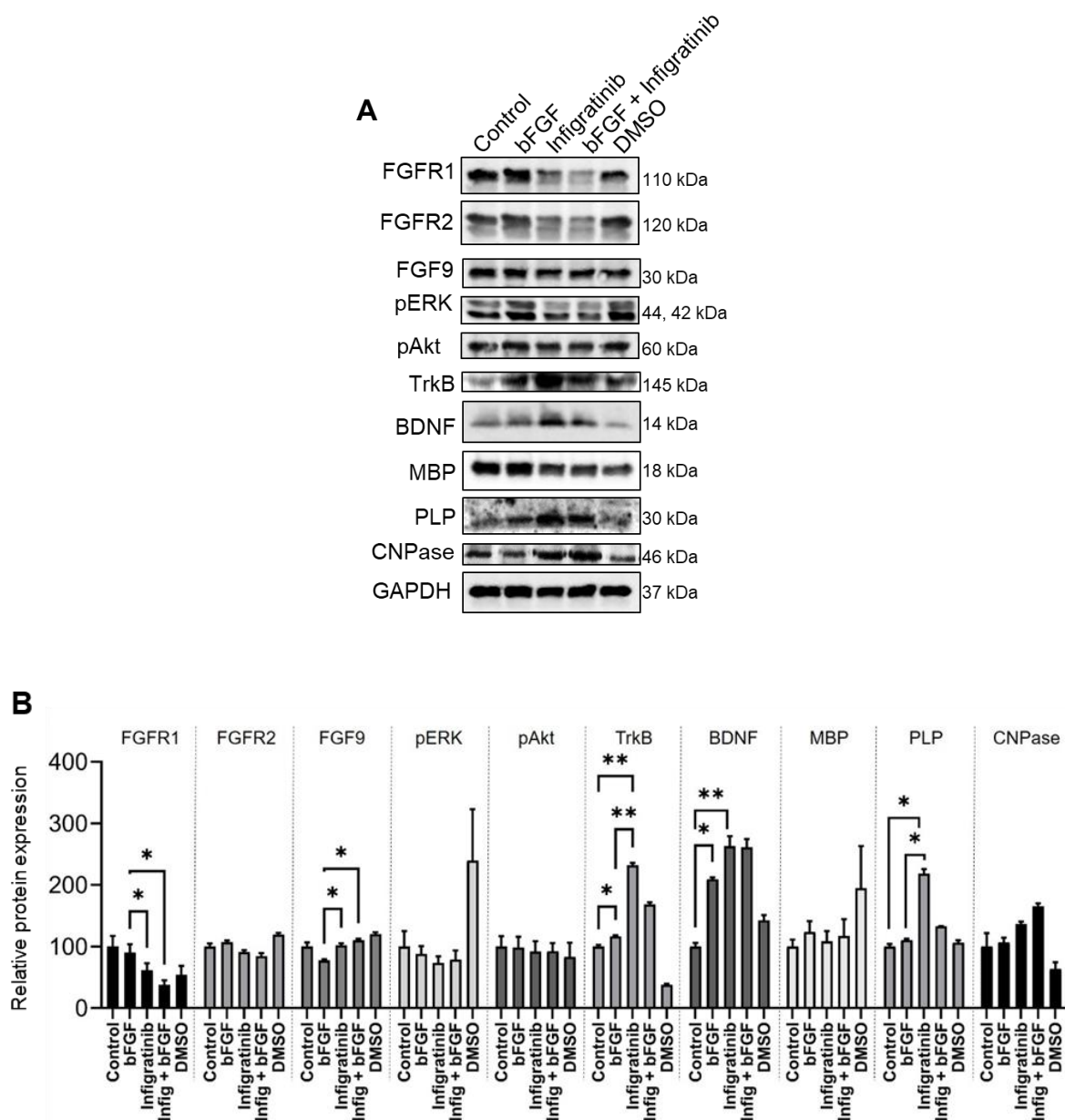


**Figure 47. Expression of FGF/FGFR dependent signalling molecules and myelin proteins.**

(A - B) There was a trend to less FGFR1/2 protein expression in infigratinib treated cells compared to untreated. FGFR1 protein expression was significantly less in cells treated with infigratinib compared to bFGF treated cells ( $P < 0.05$ ). Protein expression of BDNF, TrkB, and myelin protein PLP were increased after infigratinib ( $P < 0.05$ ). Representative western blots are shown.  $n = 3/\text{group}$ , data are presented as mean  $\pm$  SEM, ns = not significant, \*  $P < 0.05$ , \*\*  $P < 0.01$ .



## 5 DISCUSSION

In the present study, we identified that oral application of infigratinib before disease onset or after disease onset reduced disease severity and improved clinical recovery during onset, peak, and chronic phases of EAE and decreased the number of relapses in MOG<sub>35-55</sub>-induced EAE. The most significant findings are that a) infigratinib administration reduced inflammatory infiltrates into the CNS, b) reduced demyelination in CNS, c) increased axonal density in CNS, d) enhanced myelin protein expression in the spinal cord, and d) decreased remyelination inhibitors, e) increased mature oligodendrocytes population in WML, NAWM in the spinal cord. The mode of action underlying the protection in EAE includes anti-inflammatory action by reducing pro-inflammatory cytokine expression, neuroprotection by enhancing myelin proteins and neuronal growth factors/receptors and reducing myelin inhibitors expression. Our findings suggest that short-term pharmacological inhibition of FGFR by infigratinib is sufficient to reduce the EAE symptoms and evidenced the tolerability of 30 mg/kg oral infigratinib application in the MOG<sub>35-55</sub>-induced EAE model.

### 5.1 Inhibition of FGFR by infigratinib reduces severity of EAE

Our recent studies demonstrated that conditional deletion of oligodendrocyte-specific *FGFR1* and *FGFR2* resulted in less severe disease symptoms in the chronic phase of EAE (Rajendran et al., 2018; Kamali et al., 2021). In MS patients, enhanced expression of FGFR1 was observed in OPCs within active lesions (Clemente et al., 2011). The current study is the first to investigate the FGFR inhibitor infigratinib on MOG<sub>35-55</sub>-induced EAE. Our data demonstrate that oral application of infigratinib at the time of EAE induction over 10 days (days 0-9; to delay the onset of disease and to reduce disease severity) delayed the onset of EAE by 2 days, 16.7% of mice treated with infigratinib reached EAE scores of 1 and above at the end of the experiment (day 41 p.i.). Furthermore, infigratinib was applied at the time of onset of symptoms (day 10-19 p.i.) to reduce the severity of relapses, where it exhibited an immediate effect on disease severity and ameliorated EAE signs throughout the chronic phase. This is a long-lasting effect (day 42 p.i.) on MOG<sub>35-55</sub>-induced EAE. At the end of the chronic phase (day 42 p.i.), 36.8% of infigratinib treated mice had EAE scores of more than 1, whereas 77.8% of mice had score more than 1 in placebo. The reduction of EAE disease severity throughout the chronic phase was achieved in both treatment approaches.

## 5.2 Infigratinib reduces immune cell infiltration into the CNS

During acute and chronic phases of EAE, reduced FGFR signalling was associated with less infiltration of activated macrophages/microglia, CD3(+) T cells and B220(+) B cells into the spinal cord. The activated immune cells in the peripheral lymphoid organs migrate, invade into CNS, and induce inflammation (Kipp et al., 2017). Cytokines play a significant role in recruiting activated immune cells into the CNS (Filippi et al., 2018, Sinha et al., 2015 and Bakhuraysah et al., 2021). Nevertheless, through induction and peak phases of EAE, extensive infiltration of peripheral macrophages is observed in the CNS. More abundant macrophages are found in active demyelinating MS lesions (Vogel et al., 2013). In EAE, peripherally activated myelin-specific T cells infiltrate and are reactivated in the CNS, where they release pro-inflammatory cytokines (Fletcher et al., 2010). The infiltrating Th1 and Th17 cells produce a high amounts of pro-inflammatory cytokines in CNS (IFN $\gamma$ , IL17, IL12, IL23), which cause demyelination and neuronal death in the inflamed CNS (Jiang et al., 2014). In the later phase of EAE, anti-inflammatory Th2 and regulatory T cells develop and control inflammation by reducing Th1 cell activity and pro-inflammatory cytokine release (Lavasani et al., 2010). In addition, the infiltrating B cells contribute to the pathogenesis of EAE through the release of anti-myelin antibodies that contribute to demyelination (Mann et al., 2012).

Oligodendrocyte-specific deletion of *FGFR1* and *FGFR2* in MOG<sub>35-55</sub>-induced EAE showed a significant reduction of T and B lymphocytes and macrophages/microglia infiltration into the spinal cord (Rajendran et al., 2018 and Kamali et al., 2021). In accordance with prior studies, inhibition of FGFR with infigratinib led to milder clinical symptoms of MOG<sub>35-55</sub>-EAE, and was associated with reduced T and B lymphocytes and macrophages/microglia infiltration to the spinal cord in the acute and chronic phase of EAE with both treatment approaches. Thus, our investigation demonstrates that infigratinib directly regulates the infiltration of activated immune cells into the CNS and the inflammation process in EAE.

## 5.3 Modulatory effects of infigratinib on pro-inflammatory cytokines

Collectively peripheral immune cell activation, inflammatory mediators secreted by CNS-resident immune cells and recruitment of inflammatory cells into the CNS lead to inflammation, demyelination and oligodendroglial damage in MS and EAE (Filippi et al., 2018 and Van Kaer et al., 2019). Oligodendroglial *FGFR1* deletion in EAE showed decreased

expression of IL1 $\beta$ , IL6 and TNF $\alpha$  (Rajendran. et al., 2018). Similarly, oligodendroglial *FGFR2* deletion in EAE showed less expression of IL1 $\beta$  and TNF $\alpha$  (Kamali et al., 2021).

Cytokines play a significant role in recruiting activated immune cells into the CNS (Filippi et al., 2018, Sinha et al., 2015 and Bakhuraysah et al., 2021). Several preclinical and clinical data indicate a notable role of cytokines in the pathogenesis and progression of MS and EAE (Rossi et al., 2014, Lin and Edelson 2018, Rodgers and Miller 2012). Interestingly, IL1 $\beta$  has recently been demonstrated to play a role in neuronal degeneration via p53-mediated apoptosis and MS disease progression (Rossi et al., 2014). IL1 $\beta$  seems to be the crucial mediator of EAE, as IL1 $\beta$ -deficient mice were seen to resist EAE (Lin and Edelson 2018). IL1 $\beta$  promotes the differentiation of pathogenic Th17 and lymphocyte trafficking into the CNS and CNS tissue damage (Rodgers and Miller 2012). Elevated levels of IL6 were detected in active plaques of individuals suffering from MS, IL6 deficient animals were fully resistant to EAE (Gobel et al., 2018). Significant increases in IL12 levels were observed in EAE, the CSF and lesions of MS patients; further, IL12p40-deficient mice were resistant to EAE (Sun et al., 2015). TNF $\alpha$  levels were increased in active lesions in the CNS, serum and cerebrospinal fluid (CSF) of MS patients.

Increased TNF $\alpha$  in CSF also associates with the severity and progression of disease (Gobel et al., 2018). TNF $\alpha$  inhibits the proliferation and differentiation of oligodendrocyte progenitor cells and also induces mature oligodendrocyte apoptosis. Activated macrophages and T cells are the main sources of TNF $\alpha$  (Rodgers and Miller 2012). The enhanced expression of iNOS in the CNS was associated with increased apoptosis of myelinating oligodendrocytes in EAE and it can affect the remyelination process and contribute to the severity of the disease (Sonar and Lal 2019). In agreement with previous studies, inhibition of FGFR with infigratinib causes less expression of pro-inflammatory cytokines (IL1 $\beta$ , IL6, IL12, TNF $\alpha$  and iNOS) in the spinal cord of chronic phase of EAE, suggesting a lasting anti-inflammatory effect of infigratinib within the CNS and associated with disease recovery of infigratinib treated mice.

#### 5.4 Effect of infigratinib on myelin inhibitors

Lingo-1 is expressed in oligodendrocytes, overexpression of Lingo-1 led to inhibition of oligodendrocyte differentiation and axonal myelination. Increased oligodendrocyte differentiation and myelination were observed in cultured OPCs from Lingo-1 knockout mice than cells from wild-type (WT) littermates. Lingo-1 antagonists increase oligodendrocyte differentiation and facilitate CNS myelination (Mi et al., 2005, Jepson et al., 2012 and Shao et al., 2017). In co-cultures of oligodendrocytes and neurons with anti-Lingo-1 antibody promoted myelination. Lingo-1 knockout mice exhibited early-onset CNS myelination through postnatal days 5-15, then reaching the equal level of myelination as wild-type mice at adulthood (Mi et al., 2013). Inhibition of Lingo-1 activity *in vitro* and *in vivo* increases the outgrowth of oligodendrocyte processes and leads to highly developed myelinated axons (Zhou et al., 2012). Both *in vitro* and *in vivo* data suggest that blockage of Lingo-1 preserves and improves neurite growth of midbrain neurons (Inoue et al., 2007). Oligodendrocyte-specific *FGFR1* deletion decreases Lingo-1 mRNA expression in the chronic phase of EAE (Rajendran et al., 2018).

SEMA3A is inhibiting OPCs migration to demyelinated lesions in MS (Okuno et al., 2011). *In vivo* mouse model data suggest that increasing SEMA3A expression in lesions reduced OPC migration to the lesion area and inhibits its subsequent remyelination (Boyd et al., 2013). Similarly, SEMA3A negatively impairs OPC maturation and migration in demyelinating conditions (Syed et al., 2011). Significantly SEMA3A level increases after spinal cord injury, reaching its peak at one week following injury (Kaneko et al., 2006). The application of SEMA3A inhibitor increased tissue preservation, remyelination and functional recovery following spinal cord injury (Kaneko et al., 2006). *In vitro*, inhibition of FGFR in oligodendrocyte (OLN-93) reduces the gene expression of SEMA3A (Rajendran et al., 2021). Oligodendrocyte-specific *FGFR2* deletion attenuates SEMA3A mRNA expression in the acute and chronic phase of EAE (Kamali et al., 2021). Taken together, inhibition of FGFR with infigratinib decreases the expression of myelin inhibitor SEMA3A and Lingo-1. Therefore, inhibition of FGFR signalling causes myelination and intrinsically attenuates inhibition of myelination.

### 5.5 Effects of infigratinib on oligodendrocytes, demyelination and axons

Pathophysiological hallmarks of MS are inflammation, demyelination, axonal injury and impaired remyelination (Huang et al., 2017). Recent studies have suggest that oligodendrocyte damage following immune attacks contributes to the development of MS/ EAE (Stone and Lin 2015). *In vitro* data suggest that activation of oligodendroglial Fgfr1 by FGF2 is associated with a downregulation of myelin proteins (Fortin et al., 2005). Another *in vitro* study demonstrated that inhibition of FGFR signalling in oligodendrocytes results in enhanced myelin-specific proteins (Rajendran et al., 2021). The myelin sheath damage is associated with axon degeneration, which is the main underlying mechanism of permanent disability in MS patients (Thompson et al., 2018). In MS, remyelination often fails due to reduced recruitment of OPC to demyelinated areas and impaired OPC differentiation into myelinating oligodendrocytes (Kuhlmann et al., 2008). Loss of motor neurons represents an integral part of MS pathology. The infiltrating T cells in CNS inducing neuronal apoptosis (Aktas et al., 2005). T cells were detected in surrounding dying neurons in chronic active MS patients (Vogt et al., 2009).

Oligodendrocyte-specific *FGFR1* and *FGFR2* deletion attenuate demyelination and axon degeneration in EAE lesions (Rajendran et al., 2018; Kamali et al., 2021). Herein, pharmacological inhibition of FGFR by infigratinib showed increased OPC and mature oligodendrocytes in lesion areas. These results demonstrate the protection of oligodendrocytes resulting from less demyelination, axon degeneration and neuron loss in the CNS during EAE. These data collectively provide evidence that infigratinib activates differentiation of oligodendrocytes, thereby decreased demyelination in EAE. This increased the number of mature oligodendrocytes and motor neurons in CNS, suggesting that infigratinib may pass the BBB and regulate oligodendrocytes and neurons, thereby increasing remyelination. The limitation of our study is that the direct evidence of infigratinib in CNS is lacking; our attempts to test the infigratinib in the CNS by MALDI-MS were not successful.

### 5.6 Effects of infigratinib on FGFR and dependent signalling pathways

Previous studies have implicated FGF/FGFR signalling in oligodendrocyte development and remyelination. *In vivo* and *in vitro* analyses, (FGF2<sup>-/-</sup> mice) reduced FGF2 activity seems to promote the repopulation of oligodendrocytes and enhanced the rate of remyelination in lesions

by raising oligodendrocyte lineage cell differentiation without significantly changing OPCs proliferation or survival (Armstrong et al., 2002). The activation of the FGF2 signalling pathway in the adult rat CNS results in the destruction of oligodendrocytes and myelin (Butt and Dinsdale 2005). FGF2 mediated FGFR signalling inhibits oligodendrocyte differentiation and the expression of myelin proteins (Rajendran et al., 2021). Expression of FGF9 is upregulated in early active MS lesions and remains high at sites of ongoing tissue damage in patients with longstanding progressive disease. FGF9 induces a pro-inflammatory response and inhibits myelination and remyelination *in vitro* (Lindner et al., 2015). Continued high expression of FGF9 may cause a failure of remyelination (Rajendran et al., 2021). Oligodendrocyte-specific FGFR2 deletion attenuates FGF2 and FGF9 expression in the acute and chronic phase of EAE (Kamali et al., 2021).

Previous studies have shown that Akt-mTOR signalling in oligodendrocytes increases the expression of myelin genes and proteins (Zou et al., 2014; Kearns et al., 2015). Increased Akt signal transduction enhances CNS myelination (Flores et al., 2008) and Akt dysregulation causes inflammatory and autoimmune disorders (Manning and Toker 2017). ERK1/2 signalling is an essential regulator to promote oligodendrocyte myelination and myelin-sheath thickness in the CNS (Ishii et al., 2012; Xiao et al., 2012). The principal function of ERK1/2 signalling *in vivo* is in increasing active myelin growth and thickness, following oligodendrocyte differentiation and the initiation of myelination (Ishii et al., 2012). Increased myelin gene expression and myelin growth in the adult mouse CNS at both moderate and hyperactivated levels of ERK1/2 (Ishii et al., 2016). BDNF is the neurotrophin and it is less in chronic MS plaques. In MS, BDNF is reduced in serum and CSF compared to healthy controls (Nociti 2020). BDNF plays an important role in neuroinflammation modulation, neuroprotection and neuronal repair through activation of oligodendroglial TrkB (Nociti 2020; VonDran et al., 2011). Studies on the model of cuprizone-mediated demyelination in BDNF heterozygous knockout mice exhibited that BDNF plays a role in regulating the number of oligodendrocyte progenitors and the expression of myelin proteins (Luhder et al., 2013). BDNF promotes CNS myelination through activation of oligodendroglial TrkB. Increased expression of TrkB enhances oligodendrocyte differentiation and remyelination in EAE (Fletcher et al., 2018).

Activation of TrkB with TDP6, directed to higher TrkB phosphorylation in the corpus callosum, more mature oligodendrocytes, and a higher rate of remyelinated axons (Fletcher et al., 2018). Oligodendrocyte-specific *FGFR1* deletion showed increased phosphorylation of

ERK1/2 and Akt and TrkB and BDNF expression in the chronic phase associated with milder EAE disease course (Rajendran et al., 2018). Consequently, *FGFR2* deletion showed increased phosphorylation of Akt associated with increased myelin protein PLP in the chronic phase (Kamali et al., 2021). In the current study, infigratinib application as prevention and suppression of EAE showed less FGF2/9 and FGFR1/2 expression. Further, infigratinib increases the expression of FGFR signalling molecules pERK1/2, pAkt and TrkB and BDNF in the chronic phase EAE. Importantly, we found increased myelin proteins MBP, PLP and CNPase in the infigratinib treated mice suggesting infigratinib has long lasting and multi targeted effects on FGFR signalling in the CNS. Taken together, inhibition of FGFR signalling by infigratinib protects axons and neurons by enhancing myelin proteins and remyelination in the EAE model. We further confirmed the effect of infigratinib on OLN93 oligodendrocytes by *in vitro* experiments. Expression of BDNF/TrkB and myelin proteins PLP and CNPase in OLN93 oligodendrocytes is increased by FGFR Inhibition (Rajendran et al., 2021). In agreement with the previous study, infigratinib increased the protein expression of BDNF/TrkB and myelin proteins PLP, CNPase in OLN93 oligodendrocytes.

Bruton's tyrosine kinase (BTK) is expressed in B cells, myeloid cells and platelets, but not T or NK cells. *In vivo* BTK inhibitor application reduces B cell proliferation, differentiation and production of cytokines, further promotes remyelination (Martin et al., 2020, Torke et al., 2020). BTK inhibitors also inhibit other tyrosine kinases that are not involved in MS and cause unrelated tissue damage that limits their therapeutic use (Contentti and Correale 2020). In our study, infigratinib mediated FGFR tyrosine kinase inhibition broadly reduced antigen triggered activation/infiltration of T cells, B cells, macrophages/microglia and enhance remyelination through oligodendrocyte differentiation, myelin protein MBP, PLP, CNPase expression.

In a recent report, current several disease modifying drugs of MS (e.g., Glatiramer acetate, Daclizumab and Fingolimod) are identified to act on circulating T cells, B cells, macrophages, and cytokine production (Fox et al., 2019). However, the clinical potential of these drugs is restricted by side effects or their effect on off-target receptor interactions. Continued screening of small molecules that enhance mature oligodendrocytes and remyelination is an unmet need. Infigratinib has a tolerable safety profile when administered orally in humans and rodents (Nogova et al., 2017, Guagnano et al., 2011). In the present study, the infigratinib dose of 30 mg/kg/day proved effective for EAE treatment. Furthermore, infigratinib is currently undergoing clinical trials to assess safety in patients with cholangiocarcinoma (Makawita et al., 2020); preliminary results demonstrated that infigratinib is safe and has beneficial

therapeutic effects in select patients, suggesting that infigratinib would be safe as MS treatment. Importantly, analysis of the distribution of infigratinib orally administered to mice for 10 days has shown that infigratinib crosses the blood-brain barrier and inhibits FGFR expression, giving infigratinib the vast advantage of being able to exert effects directly on the CNS. Taken together, our findings provide important insights into the neural repair capacities of infigratinib through immunomodulation and enhancing remyelination and myelin expression in the experimental models of MS.

In conclusion, based on the present study, our results suggest that FGFR plays a crucial role in MS/EAE pathogenesis. Pharmacological inhibition of FGFR signalling by infigratinib ameliorates EAE progression by reducing immune cell infiltration, and decreasing remyelination inhibitor expression. On the other hand, infigratinib also enhances myelin protein expression, increases the number of mature oligodendrocytes in WML and NAWM to protect axons via remyelination. The beneficial effects of FGFR inhibition in EAE are associated with the regulation of FGF/FGFR signalling downstream proteins such as pERK, pAkt, and increased expression of BDNF and TrkB. These effects of infigratinib suggest that it has high therapeutic potential to treat multiple sclerosis.



## 6 SUMMARY

The FGF/FGFR signalling plays a vital role in diverse cellular processes in the central nervous system. The role of FGF/FGFR signalling in MS pathology and EAE is partially understood. Knockout of oligodendroglial *FGFR1* and *FGFR2* clearly showed beneficial effects in MOG<sub>35-55</sub>-induced EAE. The present investigation focuses on the efficacy of the selective FGFR inhibitor infigratinib in preventing and suppressing relapses in MOG<sub>35-55</sub>-induced EAE, an animal model for Multiple sclerosis. Interestingly, infigratinib treated mice exhibited a milder disease course of MOG<sub>35-55</sub>-induced EAE. FGFR inhibition with infigratinib caused reduced spinal cord immune cell infiltration (T-cells, B-cells, macrophages/ activated microglia), inflammation, demyelination and increased axonal density. Pro-inflammatory cytokines (IL1, IL6, IL12, TNF $\alpha$ , iNOS) lead to inflammatory immune cells activation and mediators of inflammation, which was reduced by infigratinib. Increased expression of BDNF, TrkB receptor and myelin proteins MBP, PLP, CNPase were noticed in infigratinib treated mice linked with disease recovery. Infigratinib reduced the expression of myelin inhibitor SEMA3A and Lingo-1. The number of myelin producing mature oligodendrocytes and motor neurons was increased in the white matter lesion area of infigratinib treated mice, associated with remyelination. Taken together, our findings indicate that inhibition of FGFR signalling by infigratinib protects oligodendrocytes and neurons against inflammation, enhancing myelin proteins expression and remyelination in the EAE model. Infigratinib should be considered as a therapeutic advantage for patients with MS.

## ZUSAMMENFASSUNG

Die FGF/FGFR Signalkaskade spielt eine entscheidende Rolle in verschiedenen zellulären Prozessen des zentralen Nervensystems. Die Rolle der FGF/FGFR-Signalkaskade im Zusammenhang mit den pathologischen Prozessen der Multiplen Sklerose und dem EAE-Modell ist nur teilweise verstanden. Der knockout von FGFR1 und FGFR2 in Oligodendrozyten zeigt eindeutig positive Auswirkungen im MOG<sub>35-55</sub>-induzierten EAE Tier Modell. Die vorliegende Untersuchung fokussiert sich auf die Wirksamkeit des selektiven FGFR Inhibitors Infigratinib, Rückfälle im MOG<sub>35-55</sub>-induzierten EAE Modell präventiv zu verhindern oder nach Ausbruch abzuschwächen. Interessanterweise entwickelten Mäuse unter Infigratinib-Therapie einen milderen Krankheitsverlauf der EAE. So zeigen sich nach Inhibition der FGFR durch Infigratinib eine Reduktion der Immuneinfiltration im Rückenmark (T-Zellen, B-Zellen, Makrophagen/aktivierte Mikroglia), abgeschwächte Entzündungsreaktionen, weniger Demyelinisierung und eine erhöhte Axondichte. Die Anzahl proinflammatorische Zytokine (IL1, IL6, IL12, TNF, iNOS), die pathologischer Weise zu einer Aktivierung von Immunzellen führen, wurden ebenfalls durch die Gabe von Infigratinib verringert. Außerdem konnte der mildere Krankheitsverlauf in betroffenen Mäusen mit einer gesteigerten Expression von BDNF, seinem Rezeptor TrkB und von Myelinproteinen wie MBP, PLP und CNPase in Verbindung gebracht werden. Zusätzlich konnte gezeigt werden, dass Inhibitoren der Myelinisierung (SEMA3A, LINGO-1) bei Therapie mit Infigratinib reduziert wurden. Die gesteigerte Remyelinisierung in Läsionen der weißen Substanz ist mit einer erhöhten Anzahl reifer, myelinproduzierender Oligodendrozyten und Motoneuronen assoziiert. Zusammenfassend lassen die Ergebnisse darauf schließen, dass die FGFR-Inhibition durch Infigratinib Oligodendrozyten und Neurone gegenüber entzündlichen Prozessen schützt und die Remyelinisierung durch gesteigerte Expression von Myelinproteinen fördert. Infigratinib sollte wegen seiner therapeutischen Vorteile bei der Behandlung von MS Patienten berücksichtigt werden.

---

**REFERENCES**

- Aktas, O., Smorodchenko, A., Brocke, S., Infante-Duarte, C., Schulze Topphoff, U., Vogt, J., . . . Zipp, F. (2005). Neuronal damage in autoimmune neuroinflammation mediated by the death ligand TRAIL. *Neuron*, *46*(3), 421-432. doi:10.1016/j.neuron.2005.03.018
- Ahnert J. R., Gray N, Mok T, Gainor J. What It Takes to Improve a First-Generation Inhibitor to a Second- or Third-Generation Small Molecule. *Am Soc Clin Oncol Educ Book*. 2019 Jan;39:196-205. doi: 10.1200/EDBK\_242209.
- Armstrong, R. C., Le, T. Q., Frost, E. E., Borke, R. C., & Vana, A. C. (2002). Absence of fibroblast growth factor 2 promotes oligodendroglial repopulation of demyelinated white matter. *J Neurosci*, *22*(19), 8574-8585.
- Astolfi, A., Pantaleo, M. A., Indio, V., Urbini, M., & Nannini, M. (2020). The Emerging Role of the FGF/FGFR Pathway in Gastrointestinal Stromal Tumor. *Int J Mol Sci*, *21*(9). doi:10.3390/ijms21093313
- Baecher-Allan, C., Kaskow, B. J., & Weiner, H. L. (2018). Multiple Sclerosis: Mechanisms and Immunotherapy. *Neuron*, *97*(4), 742-768. doi:10.1016/j.neuron.2018.01.021
- Bakuraysah, M. M., Theotokis, P., Lee, J. Y., Alrehaili, A. A., Aui, P. M., Figgett, W. A., . . . Petratos, S. (2021). B-cells expressing NgR1 and NgR3 are localized to EAE-induced inflammatory infiltrates and are stimulated by BAFF. *Sci Rep*, *11*(1), 2890. doi:10.1038/s41598-021-82346-6
- Bando, Y. (2015). Myelin morphology and axon pathology in demyelination during experimental autoimmune encephalomyelitis. *Neural Regen Res*, *10*(10), 1584-1585. doi:10.4103/1673-5374.165287
- Bansal, R., Kumar, M., Murray, K., Morrison, R. S., & Pfeiffer, S. E. (1996). Regulation of FGF receptors in the oligodendrocyte lineage. *Mol Cell Neurosci*, *7*(4), 263-275. doi:10.1006/mcne.1996.0020
- Bergles, D. E., & Richardson, W. D. (2015). Oligodendrocyte Development and Plasticity. *Cold Spring Harb Perspect Biol*, *8*(2), a020453. doi:10.1101/cshperspect.a020453
- Bittner, S., Afzali, A. M., Wiendl, H., & Meuth, S. G. (2014). Myelin oligodendrocyte glycoprotein (MOG<sub>35-55</sub>) induced experimental autoimmune encephalomyelitis (EAE) in C57BL/6 mice. *J Vis Exp*(86). doi:10.3791/51275

- Botrus G, Raman P, Oliver T, Bekaii-Saab T. Infigratinib (BGJ398): an investigational agent for the treatment of FGFR-altered intrahepatic cholangiocarcinoma. *Expert Opin Investig Drugs*. 2021 Apr;30(4):309-316. doi: 10.1080/13543784.2021.1864320.
- Boyd, A., Zhang, H., & Williams, A. (2013). Insufficient OPC migration into demyelinated lesions is a cause of poor remyelination in MS and mouse models. *Acta Neuropathol*, 125(6), 841-859. doi:10.1007/s00401-013-1112-y
- Butt, A. M., & Dinsdale, J. (2005). Fibroblast growth factor 2 induces loss of adult oligodendrocytes and myelin in vivo. *Exp Neurol*, 192(1), 125-133. doi:10.1016/j.expneurol.2004.11.007
- Chae, Y. K., Ranganath, K., Hammerman, P. S., Vaklavas, C., Mohindra, N., Kalyan, A., . . . Giles, F. J. (2017). Inhibition of the fibroblast growth factor receptor (FGFR) pathway: the current landscape and barriers to clinical application. *Oncotarget*, 8(9), 16052-16074. doi:10.18632/oncotarget.14109
- Clemente, D., Ortega, M. C., Arenzana, F. J., & de Castro, F. (2011). FGF-2 and Anosmin-1 are selectively expressed in different types of multiple sclerosis lesions. *J Neurosci*, 31(42), 14899-14909. doi:10.1523/JNEUROSCI.1158-11.2011
- Contentti E.C., Correale J. Bruton's tyrosine kinase inhibitors: a promising emerging treatment option for multiple sclerosis. *Expert Opin Emerg Drugs*. 2020 Dec;25(4):377-381. doi: 10.1080/14728214.2020.1822817.
- Dai S, Zhou Z, Chen Z, Xu G, Chen Y. Fibroblast Growth Factor Receptors (FGFRs): Structures and Small Molecule Inhibitors. *Cells*. 2019 Jun 18;8(6):614. doi: 10.3390/cells8060614. PMID: 31216761; PMCID: PMC6627960.
- De Angelis, F., John, N. A., & Brownlee, W. J. (2018). Disease-modifying therapies for multiple sclerosis. *BMJ*, 363, k4674. doi:10.1136/bmj.k4674
- Dobson, R., & Giovannoni, G. (2019). Multiple sclerosis - a review. *Eur J Neurol*, 26(1), 27-40. doi:10.1111/ene.13819
- Domingues, H. S., Portugal, C. C., Socodato, R., & Relvas, J. B. (2016). Oligodendrocyte, Astrocyte, and Microglia Crosstalk in Myelin Development, Damage, and Repair. *Front Cell Dev Biol*, 4, 71. doi:10.3389/fcell.2016.00071
- Doshi, A., & Chataway, J. (2016). Multiple sclerosis, a treatable disease. *Clin Med (Lond)*, 16(Suppl 6), s53-s59. doi:10.7861/clinmedicine.16-6-s53

- Facchinetti, F., Hollebecque, A., Bahleda, R., Lorient, Y., Olausson, K. A., Massard, C., & Friboulet, L. (2020). Facts and New Hopes on Selective FGFR Inhibitors in Solid Tumors. *Clin Cancer Res*, 26(4), 764-774. doi:10.1158/1078-0432.CCR-19-2035
- Farooqi, N., Gran, B., & Constantinescu, C. S. (2010). Are current disease-modifying therapeutics in multiple sclerosis justified on the basis of studies in experimental autoimmune encephalomyelitis? *J Neurochem*, 115(4), 829-844. doi:10.1111/j.1471-4159.2010.06982.x
- Filippi, M., Bar-Or, A., Piehl, F., Preziosa, P., Solari, A., Vukusic, S., & Rocca, M. A. (2018). Multiple sclerosis. *Nat Rev Dis Primers*, 4(1), 43. doi:10.1038/s41572-018-0041-4
- Fletcher, J. L., Wood, R. J., Nguyen, J., Norman, E. M. L., Jun, C. M. K., Prawdiuk, A. R., . . . Murray, S. S. (2018). Targeting TrkB with a Brain-Derived Neurotrophic Factor Mimetic Promotes Myelin Repair in the Brain. *J Neurosci*, 38(32), 7088-7099. doi:10.1523/JNEUROSCI.0487-18.2018
- Fletcher, J. M., Lalor, S. J., Sweeney, C. M., Tubridy, N., & Mills, K. H. (2010). T cells in multiple sclerosis and experimental autoimmune encephalomyelitis. *Clin Exp Immunol*, 162(1), 1-11. doi:10.1111/j.1365-2249.2010.04143.x
- Flores, A. I., Narayanan, S. P., Morse, E. N., Shick, H. E., Yin, X., Kidd, G., . . . Macklin, W. B. (2008). Constitutively active Akt induces enhanced myelination in the CNS. *J Neurosci*, 28(28), 7174-7183. doi:10.1523/JNEUROSCI.0150-08.2008
- Fortin, D., Rom, E., Sun, H., Yayon, A., & Bansal, R. (2005). Distinct fibroblast growth factor (FGF)/FGF receptor signaling pairs initiate diverse cellular responses in the oligodendrocyte lineage. *J Neurosci*, 25(32), 7470-7479. doi:10.1523/JNEUROSCI.2120-05.2005
- Fox, E. J., Buckle, G. J., Singer, B., Singh, V., & Boster, A. (2019). Lymphopenia and DMTs for relapsing forms of MS: Considerations for the treating neurologist. *Neurol Clin Pract*, 9(1), 53-63. doi:10.1212/CPJ.0000000000000567
- Glatigny, S., & Bettelli, E. (2018). Experimental Autoimmune Encephalomyelitis (EAE) as Animal Models of Multiple Sclerosis (MS). *Cold Spring Harb Perspect Med*, 8(11). doi:10.1101/cshperspect.a028977
- Gobel, K., Ruck, T., & Meuth, S. G. (2018). Cytokine signaling in multiple sclerosis: Lost in translation. *Mult Scler*, 24(4), 432-439. doi:10.1177/1352458518763094

- Gold, R., Linington, C., & Lassmann, H. (2006). Understanding pathogenesis and therapy of multiple sclerosis via animal models: 70 years of merits and culprits in experimental autoimmune encephalomyelitis research. *Brain*, *129*(Pt 8), 1953-1971. doi:10.1093/brain/awl075
- Goldenberg, M. M. (2012). Multiple sclerosis review. *P T*, *37*(3), 175-184.
- Guagnano, V., Furet, P., Spanka, C., Bordas, V., Le Douget, M., Stamm, C., . . . Graus Porta, D. (2011). Discovery of 3-(2,6-dichloro-3,5-dimethoxy-phenyl)-1-{6-[4-(4-ethyl-piperazin-1-yl)-phenylamino]-pyrimidin-4-yl}-1-methyl-urea (NVP-BGJ398), a potent and selective inhibitor of the fibroblast growth factor receptor family of receptor tyrosine kinase. *J Med Chem*, *54*(20), 7066-7083. doi:10.1021/jm2006222
- Guillemot, F., & Zimmer, C. (2011). From cradle to grave: the multiple roles of fibroblast growth factors in neural development. *Neuron*, *71*(4), 574-588. doi:10.1016/j.neuron.2011.08.002
- Halabchi, F., Alizadeh, Z., Sahraian, M. A., & Abolhasani, M. (2017). Exercise prescription for patients with multiple sclerosis; potential benefits and practical recommendations. *BMC Neurol*, *17*(1), 185. doi:10.1186/s12883-017-0960-9
- Harirchian, M. H., Tekieh, A. H., Modabbernia, A., Aghamollai, V., Tafakhori, A., Ghaffarpour, M., . . . Yazdankhah, M. (2012). Serum and CSF PDGF-AA and FGF-2 in relapsing-remitting multiple sclerosis: a case-control study. *Eur J Neurol*, *19*(2), 241-247. doi:10.1111/j.1468-1331.2011.03476.x
- Hart, F. M., & Bainbridge, J. (2016). Current and emerging treatment of multiple sclerosis. *Am J Manag Care*, *22*(6 Suppl), s159-170.
- Heinzlef, O., Molinier, G., van Hille, B., Radoszycki, L., Dourgnon, P., & Longin, J. (2020). Economic Burden of the Out-of-Pocket Expenses for People with Multiple Sclerosis in France. *Pharmacoecon Open*, *4*(4), 593-603. doi:10.1007/s41669-020-00199-7
- Huang WJ, Chen WW, Zhang X. Multiple sclerosis: Pathology, diagnosis and treatments. *Exp Ther Med*. 2017 Jun;13(6):3163-3166. doi: 10.3892/etm.2017.4410. Epub 2017 Apr 28.
- Hunter, S. F. (2016). Overview and diagnosis of multiple sclerosis. *Am J Manag Care*, *22*(6 Suppl), s141-150.
- Inoue, H., Lin, L., Lee, X., Shao, Z., Mendes, S., Snodgrass-Belt, P., . . . Isacson, O. (2007). Inhibition of the leucine-rich repeat protein LINGO-1 enhances survival, structure, and function of dopaminergic neurons in Parkinson's disease models. *Proc Natl Acad Sci U S A*, *104*(36), 14430-14435. doi:10.1073/pnas.0700901104

- Ishii, A., Furusho, M., Dupree, J. L., & Bansal, R. (2016). Strength of ERK1/2 MAPK Activation Determines Its Effect on Myelin and Axonal Integrity in the Adult CNS. *J Neurosci*, *36*(24), 6471-6487. doi:10.1523/JNEUROSCI.0299-16.2016
- Ishii, A., Fyffe-Maricich, S. L., Furusho, M., Miller, R. H., & Bansal, R. (2012). ERK1/ERK2 MAPK signaling is required to increase myelin thickness independent of oligodendrocyte differentiation and initiation of myelination. *J Neurosci*, *32*(26), 8855-8864. doi:10.1523/JNEUROSCI.0137-12.2012
- Jahn, O., Tenzer, S., & Werner, H. B. (2009). Myelin proteomics: molecular anatomy of an insulating sheath. *Mol Neurobiol*, *40*(1), 55-72. doi:10.1007/s12035-009-8071-2
- Jakimovski D, Weinstock-Guttman B, Ramanathan M, Dwyer MG, Zivadinov R. Infections, Vaccines and Autoimmunity: A Multiple Sclerosis Perspective. *Vaccines* (Basel). 2020 Jan 28;*8*(1):50. doi: 10.3390/vaccines8010050
- Jepson, S., Vought, B., Gross, C. H., Gan, L., Austen, D., Frantz, J. D., . . . Krauss, R. (2012). LINGO-1, a transmembrane signaling protein, inhibits oligodendrocyte differentiation and myelination through intercellular self-interactions. *J Biol Chem*, *287*(26), 22184-22195. doi:10.1074/jbc.M112.366179
- Jiang, Z., Jiang, J. X., & Zhang, G. X. (2014). Macrophages: a double-edged sword in experimental autoimmune encephalomyelitis. *Immunol Lett*, *160*(1), 17-22. doi:10.1016/j.imlet.2014.03.006
- Kamali, S., Rajendran, R., Stadelmann, C., Karnati, S., Rajendran, V., Giraldo-Velasquez, M., & Berghoff, M. (2021). Oligodendrocyte-specific deletion of FGFR2 ameliorates MOG<sub>35-55</sub> -induced EAE through ERK and Akt signalling. *Brain Pathol*, *31*(2), 297-311. doi:10.1111/bpa.12916
- Kammona, O., & Kiparissides, C. (2020). Recent Advances in Antigen-Specific Immunotherapies for the Treatment of Multiple Sclerosis. *Brain Sci*, *10*(6). doi:10.3390/brainsci10060333
- Kaneko, S., Iwanami, A., Nakamura, M., Kishino, A., Kikuchi, K., Shibata, S., . . . Okano, H. (2006). A selective Sema3A inhibitor enhances regenerative responses and functional recovery of the injured spinal cord. *Nat Med*, *12*(12), 1380-1389. doi:10.1038/nm1505
- Katoh, M. (2016). Therapeutics Targeting FGF Signaling Network in Human Diseases. *Trends Pharmacol Sci*, *37*(12), 1081-1096. doi:10.1016/j.tips.2016.10.003

- Kearns, C. A., Ravanelli, A. M., Cooper, K., & Appel, B. (2015). Fbxw7 Limits Myelination by Inhibiting mTOR Signaling. *J Neurosci*, *35*(44), 14861-14871. doi:10.1523/JNEUROSCI.4968-14.2015
- Kidd, T., Carey, N., Mold, F., Westwood, S., Miklaucich, M., Konstantara, E., . . . Cooke, D. (2017). A systematic review of the effectiveness of self-management interventions in people with multiple sclerosis at improving depression, anxiety and quality of life. *PLoS One*, *12*(10), e0185931. doi:10.1371/journal.pone.0185931
- Kipp, M., Nyamoya, S., Hochstrasser, T., & Amor, S. (2017). Multiple sclerosis animal models: a clinical and histopathological perspective. *Brain Pathol*, *27*(2), 123-137. doi:10.1111/bpa.12454
- Klineova, S., & Lublin, F. D. (2018). Clinical Course of Multiple Sclerosis. *Cold Spring Harb Perspect Med*, *8*(9). doi:10.1101/cshperspect.a028928
- Kommalapati, A.; Tella, S.H.; Borad, M.; Javle, M.; Mahipal, A. FGFR Inhibitors in Oncology: Insight on the Management of Toxicities in Clinical Practice. *Cancers* 2021, *13*, 2968. <https://doi.org/10.3390/cancers13122968>
- Komla-Ebri, D., Dambroise, E., Kramer, I., Benoist-Lasselín, C., Kaci, N., Le Gall, C., . . . Legeai-Mallet, L. (2016). Tyrosine kinase inhibitor NVP-BGJ398 functionally improves FGFR3-related dwarfism in mouse model. *J Clin Invest*, *126*(5), 1871-1884. doi:10.1172/JCI83926
- Kuhlmann, T., Miron, V., Cui, Q., Wegner, C., Antel, J., & Bruck, W. (2008). Differentiation block of oligodendroglial progenitor cells as a cause for remyelination failure in chronic multiple sclerosis. *Brain*, *131*(Pt 7), 1749-1758. doi:10.1093/brain/awn096
- Kuhn, S., Gritti, L., Crooks, D., & Dombrowski, Y. (2019). Oligodendrocytes in Development, Myelin Generation and Beyond. *Cells*, *8*(11). doi:10.3390/cells8111424
- Kumar, D. R., Aslinia, F., Yale, S. H., & Mazza, J. J. (2011). Jean-Martin Charcot: the father of neurology. *Clin Med Res*, *9*(1), 46-49. doi:10.3121/cmr.2009.883
- Laestander, C., & Engstrom, W. (2014). Role of fibroblast growth factors in elicitation of cell responses. *Cell Prolif*, *47*(1), 3-11. doi:10.1111/cpr.12084
- Lahiry, P., Torkamani, A., Schork, N. J., & Hegele, R. A. (2010). Kinase mutations in human disease: interpreting genotype-phenotype relationships. *Nat Rev Genet*, *11*(1), 60-74. doi:10.1038/nrg2707



- Lavasani, S., Dzhambazov, B., Nouri, M., Fak, F., Buske, S., Molin, G., . . . Westrom, B. (2010). A novel probiotic mixture exerts a therapeutic effect on experimental autoimmune encephalomyelitis mediated by IL-10 producing regulatory T cells. *PLoS One*, *5*(2), e9009. doi:10.1371/journal.pone.0009009
- Legroux, L., & Arbour, N. (2015). Multiple Sclerosis and T Lymphocytes: An Entangled Story. *J Neuroimmune Pharmacol*, *10*(4), 528-546. doi:10.1007/s11481-015-9614-0
- Lin, C. C., & Edelson, B. T. (2017). New Insights into the Role of IL-1beta in Experimental Autoimmune Encephalomyelitis and Multiple Sclerosis. *J Immunol*, *198*(12), 4553-4560. doi:10.4049/jimmunol.1700263
- Lindner, M., Thummler, K., Arthur, A., Brunner, S., Elliott, C., McElroy, D., . . . Linington, C. (2015). Fibroblast growth factor signalling in multiple sclerosis: inhibition of myelination and induction of pro-inflammatory environment by FGF9. *Brain*, *138*(Pt 7), 1875-1893. doi:10.1093/brain/awv102
- Lublin, F. D., Reingold, S. C., Cohen, J. A., Cutter, G. R., Sorensen, P. S., Thompson, A. J., . . . Polman, C. H. (2014). Defining the clinical course of multiple sclerosis: the 2013 revisions. *Neurology*, *83*(3), 278-286. doi:10.1212/WNL.0000000000000560
- Luhder, F., Gold, R., Flugel, A., & Linker, R. A. (2013). Brain-derived neurotrophic factor in neuroimmunology: lessons learned from multiple sclerosis patients and experimental autoimmune encephalomyelitis models. *Arch Immunol Ther Exp (Warsz)*, *61*(2), 95-105. doi:10.1007/s00005-012-0211-0
- Makawita S, K Abou-Alfa G, Roychowdhury S, Sadeghi S, Borbath I, Goyal L, Cohn A, Lamarca A, Oh DY, Macarulla T, T Shroff R, Howland M, Li A, Cho T, Pande A, Javle M. Infigratinib in patients with advanced cholangiocarcinoma with FGFR2 gene fusions/translocations: the PROOF 301 trial. *Future Oncol*. 2020 Oct;16(30):2375-2384. doi: 10.2217/fon-2020-0299.
- Mann, M. K., Ray, A., Basu, S., Karp, C. L., & Dittel, B. N. (2012). Pathogenic and regulatory roles for B cells in experimental autoimmune encephalomyelitis. *Autoimmunity*, *45*(5), 388-399. doi:10.3109/08916934.2012.665523
- Manning, B. D., & Toker, A. (2017). AKT/PKB Signaling: Navigating the Network. *Cell*, *169*(3), 381-405. doi:10.1016/j.cell.2017.04.001
- Marrie, R. A., Elliott, L., Marriott, J., Cossoy, M., Blanchard, J., Leung, S., & Yu, N. (2015). Effect of comorbidity on mortality in multiple sclerosis. *Neurology*, *85*(3), 240-247. doi:10.1212/WNL.0000000000001718

- Martin E, Aigrot MS, Grenningloh R, Stankoff B, Lubetzki C, Boschert U, Zalc B. Bruton's Tyrosine Kinase Inhibition Promotes Myelin Repair. *Brain Plast.* 2020 Oct 1;5(2):123-133. doi: 10.3233/BPL-200100
- McQualter, J. L., & Bernard, C. C. (2007). Multiple sclerosis: a battle between destruction and repair. *J Neurochem*, 100(2), 295-306. doi:10.1111/j.1471-4159.2006.04232.x
- Mi, S., Miller, R. H., Lee, X., Scott, M. L., Shulag-Morskaya, S., Shao, Z., . . . Pepinsky, R. B. (2005). LINGO-1 negatively regulates myelination by oligodendrocytes. *Nat Neurosci*, 8(6), 745-751. doi:10.1038/nn1460
- Mi, S., Pepinsky, R. B., & Cadavid, D. (2013). Blocking LINGO-1 as a therapy to promote CNS repair: from concept to the clinic. *CNS Drugs*, 27(7), 493-503. doi:10.1007/s40263-013-0068-8
- Mirshafiey, A., Ghalamfarsa, G., Asghari, B., & Azizi, G. (2014). Receptor Tyrosine Kinase and Tyrosine Kinase Inhibitors: New Hope for Success in Multiple Sclerosis Therapy. *Innov Clin Neurosci*, 11(7-8), 23-36.
- Mohan, H., Friese, A., Albrecht, S., Krumbholz, M., Elliott, C. L., Arthur, A., . . . Meinl, E. (2014). Transcript profiling of different types of multiple sclerosis lesions yields FGF1 as a promoter of remyelination. *Acta Neuropathol Commun*, 2, 168. doi:10.1186/s40478-014-0168-9
- Nakamura, S., Todo, T., Motoi, Y., Haga, S., Aizawa, T., Ueki, A., & Ikeda, K. (1999). Glial expression of fibroblast growth factor-9 in rat central nervous system. *Glia*, 28(1), 53-65.
- Nicholas, R., & Rashid, W. (2012). Multiple sclerosis. *BMJ Clin Evid*, 2012.
- Nociti V. What is the role of Brain derived neurotrophic factor in Multiple Sclerosis neuroinflammation?. *Neuroimmunol Neuroinflammation* 2020;7:291-299. <http://dx.doi.org/10.20517/2347-8659.2020.25>
- Nogova L, Sequist LV, Perez Garcia JM, Andre F, Delord JP, Hidalgo M, Schellens JH, Cassier PA, . . . Wolf J. Evaluation of BGJ398, a Fibroblast Growth Factor Receptor 1-3 Kinase Inhibitor, in Patients With Advanced Solid Tumors Harboring Genetic Alterations in Fibroblast Growth Factor Receptors: Results of a Global Phase I, Dose-Escalation and Dose-Expansion Study. *J Clin Oncol.* 2017 Jan 10;35(2):157-165.

- Oh LY, Denninger A, Colvin JS, Vyas A, Tole S, Ornitz DM, Bansal R. Fibroblast growth factor receptor 3 signaling regulates the onset of oligodendrocyte terminal differentiation. *J Neurosci*. 2003 Feb 1;23(3):883-94. doi: 10.1523/JNEUROSCI.23-03-00883.2003.
- Okuno, T., Nakatsuji, Y., & Kumanogoh, A. (2011). The role of immune semaphorins in multiple sclerosis. *FEBS Lett*, 585(23), 3829-3835. doi:10.1016/j.febslet.2011.03.033
- Ornitz DM, Itoh N. The Fibroblast Growth Factor signaling pathway. *Wiley Interdiscip Rev Dev Biol*. 2015 May-Jun;4(3):215-66. doi: 10.1002/wdev.176. Epub 2015 Mar 13.
- Palumbo, S., & Pellegrini, S.(2017). In I. S. Zagon & P. J. McLaughlin (Eds.), *Multiple Sclerosis: Perspectives in Treatment and Pathogenesis*. Brisbane (AU).
- Patel, J., & Balabanov, R. (2012). Molecular mechanisms of oligodendrocyte injury in multiple sclerosis and experimental autoimmune encephalomyelitis. *Int J Mol Sci*, 13(8), 10647-10659. doi:10.3390/ijms130810647
- Procaccini, C., De Rosa, V., Pucino, V., Formisano, L., & Matarese, G. (2015). Animal models of Multiple Sclerosis. *Eur J Pharmacol*, 759, 182-191. doi:10.1016/j.ejphar.2015.03.042
- Racke, M. K. (2001). Experimental autoimmune encephalomyelitis (EAE). *Curr Protoc Neurosci, Chapter 9*, Unit9 7. doi:10.1002/0471142301.ns0907s14
- Rajendran, R., Bottiger, G., Dentzien, N., Rajendran, V., Sharifi, B., Ergun, S., . . . Berghoff, M. (2021). Effects of FGFR Tyrosine Kinase Inhibition in OLN-93 Oligodendrocytes. *Cells*, 10(6). doi:10.3390/cells10061318
- Rajendran, R., Giraldo-Velasquez, M., Stadelmann, C., & Berghoff, M. (2018). Oligodendroglial fibroblast growth factor receptor 1 gene targeting protects mice from experimental autoimmune encephalomyelitis through ERK/AKT phosphorylation. *Brain Pathol*, 28(2), 212-224. doi:10.1111/bpa.12487
- Rodgers, J. M., & Miller, S. D. (2012). Cytokine control of inflammation and repair in the pathology of multiple sclerosis. *Yale J Biol Med*, 85(4), 447-468.
- Rossi, S., Motta, C., Studer, V., Macchiarulo, G., Volpe, E., Barbieri, F., . . . Centonze, D. (2014). Interleukin-1beta causes excitotoxic neurodegeneration and multiple sclerosis disease progression by activating the apoptotic protein p53. *Mol Neurodegener*, 9, 56. doi:10.1186/1750-1326-9-56

- Rottlaender, A., Villwock, H., Addicks, K., & Kuerten, S. (2011). Neuroprotective role of fibroblast growth factor-2 in experimental autoimmune encephalomyelitis. *Immunology*, *133*(3), 370-378. doi:10.1111/j.1365-2567.2011.03450.x
- Sarchielli, P., Di Filippo, M., Ercolani, M. V., Chiasserini, D., Mattioni, A., Bonucci, M., . . . Calabresi, P. (2008). Fibroblast growth factor-2 levels are elevated in the cerebrospinal fluid of multiple sclerosis patients. *Neurosci Lett*, *435*(3), 223-228. doi:10.1016/j.neulet.2008.02.040
- Seiwert T. Y. (2018). Phase IIa study of the efficacy of BGJ398 (infigratinib) in FGFR1-3 translocated, mutated, or amplified squamous cell carcinoma of the head and neck. (clinicaltrials.gov)
- Shao, Z., Lee, X., Huang, G., Sheng, G., Henderson, C. E., Louvard, D., . . . Mi, S. (2017). LINGO-1 Regulates Oligodendrocyte Differentiation through the Cytoplasmic Gelsolin Signaling Pathway. *J Neurosci*, *37*(12), 3127-3137. doi:10.1523/JNEUROSCI.3722-16.2017
- Simons, M., & Nave, K. A. (2015). Oligodendrocytes: Myelination and Axonal Support. *Cold Spring Harb Perspect Biol*, *8*(1), a020479. doi:10.1101/cshperspect.a020479
- Sinha, S., Boyden, A. W., Itani, F. R., Crawford, M. P., & Karandikar, N. J. (2015). CD8(+) T-Cells as Immune Regulators of Multiple Sclerosis. *Front Immunol*, *6*, 619. doi:10.3389/fimmu.2015.00619
- Sonar, S. A., & Lal, G. (2019). The iNOS Activity During an Immune Response Controls the CNS Pathology in Experimental Autoimmune Encephalomyelitis. *Front Immunol*, *10*, 710. doi:10.3389/fimmu.2019.00710
- Stadelmann, C., Timmler, S., Barrantes-Freer, A., & Simons, M. (2019). Myelin in the Central Nervous System: Structure, Function, and Pathology. *Physiol Rev*, *99*(3), 1381-1431. doi:10.1152/physrev.00031.2018
- Stone, S., & Lin, W. (2015). The unfolded protein response in multiple sclerosis. *Front Neurosci*, *9*, 264. doi:10.3389/fnins.2015.00264
- Sun, L., He, C., Nair, L., Yeung, J., & Egwuagu, C. E. (2015). Interleukin 12 (IL-12) family cytokines: Role in immune pathogenesis and treatment of CNS autoimmune disease. *Cytokine*, *75*(2), 249-255. doi:10.1016/j.cyto.2015.01.030
- Syed, Y. A., Hand, E., Mobius, W., Zhao, C., Hofer, M., Nave, K. A., & Kotter, M. R. (2011). Inhibition of CNS remyelination by the presence of semaphorin 3A. *J Neurosci*, *31*(10), 3719-3728. doi:10.1523/JNEUROSCI.4930-10.2011

- t Hart, B. A., Gran, B., & Weissert, R. (2011). EAE: imperfect but useful models of multiple sclerosis. *Trends Mol Med*, *17*(3), 119-125. doi:10.1016/j.molmed.2010.11.006
- Tafti, D., Ehsan, M., & Xixis, K. L. (2021). Multiple Sclerosis. In *StatPearls*. Treasure Island (FL).
- Tintore, M., Vidal-Jordana, A. & Sastre-Garriga, J. Treatment of multiple sclerosis — success from bench to bedside. *Nat Rev Neurol* *15*, 53–58 (2019). <https://doi.org/10.1038/s41582-018-0082-z>
- Thompson, A. J., Banwell, B. L., Barkhof, F., Carroll, W. M., Coetzee, T., Comi, G., . . . Cohen, J. A. (2018). Diagnosis of multiple sclerosis: 2017 revisions of the McDonald criteria. *Lancet Neurol*, *17*(2), 162-173. doi:10.1016/S1474-4422(17)30470-2
- Thompson, A. J., Baranzini, S. E., Geurts, J., Hemmer, B., & Ciccarelli, O. (2018). Multiple sclerosis. *Lancet*, *391*(10130), 1622-1636. doi:10.1016/S0140-6736(18)30481-1
- Tiong, K. H., Mah, L. Y., & Leong, C. O. (2013). Functional roles of fibroblast growth factor receptors (FGFRs) signaling in human cancers. *Apoptosis*, *18*(12), 1447-1468. doi:10.1007/s10495-013-0886-7
- Torke S, Pretzsch R, Häusler D, Haselmayer P, Grenningloh R, Boschert U, Brück W, Weber MS. Inhibition of Bruton's tyrosine kinase interferes with pathogenic B-cell development in inflammatory CNS demyelinating disease. *Acta Neuropathol*. 2020 Oct;140(4):535-548. doi: 10.1007/s00401-020-02204-z.
- Van Kaer, L., Postoak, J. L., Wang, C., Yang, G., & Wu, L. (2019). Innate, innate-like and adaptive lymphocytes in the pathogenesis of MS and EAE. *Cell Mol Immunol*, *16*(6), 531-539. doi:10.1038/s41423-019-0221-5
- Vermersch P, Oh J, Cascione M, Oreja-Guevara C, Gobbi C, Travis LH, Myhr KM, Coyle PK. Teriflunomide vs injectable disease modifying therapies for relapsing forms of MS. *Mult Scler Relat Disord*. 2020 Aug;43:102158. doi: 10.1016/j.msard.2020.102158
- Vogel, D. Y., Vereyken, E. J., Glim, J. E., Heijnen, P. D., Moeton, M., van der Valk, P., . . . Dijkstra, C. D. (2013). Macrophages in inflammatory multiple sclerosis lesions have an intermediate activation status. *J Neuroinflammation*, *10*, 35. doi:10.1186/1742-2094-10-35
- Vogt, J., Paul, F., Aktas, O., Muller-Wielsch, K., Dorr, J., Dorr, S., . . . Zipp, F. (2009). Lower motor neuron loss in multiple sclerosis and experimental autoimmune encephalomyelitis. *Ann Neurol*, *66*(3), 310-322. doi:10.1002/ana.21719

- VonDrän, M. W., Singh, H., Honeywell, J. Z., & Dreyfus, C. F. (2011). Levels of BDNF impact oligodendrocyte lineage cells following a cuprizone lesion. *J Neurosci*, *31*(40), 14182-14190. doi:10.1523/JNEUROSCI.6595-10.2011
- Wang, M., Yang, Y., Cansever, D., Wang, Y., Kantores, C., Messiaen, S., . . . Bhushan, S. (2021). Two populations of self-maintaining monocyte-independent macrophages exist in adult epididymis and testis. *Proc Natl Acad Sci U S A*, *118*(1). doi:10.1073/pnas.2013686117
- Wohrle, S., Henninger, C., Bonny, O., Thuery, A., Beluch, N., Hynes, N. E., . . . Graus Porta, D. (2013). Pharmacological inhibition of fibroblast growth factor (FGF) receptor signaling ameliorates FGF23-mediated hypophosphatemic rickets. *J Bone Miner Res*, *28*(4), 899-911. doi:10.1002/jbmr.1810
- Xiao, J., Ferner, A. H., Wong, A. W., Denham, M., Kilpatrick, T. J., & Murray, S. S. (2012). Extracellular signal-regulated kinase 1/2 signaling promotes oligodendrocyte myelination in vitro. *J Neurochem*, *122*(6), 1167-1180. doi:10.1111/j.1471-4159.2012.07871.x
- Xie, Y., Su, N., Yang, J., Tan, Q., Huang, S., Jin, M., . . . Chen, L. (2020). FGF/FGFR signaling in health and disease. *Signal Transduct Target Ther*, *5*(1), 181. doi:10.1038/s41392-020-00222-7
- Yamout, B. I., & Alroughani, R. (2018). Multiple Sclerosis. *Semin Neurol*, *38*(2), 212-225. doi:10.1055/s-0038-1649502
- Zhou, Y. X., Pannu, R., Le, T. Q., & Armstrong, R. C. (2012). Fibroblast growth factor 1 (FGFR1) modulation regulates repair capacity of oligodendrocyte progenitor cells following chronic demyelination. *Neurobiol Dis*, *45*(1), 196-205. doi:10.1016/j.nbd.2011.08.004
- Zhou, Z. D., Sathiyamoorthy, S., & Tan, E. K. (2012). LINGO-1 and Neurodegeneration: Pathophysiologic Clues for Essential Tremor. *Tremor Other Hyperkinet Mov (N Y)*, *2*. doi:10.7916/D8PZ57JV
- Zipp, F., Oh, J., Frago, Y. D., & Waubant, E. (2019). Implementing the 2017 McDonald criteria for the diagnosis of multiple sclerosis. *Nat Rev Neurol*, *15*(8), 441-445. doi:10.1038/s41582-019-0194-0
- Zou, Y., Jiang, W., Wang, J., Li, Z., Zhang, J., Bu, J., . . . Xiao, B. (2014). Oligodendrocyte precursor cell-intrinsic effect of Rheb1 controls differentiation and mediates mTORC1-dependent myelination in brain. *J Neurosci*, *34*(47), 15764-15778. doi:10.1523/JNEUROSCI.2267-14.2014

## ACKNOWLEDGEMENTS

First and foremost, I would like to expose my sincere and warm thankfulness to my supervisor, **Prof. Dr. Martin Berghoff**, for accepting me to work in his research group. He has given me constant guide and supervision during these past four years and always encouraged me to attend conferences. He has been very supportive and has provided me the confidence to work with new collaborators. He has apprised me at the right time to start writing my thesis. He has advised me with his persistence, motivation, and extensive expertise throughout my work and thesis. I am incredibly grateful to him for allowing me to work under his tutelage.

I like to express my very grateful to **Prof. Dr. Reinhard Lakes-Harlan**. He was accepted as my first supervisor for my Dr.rer.nat.

I further praise our collaborator **Prof. Dr. Srikanth Karnati**, Institute for Anatomy and Cell Biology, Würzburg, Germany, provides new sight to my project with advanced scientific approaches. He has always given the first preference to my research to get a technical assistantship and valuable discussions with his extensive knowledge. He handled me as his own brother and gave me strong motivation, worthy guidance for my research and further career growth. I would like to extend my thankfulness to our collaborator, **Prof. Dr. Christina Stadelmann**, Institute for Neuropathology, Göttingen, Germany, to share her knowledge and provide technical assistantship to make staining in her lab.

My hearty thanks to my brother and post-doctoral fellow **Dr. Ranjithkumar Rajendran**, Experimental Neurology, Justus-Liebig University, Giessen, Germany. He had given the solid support to set up my new career path and to provide help during my initial days in Germany. In every experiment in the lab, he helped me with his widespread knowledge. I like to thank **Dr. Guido Haschke**, animal welfare officer, JLU, Giessen, **Dr. med. vet. Daniel Zahner** and animal caretakers for their support to do animal experiments. Many thanks to the “**Giessen Graduate school of Life Sciences**” (GGL), where I had the opportunity to gain scientific knowledge. I thank my fellow graduate **Tahira Zar** (now Dr. Zar) for help in the lab and her friendly discussions, to **Edith Löffler** for her welcoming manner towards me when I was new to the lab.

My sincere thanks to **Dr. S. P. Vijeikumar, Kavitha MSc, Dr. M. Shabana Begum** for spurring scientific research during my earlier days of my bachelors. My sincere and heartily thanks to my friends **Dr. Tamilarasan Selvaraj, Benedict Vincent Albert** and **Naveen Chandar Bharathi** for their moral support and assistance in every possible way in Germany. I would also like to thank my friends who are living in India. Especially **Rajesh, Sudar Kumar, Ramasubramaniam, Christiana** and **Sudharsan** who have helped and encouraged me a lot.

I mainly praise my grandma **Mrs. Chellamal Raja Gounder**, my parents **Mr. Rajendran & Mrs. Pappathi** and my aunt **Ms. Vennila**. My grandma worked hard in our farmland to get good education and wealth for my brother and me. She gave pure love and care. I am very much thankful to my beloved wife **Nivetha** for being my better half and for her support and care in every part of my life. I love them so much, and I would not have made it this far without them.

I also have to thank the members of my Dr.rer.nat committee for their helpful career advice and suggestions in general.

I am grateful to Novartis Phastmaceutical who has sponsored my thesis.



## PUBLICATIONS

1. Rajendran, R.\* , **Rajendran, V.\***, Megalofonou, F., Gurski, F., Stadelmann, S., Karnati, S., Berghoff, M. (2021). Oligodendrocyte-specific deletion of *FGFR1* reduces cerebellar inflammation and neurodegeneration in MOG<sub>35-55</sub>-induced EAE. *International Journal of Molecular Sciences*. Aug 31;22(17):9495. doi: 10.3390/ijms22179495 (IF: 5.9). \*Authors equally contributed
2. Rajendran, R., Bottiger, G., Dentzien, N., **Rajendran, V.**, Sharifi, B., Ergun, S., Berghoff, M. (2021). Effects of FGFR Tyrosine Kinase Inhibition in OLN-93 Oligodendrocytes. *Cells*, May 25;10(6):1318. doi:10.3390/cells10061318 (IF: 6.6)
3. Kamali, S., Rajendran, R., Stadelmann, C., Karnati, S., **Rajendran, V.**, Giraldo-Velasquez, M., & Berghoff, M. (2021). Oligodendrocyte-specific deletion of *FGFR2* ameliorates MOG<sub>35-55</sub>-induced EAE through ERK and Akt signalling. *Brain Pathol*, 31(2), 297-311. doi:10.1111/bpa.12916 (IF: 6.5)
4. **Rajendran, V.\***, Rajendran, R.\* , Kissel, F., Megalofonou, F., Chen, K., Stadelmann, S., Karnati, S., Berghoff, M. (2021). Differential regulation of FGFR signalling in spinal cord, cerebellum and brain stem of oligodendroglial FGFR1 knock out C57BL/6 mice. **Manuscript in preparation.** \*Authors equally contributed

### Publication originated from this dissertation

1. Rajendran, R.\* , **Rajendran, V.\***, Böttiger, G., Shirvanchi, K., Westbrook, V., Wallendszus, N., Bhushan, S., Ratering, S., Schnell, S., Liebisch, G., Stadelmann, S., Karnati, S., Berghoff, M. (2021). The selective FGFR inhibitor infigratinib exerts anti-inflammatory and neuroregenerative effects of in an EAE disease model of multiple sclerosis. **Submitted to *Nature medicine* (IF: 53.44).** \*Authors equally contributed
2. Rajendran, R.\* , **Rajendran, V.\***, Wallendszus, N., Liebisch, G., Stadelmann, S., Karnati, S., Berghoff, M. (2021). Effect of infigratinib on lipid metabolism in spinal cord and spleen during MOG<sub>35-55</sub>-induced EAE. **Manuscript in preparation.** \*Authors equally contributed

## Presentations and posters

1. **Rajendran, V.,** Rajendran, R., Berghoff, M. (2018). Myelin related gene expression in oligodendrocytes is regulated by FGFR inhibition with BGJ398 *in vitro*. ECTRIMS Online Library. Rajendran V. 10/10/18; 229340; EP1502.
2. **Rajendran, V.,** Rajendran, R., Berghoff, M. (2018). Inhibition of FGFR1/2 decreases oligodendrocyte proliferation through ERK signaling *in vitro*. American Academy of Neurology Annual Congress. Los Angeles, California, USA. [https://n.neurology.org/content/90/15\\_Supplement/P1.398](https://n.neurology.org/content/90/15_Supplement/P1.398)
3. **Rajendran, V.,** Rajendran, R., Stadelmann, S., Karnati, S., Berghoff, M. (2019). The FGFR inhibitor BGJ398 ameliorates motor deficits in experimental autoimmune encephalomyelitis, an animal model of multiple sclerosis. Poster. 12th Annual GGL Conference 2019, Giessen, Germany.
4. **Rajendran, V.,** Rajendran, R., Berghoff, M. (2019). Differential regulation of ERK and AKT phosphorylation in the CNS of oligodendroglial FGFR1 knockout mice. Research Day MS and Oppenheim Förderprizes für MS, Novartis Pharmaceuticals, Berlin, Germany.
5. **Rajendran, V.,** Rajendran, R., Stadelmann, C., Karnati, S., Berghoff, M. (2020). FGFR inhibitor BGJ398 protects against inflammation and demyelination in EAE through ERK/Akt phosphorylation. Poster. 1<sup>st</sup> Digital GGL Conference on Life Sciences, Giessen, Germany.
6. **Rajendran, V.,** Kissel, F., Rajendran, R., Berghoff, M. (2020). Oligodendroglial Specific Deletion of *FGFR1* Protects Myelin in C57BL/6 Mice. American Academy of Neurology Annual Congress. [https://n.neurology.org/content/94/15\\_Supplement/990](https://n.neurology.org/content/94/15_Supplement/990)